Modeling of General Medium Constitutive Relationships in the Transmission Line Matrix Method (TLM)

by

Leonardo Rodrigues Araujo Xavier de Menezes
M.Sc. degree, University of Brasilia, Brazil, 1992

A Dissertation Submitted in Partial Fulfillment of the Requirements for the Degree of

Doctor of Philosophy

in the Department of Electrical & Computer Engineering

We accept this thesis as conforming to the required standard

Dr. W. J. R. Hoefer, Supervisor
Professor, Department of Electrical and Computer Engineering

Dr. M. Stuchly, Departmental Member
Professor, Department of Electrical and Computer Engineering

Dr. R. Vahldieck, Departmental Member
Professor, Department of Electrical and Computer Engineering

Dr. R. N. Horspool, Outside Member
Professor, Department of Computer Science

Dr. J. LoVetri, External Examiner
Professor, Department of Electrical Engineering, University of Western Ontario

Supervisor: Dr. W. J. R. Hoefer

ABSTRACT

This thesis presents the modeling of general medium constitutive relationships in the Transmission Line Matrix (TLM) method. The technique is shown for two- and three-dimensional cases. The procedure consists of decoupling the impulse scattering at the nodes from equations describing the medium. This is achieved by using nodal sources connected to the TLM node. The nodal sources are implemented with the state-variable description of the constitutive relationships. The technique requires only few modifications to the TLM algorithm. The procedure is validated for frequency-dependent, nonlinear, anisotropic and gyromagnetic media.

This thesis also presents a dispersion analysis of TLM with frequency-dependent dielectrics. This study is performed in two- and three-dimensions by solving the dispersion relationship of TLM with nodal sources. The sources are used to model the frequency dependent dielectric. The study shows that the nodal source and stub-loaded models are equivalent for frequency independent dielectrics. The accuracy bounds of the TLM frequency-dependent dielectric model are presented.

This thesis also investigates the physical origin of the coarseness and dispersion errors influencing two-dimensional TLM solutions of Maxwell's equations. The study is performed by solving the difference equations of the numerical method analytically. The results confirm a reduction of the accuracy of the discrete solution near field singularities. The solution of a partially filled waveguide is also investigated. The results show that TLM can have positive or negative frequency shifts, depending on the dielectric filling, excited mode and geometry. These results are also valid for the finite difference time domain method (FDTD).

Examiners:

Dr. W. J. R. Hoefer, Supervisor
Professor, Department of Electrical and Computer Engineering

Dr. M. Stuchly, Departmental Member
Professor, Department of Electrical and Computer Engineering

Dr. R. Vahldieck, Departmental Member
Professor, Department of Electrical and Computer Engineering

Dr. R. N. Horspool, Outside Member
Professor, Department of Computer Science

Dr. J. LoVetri, External Examiner
Professor, Department of Electrical Engineering, University of Western Ontario

Table of Contents

List of Tables

List of Figures

Acknowledgments

I would like to thank the many friends who helped me in this most interesting journey.

First, I would like to express my gratitude to my supervisor, Prof. Wolfgang J.R. Hoefer. Without his help and advice none of this would been possible. He taught and guided me through whole process. I learned much from him.

I also wish to thank my former supervisor, Prof. Humberto Abdalla, University of Brasilia, Brazil, for keeping my mind open to the interesting problems of electromagnetism.

Thanks to the many members of the NSERC/MPR Teltech Research group: Lucia Cascio, Dr. Eswarappa Channabasappa, Sherri Cole, John Damaschke, Christof Fuchs, Dr. Jonathan Herring, Dr. Poman So, Dr. Mario Righi, Giampaolo Tardioli, Jesus Torre and Dr. Qi Zhang. I thank you all for the inspiring discussions, helpful ideas, the exciting suggestions, and the nice and relaxing coffee breaks.

A very special thanks to Sherri Cole (again), Lynne Barret, Vicky Smith and Maureen Denning for making the presentation of this thesis a reality. Without their help, I don not know if I could have presented this work.

The financial support of the Conselho Nacional de Pesquisa (CNPq) is also gratefully acknowledged. The members of this agency were the ones who made possible my coming to the University of Victoria

Thanks also to my brazilian friends in Victoria: Marcello, Sergio, Luciana, Vera, Peixoto and Lane. And thanks also to my portuguese friend: Isabel de Campos

And last but not least: I acknowledge the support from my family in Brazil. I thank each one of you: Raimundo, Niceas, Ricardo and Leticia. You are the reason I keep trying to do my best.

Dedication

To my friends and family, for being there

And to the lights burning bright all alone in the night.

List of symbols

The following symbols are used throughout this thesis:

a	incident pulse at the node
b	scattered pulse from the node
c	speed of light
dt	Infinitesimal temporal step
dr	infinitesimal spatial step
e	charge of the electron
f	frequency
g	Lande g-factor
i	current
j	$\sqrt{-1}$
k_u	propagation constant
k	timestep (iteration) number
l	index in the y-direction (y=j Δy)
m	normalized magnetization density
m	mass of the electron
m	index in the x-direction (x=j Δx)
n	index in the y-direction (z=j Δz)
p	normalized polarization density
s	Laplace transform variable
t	time
v_p	phase velocity
v	voltage
y	normalized stub admittance
z	normalized stub impedance
B	magnetic flux density
B	reactance
C	capacitance
[C]	connection matrix
D	electric displacement
E	electric field
[F]	electric susceptibility tensor
[G]	magnetic susceptibility tensor
H	magnetic field
H_0	bias magnetic field
J	total angular moment
$[J_s]$	Source vector
L	inductance
<L>	mean orbital angular moment

M	magnetization density
M_0	saturation magnetization
P	polarization density
[P]	propagation matrix
R	resistance
[S]	scattering matrix
[U]	identity matrix
V	voltage.
Y	admittance
Y_o	characteristic admittance
Y_r	normalized link-line admittance
Z	impedance
Z_o	characteristic impedance
Z_r	normalized link-line impedance
α	nonlinear coupling constant
β	propagation constant
δ_0	Loss factor
ε	absolute permittivity
ε_o	permittivity of free space
ε_r	relative permittivity
ε_s	static permittivity
λ	wavelength
λ_o	wavelength in free space
μ	absolute permeability
μ_o	permeability of free space
μ_r	relative permeability
$\langle\mu\rangle$	mean magnetic moment
ω	angular frequency
ω_0	resonance frequency
χ	susceptibility
τ_0	relaxation time
Δf	frequency step
Δl	space discretization step
Δt	temporal discretization step
[A]	matrix composed of elements $[a_{ij}]$
[a]	array composed of elements $[a_i]$

Prefixes

A subscript prefix is used to denote the timestep (iteration) number.

Suffixes

The following superscript suffixes are used:

i	pulse incident upon a node
r	pulse reflected from a node

The following subscript suffixes are used:

1..18	pulse on link lines 1 to 18
u	polarization along the u direction
s	source voltages
e	electric source
u	magnetic source

Common abbreviations

TLM	Transmission Line Matrix
FDFD	Finite Differences in the Frequency Domain
FDTD	Finite Differences in the Time Domain
ABC	Absorbing Boundary Condition
TEM	Transverse Electromagnetic
TE	Transverse Electric
TM	Transverse Magnetic
2D	Two-dimensional
3D	Three-dimensional
DUT	Device Under Test

Chapter 1

Introduction

1.1 Field modeling tools

Accurate numerical field modeling tools are crucial for the development and understanding of new technologies. Today, numerical simulation of electromagnetic problems is an important step in the design of new components and validation of novel concepts, [1]-[3]. Simulation tools allow shorter design cycles. They also improve the competitiveness by shortening the development of new products.

As the use of software packages for field modeling increases, the need to enhance the modeling capabilities of these programs also grows. The inclusion of complex medium behavior with frequency dependency, anisotropy and non-linearity is important since Microwave Monolithic Integrated Circuits (MMIC's) are built with materials having these properties. Complex modeling capability is also important in the field of biological effects of RF ([4]-[5]), non-reciprocal devices ([6]-[8]), plasma modeling ([9]) and full wave analysis of semiconductor devices ([10]-[11]).

Moreover, the capability to expand the model of the medium is desirable. The modeling capability of a simulator should grow as the understanding of the physics of the medium increases. This allows the use of simple models in early stages of the design and more complex ones in the final stages.

The most important element in the modeling process is the field solver tool. The numerical solution of Maxwell equations must be performed using a particular numerical method [1]-[3]. In the development of new technologies the field solver tool must be general. Therefore the method should be able to:

- Analyze arbitrary geometries

In system design or in high field applications, it is also necessary to impose a second condition for the field solver tool:

- Include non-linear effects

These two restrictions rule out several methods. These methods are either geometry specific (therefore computationally more efficient), or use the principle of superposition (therefore linear) in their formulation.

The second restriction affects most of the frequency domain methods. The reason is the generation of harmonics and sub-harmonics in nonlinear problems [12]. This effect demands the use of harmonic balance techniques, which involve the iterative solution of the same problem at the same frequency several times.

This restriction is avoided if the numerical method solves the problem in the time domain. This leads to three choices [1]-[3]:

- Methods based on the integral (or variational) formulation of the field equations, in the time domain,
- Methods based on the differential formulation of the equations, in the time domain.

The first approach is global in the solution, with boundary and initial conditions included in the formulation. The Method of Moments (MoM) and the Finite Element Method (FEM) are the leading technique used in this case.

The second approach is local and includes the boundary and initial conditions as the algorithm marches in time. The Finite Difference Time Domain (FDTD) and the Transmission Line Matrix (TLM) methods are the leading techniques in this case.

Both approaches lead to systems of algebraic equations that must be solved at each timestep. Each one has particular advantages over the other, depending on the problem [1]-[3]. The integral formulation can solve open problems (antennas, scattering) and treat complex geometries easily. The differential formulation can solve closed problems with different media more easily.

1.2 Time domain differential methods and TLM

The major time domain differential techniques are the FDTD and TLM.

The most frequently used technique is the Finite Difference Time Domain (FDTD)

method. It is based on the direct discretization of Maxwell's equations using the leapfrog scheme [13]. The FDTD method leads to a set of equations that are solved recursively at each timestep.

The Transmission Line Matrix (TLM) method is a time domain method based on the physical approximation of the field components by circuit quantities [14]-[16]. These quantities (voltages and currents) obey the same equations as the fields. The equations are governed by the transmission line circuit topology.

It is important to mention that a new technique has recently emerged; it is called Multi-Resolution in Time Domain (MRTD) [17]-[18]. It uses wavelets as basis functions in its derivation from Maxwell equations. This technique leads to improved dispersion characteristics with large savings in computer memory. The only apparent drawback of the method seems to be the difficulty to enforce the boundary conditions.

The advantages of the FDTD method over TLM are:

- It uses less variables than TLM [13], [14]. In two-dimensional TLM, four variables are used, while in FDTD only three are needed. In three-dimensional TLM, twelve variables are used in TLM, compared to six in FDTD.
- It is simpler and more efficient to implement the Perfect Matched Layer (PML) absorbing boundary condition in FDTD than in TLM [19], [20].
- In certain cases, it can have less dispersion error than TLM [21]-[27].
- No spurious solutions

The advantages of the TLM method over FDTD are:

- All the field components are obtained at the same point in space and time [14],[28]. There is no difficulty in the modeling of electric, magnetic and dielectric boundaries at the same point in space, providing twice the spatial resolution of the other leading method.
- The equivalent circuit of linear passive structures can be directly obtained from a TLM solution and interfaced to other TLM problems [29]-[30].
- In certain cases, it can have less dispersion than FDTD [22]-[27].

A comparison between TLM and FDTD shows that the methods can be considered complementary rather than competing. Both methods are simple to implement in a

sequential or parallel form and can be interfaced with other methods of analysis.

1.3 Outline of this thesis

The fact that the TLM network can be easily combined with arbitrary lumped-element circuits [29]-[30] is a decisive advantage for the modeling of general constitutive relationships. In this thesis, the Transmission Line Matrix (TLM) method is therefore used for this purpose.

Chapter 2 discusses the TLM method. The discrete Huygens' principle is used to explain the basic TLM formulation.

Chapter 3 discusses the modeling of general constitutive relationships in TLM. The medium equation can be expressed as a circuit equation, since the voltages and currents in equivalent circuits follow the same relations as the polarization and magnetization vectors and the electric and magnetic fields. This allows the modeling of very general circuit relationships since numerical techniques for the solution of the circuits can be used to include very general circuit topologies in the TLM mesh.

Chapter 4 validates the proposed approach. The TLM model for several kinds of medium relationships is discussed. The approach is validated with examples of frequency dependent, nonlinear and anisotropic relationships. The validation is performed for both the two and three-dimensional TLM methods.

Chapter 5 deals with the accuracy of the TLM method. The dispersion analysis of frequency dependent dielectrics is performed for the two and three-dimensional TLM. The analysis shows that the accuracy of frequency dependent materials in TLM is a function of the timestep, relaxation time and the resonant frequency of the medium. The dispersion analysis of the numerical method provides the maximum ranges of isotropy, accuracy and bandwidth of the technique. It shows the approximations involved in the numerical method and defines the range of applicability of the technique. The dispersion of TLM is obtained by solving the matrix equations of TLM in the steady-state, assuming an infinite mesh.

Chapter 5 also presents a new method of error analysis for TLM. The technique is based on the solution of the difference equations of the numerical method. These equations are solved by including the boundary conditions of the problems. Since the solution can only be obtained in certain cases, only three special cases are treated. However, these

examples show that TLM and FDTD can be less than second order accurate in the presence of logarithmic discontinuities (thin edges).

The last chapter concludes the thesis by summarizing its new contributions to the field of electromagnetic modeling: modeling of general media in TLM, dispersion analysis of TLM with frequency dependent dielectrics and the solution of difference equations. This chapter also points out some of the possible applications and future work. One application of medium modeling in TLM is the solution of coupled problems. The difference equation approach can be used to quantify the errors in staircase and conformal mapping modeling of certain structures.

Chapter 2

The Transmission Line Matrix Method

2.1 Introduction

This chapter is a review of the Transmission Line Matrix (TLM) method.

The TLM method is a powerful numerical technique for solving electromagnetic problems. The method uses transmission line networks to represent the behavior of electromagnetic fields [14]-[16]. In this model, voltages and currents follow equations identical to those governing electric and magnetic fields in space and time.

Therefore, concepts of transmission line analysis can be used to describe the electromagnetic phenomena. The TLM method uses scattering and propagation matrices to simulate the propagation of electromagnetic fields. The space is divided into a mesh of transmission lines interconnected at discrete points in space. At each of these points, the incident and reflected pulses are scattered and transmitted to other points of the mesh.

A simple two-dimensional version of the TLM method can be obtained by applying Huygens' principle and the conservation of energy [16]. This formulation shows the basic concepts involved in the method.

There are two distinct nodes used to model electric or magnetic fields. The nodes represent the two different polarizations for a wave propagating on a plane [31]-[33]. These are the cases where electric (TE) or magnetic (TM) field is perpendicular to the plane of propagation.

The transmission line analogy characterizes the first case as the shunt node case and the second as series node case. This follows from the topology of the network of transmission lines.

A three-dimensional version of the method is obtained by assembling a 3D array of two-dimensional nodes. For each direction one series and one shunt node is used to represent the magnetic and electric field component in that direction [34]. The complete node will describe the behavior of six field components.

Permittivity and permeability are modelled by stubs connected to the node [15]-[16]. In the shunt node case, an open-circuited stub models the relative permittivity of the region. In the series node case, a short-circuited stub models the relative permeability. In this representation the relative permittivity and permeability of the medium are frequency independent and isotropic.

The TLM method can be solved either in the time or in the frequency domain. In the time domain, the evolution of the propagation of pulses through the transmission lines determines the state of the system. The resulting scheme can be used to analyze transient behavior of electromagnetic structures [14]-[16]. The frequency domain version of TLM transforms the domain into an eigenvalue problem solved at each frequency point [35]. The time-domain TLM yields a wide-band response of the electromagnetic problem.

2.2 The discrete Huygens' principle

The TLM method can be viewed as the discrete equivalent of Huygens' principle [16],[36]. In this view a wavefront W2 at a particular time is obtained from the wavefront W1 at a previous time instant. The wavefront W2 is obtained by considering each point of the wavefront W1 at the previous time as a secondary radiator. The radiated secondary waves from all the points in W2 are interpolated. The result is the wavefront W1. This process is shown in Figure 2.1.

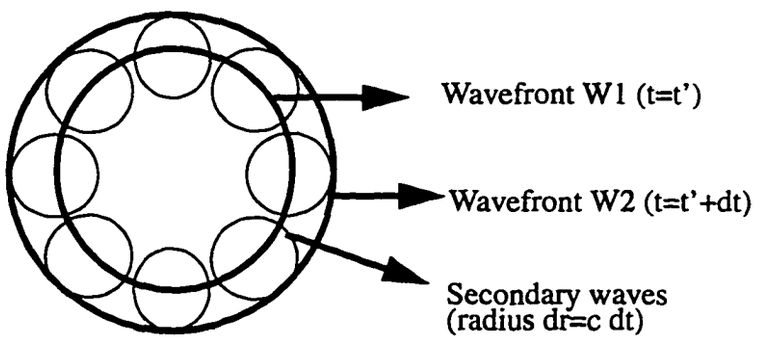

Figure 2.1 Huygens' principle: The wavefront W2 is composed by secondary wavefronts obtained from the primary wavefront W1.

In the continuous Huygens' principle, the secondary wavefronts would form a circle of radius:

$$dr = cdt \tag{2.1}$$

where dt is the differential timestep, dr is the differential radius and c is the velocity of propagation of light in the medium.

In the discrete equivalent, the radius of the wavefronts would be:

$$\Delta r = v\Delta t \tag{2.2}$$

where Δt is the discretized timestep, Δr is the discretized spatial step and v is velocity of propagation of light in the medium.

In the discrete equivalent, the propagation takes place along the Cartesian axes of space. The process is simplified to the propagation of pulses along the axial directions [2]. The pulses are scattered at the nodes and form secondary radiators. The primary wavefront is composed by all these radiators.

There are two different kinds of pulses in the mesh: pulses incident at the nodes and pulses transmitted to other nodes. The pulses scattered at a node become incident at the adjacent ones after a time delay. The delay is due to the distance between nodes and the finite speed of light.

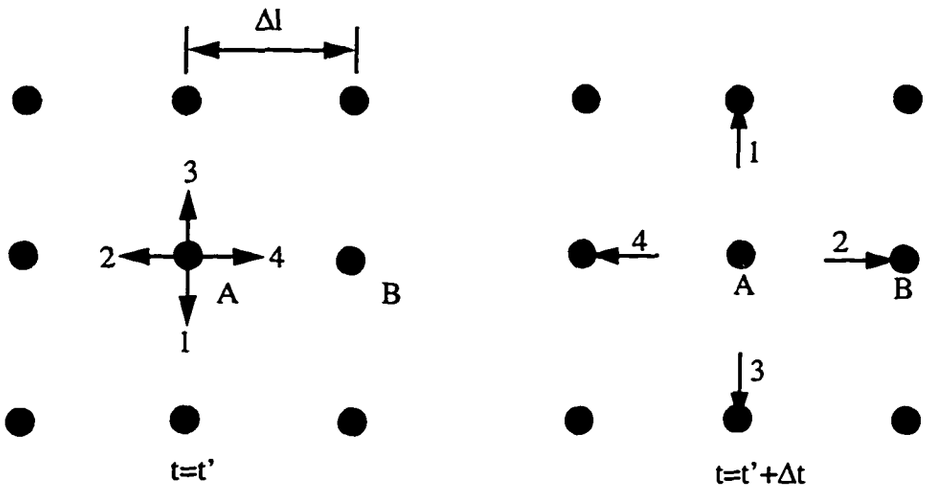

Figure 2.2 Scattering and propagation of pulses in a discrete model of Huygens' principle.

In Figure 2.2, the pulse incident on node B from the direction 2, $a_2^B(k\Delta t)$, is related to the pulse scattered at node A in the direction 4, $b_4^A(k\Delta t)$, by:

$$a_2^B(k\Delta t) = b_4^A(k\Delta t - \Delta t) \tag{2.3}$$

Applying the same idea to all nodes yields the global relationship between incident and scattered pulses:

$$[\mathbf{a}]_{k\Delta t} = [\mathbf{C}]\,[\mathbf{b}]_{(k-1)\Delta t} \tag{2.4}$$

where **a** is the vector of incident pulses, **b** is the vector of reflected pulses and **C** is a connection matrix, describing the connection between nodes.

The connection matrix **C** depends on the boundary conditions, since nodes near the boundary are also included in (2.4).

The characterization of the boundary conditions depends on the polarization of the wave, Figure 2.3. In the two-dimensional propagation there are two possible polarizations [31]-[33]. The first polarization is the TM to the plane (electric field perpendicular to the plane). The second is the TE polarization (magnetic field perpendicular to the plane).

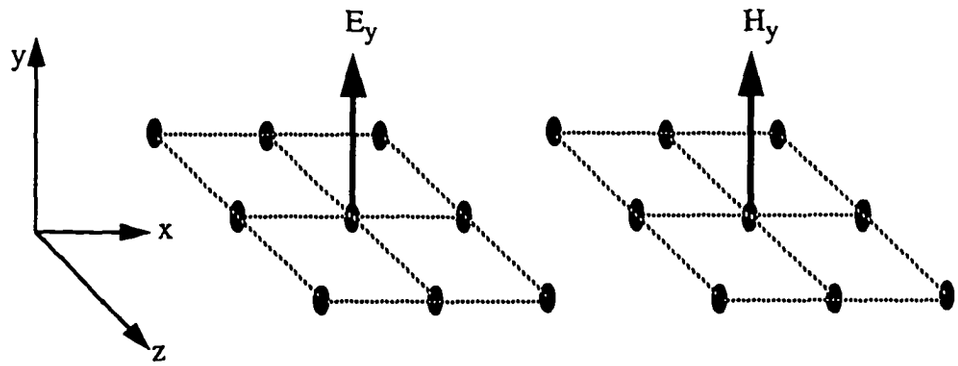

Figure 2.3 TM (Transverse Magnetic) and TE (Transverse Electric) polarizations of the field. These cases correspond to shunt and series TLM nodes respectively.

The relationship between the total field and the incident and scattered pulses is defined using the condition of field continuity between nodes. In the TM case:

$$\begin{aligned} a_1 &= \frac{1}{2}(E_y - Z_0 H_x) & a_2 &= \frac{1}{2}(E_y + Z_0 H_z) \\ a_3 &= \frac{1}{2}(E_y + Z_0 H_x) & a_4 &= \frac{1}{2}(E_y - Z_0 H_z) \\ b_1 &= \frac{1}{2}(E_y + Z_0 H_x) & b_2 &= \frac{1}{2}(E_y - Z_0 H_z) \\ b_3 &= \frac{1}{2}(E_y - Z_0 H_x) & b_4 &= \frac{1}{2}(E_y + Z_0 H_z) \end{aligned} \tag{2.5}$$

In the TE case:

$$\begin{aligned} a_1 &= \frac{1}{2}(H_y - Y_0 E_x) & a_2 &= \frac{1}{2}(H_y + Y_0 E_z) \\ a_3 &= \frac{1}{2}(H_y + Y_0 E_x) & a_4 &= \frac{1}{2}(H_y - Y_0 E_z) \\ b_1 &= \frac{1}{2}(H_y + Y_0 E_x) & b_2 &= \frac{1}{2}(H_y - Y_0 E_z) \\ b_3 &= \frac{1}{2}(H_y - Y_0 E_x) & b_4 &= \frac{1}{2}(H_y + Y_0 E_z) \end{aligned} \tag{2.6}$$

where Z_0 is the free-space impedance and Y_0 is the free-space admittance.

The last process in the propagation description is the scattering. The scattering is described as a linear combination between all incident impulses at the node:

$$b_i = \sum_{j=1}^{4} s_{ij} a_j \tag{2.7}$$

where i indicates which branch is being considered (i=1,2,3,4).

The representation of the scattering process for all branches result in the matrix equation:

$$[\mathbf{b}] = [\mathbf{S}]\,[\mathbf{a}] \tag{2.8}$$

Applying the condition of isotropy and energy conservation to the matrix results in:

$$[\mathbf{S}] = \frac{1}{2}\begin{bmatrix} -1 & 1 & 1 & 1 \\ 1 & -1 & 1 & 1 \\ 1 & 1 & -1 & 1 \\ 1 & 1 & 1 & -1 \end{bmatrix} \tag{2.9}$$

The result is equivalent to the shunt node scattering matrix obtained with the trans-

mission line concept [14]. The series node can also be obtained in this form by modifying the mapping of field components for the TE case. The same results can be obtained using transmission line concepts with greater simplicity.

2.3 Transmission-line analogy

The use of models to represent electromagnetic phenomena is not new. Since the beginning of electrical engineering, mechanical models of circuits have been used to explain the qualitative behavior of systems [37]. Even the transmission of currents in wires was once represented by the flux of water in a hollow pipe. The transmission line model is a simple representation of the electromagnetic field. Instead of using curl equations, it represents the field behavior by transmission and reflection of pulses on transmission lines.

The representation of the discrete Huygens' principle by a transmission line formulation is straightforward. The transmission lines are connected at the nodes. At each node, a scattering matrix is used to obtain the reflected pulses from the incident ones. The reflected pulses are transmitted to adjacent nodes, transforming into incident pulses. The process is repeated at each timestep.

The equivalent transmission line circuit for the TM case is a shunt circuit, Figure 2.4. Two transmission lines are connected in parallel.

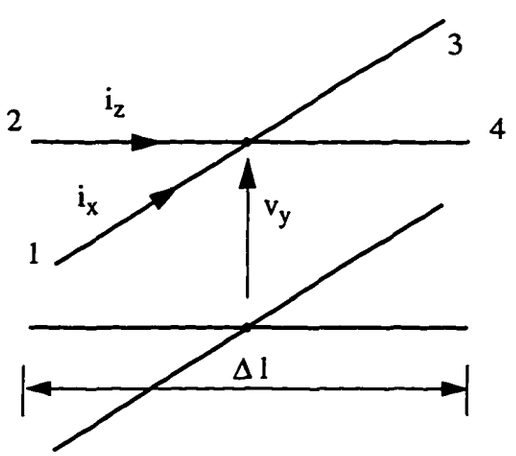

Figure 2.4 TLM shunt node. Two transmission lines are connected in parallel.

The total voltage across the shunt node is, [2]:

$$v_y = \frac{1}{2}(v_1^i + v_2^i + v_3^i + v_4^i) \tag{2.10}$$

The equivalent transmission line circuit for the TE case is a series circuit, Figure 2.5. The transmission lines are connected in series

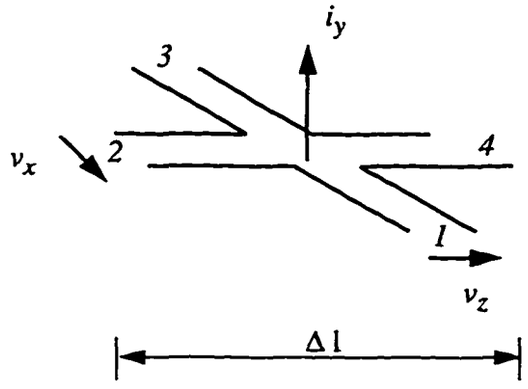

Figure 2.5 TLM series node. Two transmission lines are connected in series.

The total current across the series node is [2]:

$$i_y = \frac{1}{2Z_0}(-v_1^i + v_2^i + v_3^i - v_4^i) \tag{2.11}$$

The scattering and transmission matrices remain the same. The boundary conditions are enforced using transmission line concepts [16].

In the shunt node a metallic wall placed between nodes will reflect an incident pulse with a reflection coefficient of -1. A wall of symmetry has a reflection coefficient of one. In the series case the situation is reversed.

The representation of an absorbing boundary condition (ABC) is more complex [2]. This kind of boundary is necessary for the truncation of the computational domain. In the simulation of an infinite waveguide, the domain is truncated using a matched load condition.

The problem is the representation of this condition (ABC) in a time domain simulation. These boundaries are dispersive. The frequency domain value of the load is dependent on the wavenumber. The solution is usually an approximation of the exact absorbing boundary condition [38].

The frequency behavior of TLM is quantified by a dispersion analysis [22]-[27]. However, the qualitative behavior of the transmission line model can be explained using a simplified dispersion analysis.

In the shunt node case, the capacitance of the node will be twice the value of single transmission line, since the lines are connected in parallel. The consequence is that the propagation velocity of signals in the mesh is reduced by [2]:

$$v_p = \frac{c}{\sqrt{2}} \tag{2.12}$$

This is the low frequency speed of the transmission lines. Since the model is a discrete approximation of a continuous process, the accuracy is dependent on the frequency of the signal.

In free-space, the velocity error of TLM limits the accuracy of the method [2]. The TLM method is valid in the low frequency range. This range is determined by the discretization of the domain. As a rule of thumb, the TLM method has a 1% accuracy when the mesh size is 1/10th of the wavelength.

2.4 Three-dimensional TLM

The method can be expanded to three dimensions by combining the two-dimensional nodes [34]. A shunt node represents the electric field in the direction normal to the plane of propagation. A series node represents the magnetic field perpendicular to the plane of propagation. Using a suitable arrangement of three series and three shunt nodes, the TLM method can represent the behavior of all six field components.

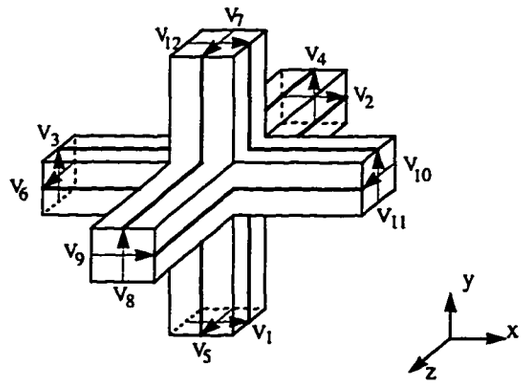

Figure 2.6 Symmetrical Condensed node. The node is composed of three shunt and three series two-dimensional nodes in a special configuration.

The most frequently used three-dimensional TLM node is the symmetrical condensed node [28], Figure 2.6. In this node, all six field components are represented in the same point in space. The scattering matrix is obtained from the total voltages at the shunt node and currents at the series nodes in all three spatial directions (x,y and z) [34].

$$
\begin{aligned}
v_1^r &= v_x(t) - z_0 i_z(t) - v_{12}^i & v_7^r &= v_z(t) - z_0 i_x(t) - v_5^i \\
v_2^r &= v_x(t) + z_0 i_y(t) - v_9^i & v_8^r &= v_y(t) + z_0 i_x(t) - v_4^i \\
v_3^r &= v_y(t) + z_0 i_z(t) - v_{11}^i & v_9^r &= v_x(t) - z_0 i_y(t) - v_2^i \\
v_4^r &= v_y(t) - z_0 i_x(t) - v_8^i & v_{10}^r &= v_z(t) + z_0 i_y(t) - v_6^i \\
v_5^r &= v_z(t) + z_0 i_x(t) - v_7^i & v_{11}^r &= v_y(t) - z_0 i_z(t) - v_3^i \\
v_6^r &= v_z(t) - z_0 i_y(t) - v_{10}^i & v_{12}^r &= v_x(t) + z_0 i_z(t) - v_1^i
\end{aligned}
\tag{2.13}
$$

2.5 Modeling dielectric and magnetic media

The TLM method can model heterogeneous media [15]-[16]. Dielectric and magnetic media are modelled by changing the impedance of the node. This can be done by adding a capacitance or inductance to the node. The change of inductance models magnetic materials and the change of capacitance models dielectric media.

Extra capacitances and inductances are added to the node in the form of stubs. In the low frequency approximation an open-circuited stub behaves as a capacitance and a short-circuited stub as an inductance [2].

In the two-dimensional case, these stubs are connected either to the shunt or series nodes. The open-circuited stub is connected to the shunt node, representing a medium with permittivity larger than vacuum. The short-circuited stub is connected to the series node, representing a medium with permeability larger than air.

The use of stubs in the node does not require special boundary or interface treatment. Since the transmission lines connecting the nodes (link lines) do not change, no boundary reflection and transmission coefficients are introduced. Therefore, the connection matrix of TLM is not changed by the introduction of stubs.

The scattering part of TLM, however, is changed by the use of stubs [2]. The scattering matrix will have an extra term describing the reflection of a pulse in the stub.

The scattering matrix equation of the shunt node with an open-circuited stub is [2]:

$$\begin{bmatrix} v_1 \\ v_2 \\ v_3 \\ v_4 \\ v_5 \end{bmatrix}_k^r = \frac{1}{y+4} \begin{bmatrix} -(2+y) & 2 & 2 & 2 & 2y \\ 2 & -(2+y) & 2 & 2 & 2y \\ 2 & 2 & -(2+y) & 2 & 2y \\ 2 & 2 & 2 & -(2+y) & 2y \\ 2 & 2 & 2 & 2 & y-2 \end{bmatrix}_k \begin{bmatrix} v_1 \\ v_2 \\ v_3 \\ v_4 \\ v_5 \end{bmatrix}_k^i \tag{2.14}$$

$$y = 4(\varepsilon_r - 1)$$

In the series case, the matrix equation is [2]:

$$\begin{bmatrix} v_1 \\ v_2 \\ v_3 \\ v_4 \\ v_5 \end{bmatrix}_k^r = \frac{1}{z+4} \begin{bmatrix} z+2 & 2 & 2 & -2 & -2 \\ 2 & z+2 & -2 & 2 & 2 \\ 2 & -2 & z+2 & 2 & 2 \\ -2 & 2 & 2 & z+2 & -2 \\ -2z & 2z & 2z & -2z & 4-z \end{bmatrix}_k \begin{bmatrix} v_1 \\ v_2 \\ v_3 \\ v_4 \\ v_5 \end{bmatrix}_k^i \tag{2.15}$$

$$z = 4(\mu_r - 1)$$

This media representation is valid only for non-dispersive isotropic dielectrics. The representation of general media in TLM is introduced in Chapter 3.

2.6 Data extraction in TLM

The TLM method generates large amounts of data at each simulation [2]. The processing of these data provides valuable insight into the behavior of the simulated structure. However, it is important to understand how to excite the TLM mesh and how to extract signals from it.

TLM is an excellent model for complex electromagnetic wave propagation. The accuracy of its results depends not only on the model itself, but also on the modeling of sources and on the way the field information is extracted. If the source region is not properly modeled, the results can be erroneous.

In time-domain TLM, the system is excited with a time domain source function at certain points of the mesh. These are called source points. In the simulation of a two-port device, the input port is connected to the source region.

In the source region, the dominant mode of propagation of the structure should be

adequately represented. This can be done by using templates. If the dominant mode is not properly represented, the number of timesteps needed to obtain the response may increase. The reason is the excitation of higher order modes. These modes can introduce resonances prolonging the time domain output sequence. They can also contribute to the excitation of an unwanted field distribution, for instance an even mode field distribution in a coplanar to microstrip transition. In the case of complex guided wave structures, the accuracy of the result depends on the proper source excitation.

The source function also has a time dependence. It consists of a sequence of pulses injected into the mesh as time progresses. The most frequently used distributions are the Dirac delta and the Gaussian functions. The advantage of using Gaussian functions is its bandwidth. Since these functions are band-limited (unlike the Dirac delta), higher frequency modes are not excited. In frequency domain TLM, this time component of the source is considered harmonic.

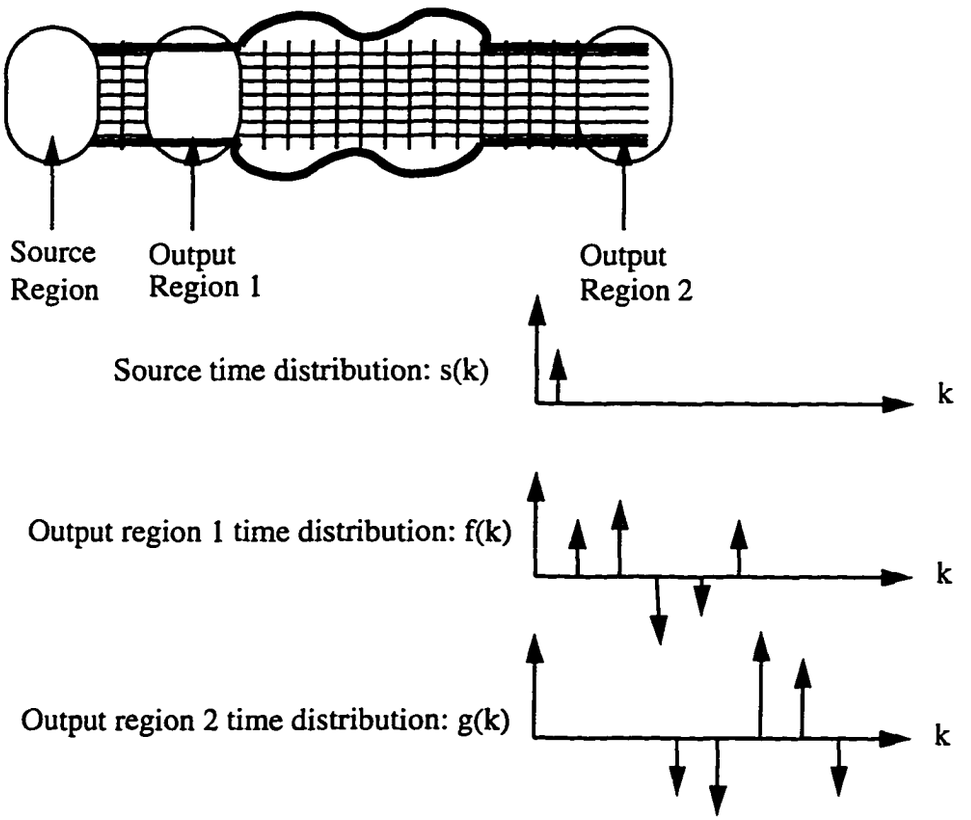

Figure 2.7 Data extraction from the TLM simulation of a two-port device. The S-parameters of the structure can be extracted using the output sequences and the response from a reference structure.

The response of TLM is the time-domain behavior of the field at all points of the mesh. The response of a two-port device is usually a sequence of pulses in time [2], taken at the output ports of the device.

The frequency response is obtained from the time-domain response with the Discrete Fourier Transform (DFT). The frequency-domain transformation of the time-domain sequences result in the wide-band representations of the fields in the output regions. These results are used to characterize the simulated structure.

In S-parameter calculation of devices, the data extraction procedure is similar to using a network analyzer. The time domain sequence is sampled at one output point in a reference structure. The device under test (DUT) is also simulated and the results at two output points are obtained. The S-parameters of the DUT are calculated with the data obtained from these simulations,

The output regions can also include several mesh points. In this case, the spatial distribution of the fields can be visualized. This can be done either in time or frequency domains. In the time-domain visualization, a dynamic representation of the evolution of the fields through the structure can be displayed. In frequency-domain, the fields can be displayed at any particular frequency. The result ia an accurate representation of the field interaction at the chosen frequency.

2.7 Conclusions

This chapter presented a review of the Transmission Line Matrix (TLM) method.

The TLM method uses transmission line models to describe the behavior of electromagnetic fields. In these models, the equations govering the propagation of voltages and currents are of the same from as Maxwell's equations that describe the behavior of electric and magnetic fields in continuous space. The mathematical representation of the array of transmission lines thus models the fields described by Maxwell's equations.

The TLM method uses scattering and propagation matrices to simulate the propagation of electromagnetic fields. The space is divided into a mesh of transmission lines interconnected at discrete points in space. At each of these points, the voltages and currents and scattered and transmitted to other points of the mesh.

A three-dimensional version of the method is obtained by assembling an array of two-dimensional nodes. A series and a shunt node are used to represent each magnetic

and electric field component respectively. The complete node will describe the behavior of six field components.

The modeling of the medium is performed by stubs connected to the node. In the the series node case, a short circuited stub models the relative permeability.

Chapter 3

Modeling General Constitutive Relationships in TLM

3.1 Introduction

In the basic TLM formulation, the medium is modeled by stubs connected to the TLM node [2]. An open-circuited stub represents the dielectric material, and a short-circuited stub represents the magnetic material. This method is very robust and efficient when the medium parameters are constant. However, the representation of complex materials is not possible with this approach.

In the representation by stubs the relative permittivity and permeability of the medium are frequency independent and isotropic. However, this is only an approximation of the behavior of real media [39]-[40] valid only under certain conditions (low intensity, narrow band fields). The interaction between the medium and electromagnetic waves can be very complex in some cases.

In some cases, the nonlinear, anisotropic or frequency dependent behavior can be neglected. Under low field conditions the response of a medium can be considered linear [39], [42]-[49]. The anisotropy of a crystal lattice cannot be neglected at shorter wavelengths [50]-[52]. The frequency dependent permittivity and permeability are only important in wideband operating conditions [39].

In other cases, these effects cannot be neglected. Semiconductor materials under high field conditions present nonlinear medium behavior [10]. Certain non-reciprocal devices are constructed using anisotropic materials [6]-[8]. High-moisture content materials display frequency dependent behavior [53]-[57].

This chapter reviews some of the complex interactions of electromagnetic waves with media. Among these effects are resonance, relaxation of materials, and anisotropy.

The chapter also presents the modeling of these complex phenomena in TLM. The representation relies on the modification of the node scattering matrix to include the medium behavior in the TLM procedure.

The modification of the matrix is shown for two implementation procedures. The first one is the modified matrix approach. In this case the node scattering matrix is changed to represent the medium being modeled. The consequence is that different medium relationships yield different TLM node scattering matrices.

The second approach is called the nodal source technique. In this approach, sources connected to the TLM nodes represent the constitutive equation of the medium. In this technique the TLM scattering matrix is independent of the medium. Only the sources change according to the constitutive equations of the medium.

A comparison between the techniques shows that it is advantageous to use the nodal source approach. While the modified matrix is more efficient, the nodal source is more general. In the former, the elements and the order of the matrix are dependent on the modeled medium. This reason alone is sufficient to choose the source technique.

The source approach has a physical interpretation. The sources represent the polarization and magnetization densities of the medium [39]. The medium independent scattering matrix represents the free-space constitutive equations. Without dielectric and magnetic media, the sources vanish.

In the case of a passive medium, the sources will absorb and/or store energy. A passive network connected to the node represents this absorption and/or storage. The circuit is solved at each TLM timestep using a circuit equivalent of the node.

In the two-dimensional case, the source is connected either to a shunt or to a series node. When connected to the shunt node, the source represents the dielectric behavior. In the series case, the source models the permeability of the medium. The shunt node is represented by its Norton equivalent, and the series node by its Thevenin equivalent. The solution procedure is the same for both nodes.

In the three-dimensional case, the sources modify the electric and magnetic fields. The sources are attached to a combination of shunt and series nodes. Since the three-dimensional TLM nodes can be assembled from three shunt and three series nodes, the

generalization of the nodal source approach to three dimensions is straightforward. Each of the shunt and series nodes has a scattering matrix independent of the medium, and a nodal source is connected to it. The combination of these nodes forms the three-dimensional TLM node

3.2 Review of constitutive relationships of materials

The constitutive relations describe the interaction of an externally applied field with charges inside the medium. The macroscopic behavior is an average of the interaction of the field with several molecules or atoms [39]. This effect is described by the polarization and magnetization of the medium.

In the linear case the medium is described by its permittivity and permeability constants. Their definition is based on the proportionality between the polarization and magnetization densities and the macroscopic fields.

In the general case, the medium behavior is best described by using the polarization and magnetization densities. The relationships between these and the applied field are the constitutive equations of the medium.

$$\begin{aligned} \mathbf{P}(t) &= \int_{-\infty}^{t} g(\mathbf{E}(\tau), \mathbf{H}(\tau))\, d\tau \\ \mathbf{M}(t) &= \int_{-\infty}^{t} f(\mathbf{E}(\tau), \mathbf{H}(\tau))\, d\tau \end{aligned} \tag{3.1}$$

where **P** is the polarization density, **M** is the magnetization density, **E** is the electric field, and **H** is the magnetic field.

The polarization density describes the macroscopic average interaction between the electric field and the electric charges in the medium. The magnetization density describes the macroscopic average interaction between the magnetic field and the moving charges (currents) in the medium.

$$\begin{aligned} \mathbf{P} &= \sum \mathbf{p}(\mathbf{E}_{local}, \mathbf{H}_{local}) \\ \mathbf{M} &= \sum \mathbf{m}(\mathbf{E}_{local}, \mathbf{H}_{local}) \end{aligned} \tag{3.2}$$

where **p** is the microscopic dipole moment, **m** the microscopic magnetic moment, $\mathbf{E}_{local}$ the microscopic electric field, and $\mathbf{H}_{local}$ the microscopic magnetic field. The macro-

scopic densities are obtained by the sum of the contributions from all atoms and molecules.

These densities can describe the flow of current as well as the storage of electric and magnetic energy in the medium. Therefore, the use of polarization and magnetization densities provide a complete description of its interaction with electromagnetic fields.

Although, the analysis presented in this chapter was developed with classical physics, the modeling of quantum phenomena (using the density matrix approach [39]) is also possible with this formulation. The main effects discussed here are the classical effects of relaxation, resonance, anisotropy, gyromagnetism and non-linearity.

In the general case, all these effects are combined. However, in most cases, one or two effects dominate the behavior of the material under most operating conditions.

3.2.1 Relaxation phenomena

Relaxation is caused by the time delay in the alignment of permanent dipole molecules with the field [39], [58]. This is common in polar materials such as water. These materials have a molecular configuration that causes a permanent dipole moment. The molecules are arranged randomly; therefore, no external dipole moment exists, in the absence of external fields.

The qualitative behavior of these materials under the influence of external fields is simple. In the low frequency range, the time delay is much smaller than the period of the wave. Therefore, the medium behaves as a low loss dielectric. In a certain frequency range, the time delay is comparable to the period of the wave. In this range, the medium appears to be lossy. In the higher frequency range, the period is much smaller than the time delay and no appreciable delay can be observed. The medium behaves as the vacuum.

In water the permanent dipole causes a rotation of the molecule in a time-harmonic field [58]. Its moment of inertia causes a delay in the orientation. The mathematical description of this process was formulated by Peter Debye in 1930. This kind of material is thus called a first-order Debye material.

The polarization density equation of this kind of medium is:

$$\mathbf{P} + \tau_0 \frac{d\mathbf{P}}{dt} = (\varepsilon_s - 1)\,\mathbf{E} + (\varepsilon_\infty - 1)\,\tau_0 \frac{d\mathbf{E}}{dt} \tag{3.3}$$

where τ_0 is the relaxation time constant of the medium, ε_∞ is the permittivity at infinite frequency and ε_s is the static permittivity.

This process is also observed in the transport of ions in some materials [39]. In this case, the relaxation is caused by collisions with other ions. Although the two processes are different (Figure 3.1), the phenomenological expression is the same.

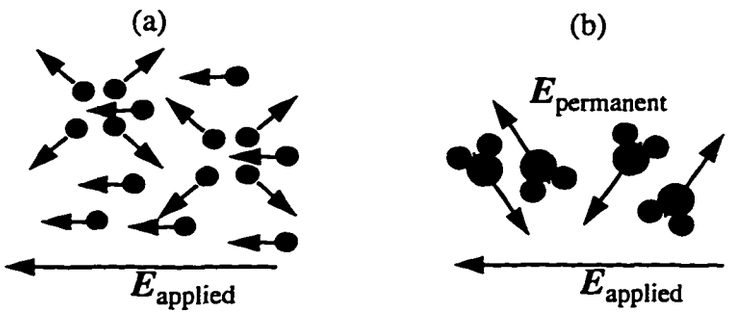

Figure 3.1 The two major microscopic processes that cause the relaxation phenomena. (a) - The transport and collisions of free ions. (b) - The alignment of the permanent dipole moment of a polar molecule.

The generalized relative permittivity of this medium can be expressed by considering a time-harmonic excitation of fields [31]-[33]:

$$\varepsilon_r(\omega) = \varepsilon_\infty + \frac{\varepsilon_s - \varepsilon_\infty}{1 + j\omega\tau_0} \tag{3.4}$$

In the ionic transport process, the relaxation time constant is usually larger than 0.1 ns.

3.2.2 Resonance phenomena

Resonance phenomena are caused by the oscillation of electrons and nuclei subject to an applied field [39]. Both oscillate in space around their equilibrium position. The kinetic energy dissipated in this process is detectable in the form of heat. The energy is totally supplied by the electric field.

This process is also simple to describe qualitatively. In the resonance region, the medium behaves as a very high permittivity dielectric. In the high frequency region, the medium behaves like the vacuum.

This phenomenon is common in all materials. In a single atom, the process is caused by the oscillation of the nucleus and the electrons around their equilibrium position, Figure 3.2. The motion of the nuclei is much smaller compared to the motion of the electrons.

Lorentz was the first to study such phenomena when developing the theory of the electron [58]. This kind of resonant material is called a second-order Lorentz material. The polarization density equation of such a medium is:

$$\mathbf{P} + \delta_0 \frac{d\mathbf{P}}{dt} + \frac{d^2\mathbf{P}}{dt^2} = \omega_0^2 (\varepsilon_s - 1)\,\mathbf{E} + (\varepsilon_\infty - 1)\,\delta_0 \frac{d\mathbf{E}}{dt} + (\varepsilon_\infty - 1)\frac{d^2\mathbf{E}}{dt^2} \tag{3.5}$$

where ω_0 is the resonant frequency, δ_0 is the loss factor of the medium, ε_∞ is the permittivity at infinite frequency, and ε_s is the static permittivity.

The polarization can be understood as a displacement of the electron and nucleus around their equilibrium positions. If the applied field is not DC, the nucleus and the electron will tend to oscillate around their equilibrium positions. At higher frequencies, the motion is limited by inertia.

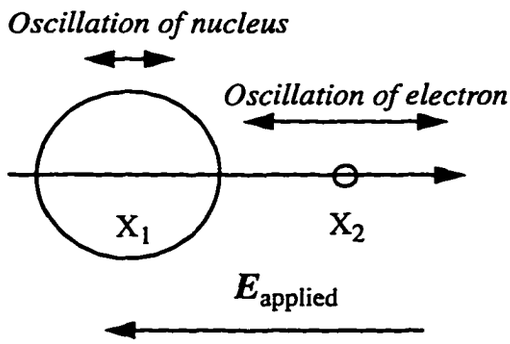

Figure 3.2 Microscopic process that causes resonance. The time varying applied electric field causes an oscillation of the position of nucleus and electron. At the resonant frequency the medium absorbs all applied energy.

The generalized relative permittivity of a second-order Lorentz medium is [31]-[33]:

$$\varepsilon_r(\omega) = \varepsilon_\infty + \frac{(\varepsilon_s - 1)\,\omega_0^2}{\omega_0^2 + j\omega\delta_0 - \omega^2} \tag{3.6}$$

3.2.3 Anisotropic materials

In an isotropic medium, the polarization density is in parallel to the electric field, and so is the magnetization density to the magnetic field [39]. This kind of medium has a random spatial distribution of molecules. In this case there are no symmetry axes, and the propagation vector is the same for all directions.

Due to the anisotropy of the crystal structure ([50]-[52], [59]), the relationship between the field vector E and the polarization density P is no longer independent of the direction but becomes a tensor equation of the form:

$$\begin{aligned} P_x &= g(E_x, E_y, E_z) \\ P_y &= h(E_x, E_y, E_z) \\ P_z &= r(E_x, E_y, E_z) \end{aligned} \tag{3.7}$$

In the limit of the linear approximation, this relationship can be simplified by expressing the general functions g, h, and r by a Taylor series and neglecting the higher-order terms:

$$\begin{aligned} P_x &= E_x\frac{dP_x}{dE_x} + E_y\frac{dP_x}{dE_y} + E_z\frac{dP_x}{dE_z} \\ P_y &= E_x\frac{dP_y}{dE_x} + E_y\frac{dP_y}{dE_y} + E_z\frac{dP_y}{dE_z} \\ P_z &= E_x\frac{dP_z}{dE_x} + E_y\frac{dP_z}{dE_y} + E_z\frac{dP_z}{dE_z} \end{aligned} \tag{3.8}$$

All the partial derivatives can be grouped into the susceptibility tensor, and the relation becomes simply:

$$[\mathbf{P}] = [\chi]\,[\mathbf{E}] \tag{3.9}$$

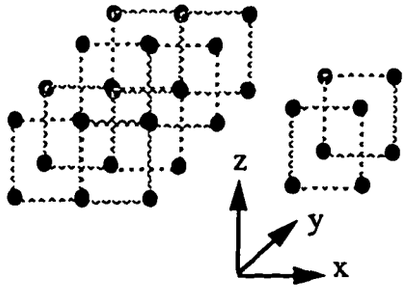

Figure 3.3 Crystalline atomic structure. The polarizability is the same along the x, y and z axis. However, it is different along the diagonal directions.

The relationship between the susceptibility and permittivity tensor is:

$$[\chi] = [\varepsilon] - [U] = \begin{bmatrix} \varepsilon_{xx} - 1 & \varepsilon_{xy} & \varepsilon_{xz} \\ \varepsilon_{yx} & \varepsilon_{yy} - 1 & \varepsilon_{yz} \\ \varepsilon_{zx} & \varepsilon_{zy} & \varepsilon_{zz} - 1 \end{bmatrix} \tag{3.10}$$

where [U] is the unitary matrix.

3.2.4 Magnetic interactions

The interaction of a medium with magnetic fields is different from the electric field case. Magnetic materials can be classified as diamagnetic, paramagnetic or ferromagnetic depending on the interaction with the field. A diamagnetic substance is repelled by magnetic fields. A paramagnetic substance has the opposite behavior. Most materials are either diamagnetic or paramagnetic. These are weak interactions. Ferromagnetism behaves in the same way as paramagnetism. The difference between the two cases is the strength of the interaction. Ferromagnetic materials are strongly attracted to magnetic fields.

In diamagnetic substances there are no permanent magnetic moments. The applied magnetic field induces extra currents in the atoms. These currents are in such direction as to oppose the increasing field. Therefore, the induced magnetic moments are directed opposite to the magnetic field. In the case of a gas with n atoms, the magnetization vector can be expressed as:

$$\mathbf{M} = n\langle\mu\rangle = \frac{ne}{2m}\langle\mathbf{L}\rangle - \frac{ne^2\langle R^2\rangle}{4m}\mathbf{B} \tag{3.11}$$

where n is the number of atoms in the gas, e is the electric charge, $\langle R^2\rangle$ is the mean classical radius of the hydrogen atom, $\langle\mathbf{L}\rangle$ is the mean orbital angular moment of the atoms, **B** is the applied magnetic field, $\langle\mu\rangle$ is the mean magnetic moment of the sample and m is the mass of the electron.

In a medium with no permanent magnetic moments, $\langle\mathbf{L}\rangle$ is zero (all orientations are equally probable). Therefore, the magnetic susceptibility is given by the factor multiplying **B** in (3.11). This is the cause of the diamagnetic effect.

However, in substances with permanent magnetic moment, there is also, besides of the diamagnetic effect, the lining up of the individual magnetic moments. The induced

magnetic moments tend to enhance the magnetic field. In these paramagnetic materials the interaction is caused by the total angular momentum of the atom. The momentum is composed by and orbital and a spin paramagnetic components.

$$\mathbf{J} = \langle \mathbf{L} + \mathbf{S} \rangle \tag{3.12}$$

where **J** is the total angular moment and <**L+S**> is the mean value of the contributions of the orbital (**L**) and spin (**S**) paramagnetic components. The magnetic moment is expressed as:

$$\mu = \gamma \mathbf{J} = -g\frac{e}{2m}\mathbf{J} \tag{3.13}$$

where γ is the gyromagnetic ratio, e is the charge of the electron, m is the mass of the electron and g is the Lande g-factor which depends of the state of the atom (1 for pure orbital moment and 2 for pure spin moment and some number is between for complex atomic systems).

Since the magnetic moment is proportional to the angular moment, an atomic system placed in a magnetic field will precess. The system experiences a torque τ which tries to align μ with the applied magnetic field. However, since the system is essentially a gyroscope, the torque will not cause the moment to align with the field. Instead the system will precess about an axis parallel to the applied field. The precession angular frequency is:

$$\omega_p = g\frac{eB}{2m} = g\omega_L \tag{3.14}$$

ω_L is called the Larmor frequency.

Ferromagnetism is much stronger than paramagnetism. This interaction is related to the tendency of nearby spins of an atom to line up in one direction. This has to do with quantum mechanics and the Pauli exclusion principle. However, some of the ferromagnetic effects (as ferromagnetic resonance) can be studied as paramagnetic interactions as long as a demagnetization factor is included. This factor is related to the shape of the medium sample. Ferromagnetism is the reason for gyromagnetic phenomena.

This relationship is described in the next section.

3.2.5 Gyromagnetic phenomena

A gyromagnetic material presents different propagation characteristics for waves with polarization directions. In a gyromagnetic material, clockwise and counter-clockwise polarized waves behave differently, Figure 3.4. The explanation for this behavior is the ferromagnetic resonance of the sample.

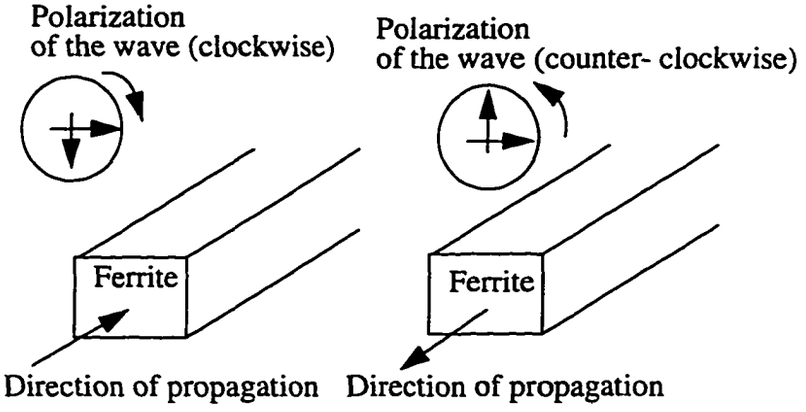

Figure 3.4 Propagation of circularly polarized waves in a ferrite medium. The clockwise and counter-clockwise waves will have different propagation constants.

The effect can be described as classical magnetic resonance. Applying a magnetic field to an atomic system shown in Figure 3.5 causes a torque in the system:

$$\tau = \frac{dJ}{dt} = \gamma(J \times B) \tag{3.15}$$

The magnetic resonance described by the torque equation (3.15) is the cause of the gyromagnetic effect [39], [7].

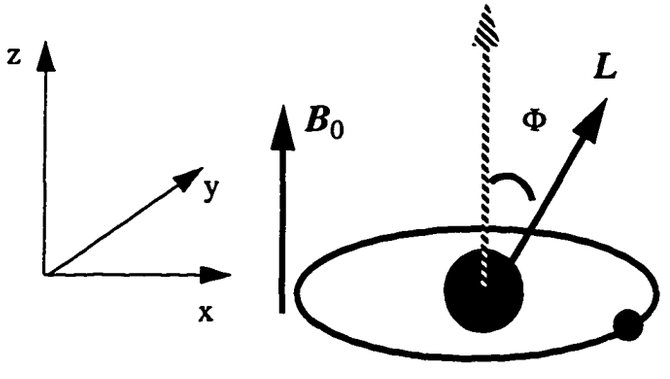

Figure 3.5 Classical magnetic resonance. The angular moment L tends to align with the applied magnetic field. The nutational frequency is determined by the applied field.

In the case of Figure 3.5, **B** is composed of a static component $\mathbf{B}_0$ and a sinusoidally varying component $\mathbf{B}_t$. The time-varying component B_t is a constant rotating vector in the xy plane and $\mathbf{B}_0$ lies along the z axis. The magnetic dipole axis precesses around $\mathbf{B}_0$ in synchronism with $\mathbf{B}_t$. The angle of precession depends on whether the rotation is clockwise or counter-clockwise.

The precession angle in the counter-clockwise rotation case is:

$$\Phi = \operatorname{asin}\left[\frac{\gamma B_t}{\sqrt{(\gamma B_0 + \omega)^2 + (\gamma B_t)^2}}\right] \tag{3.16}$$

In the clockwise case, the angle is:

$$\Phi = \operatorname{asin}\left[\frac{\gamma B_t}{\sqrt{(\gamma B_0 - \omega)^2 + (\gamma B_t)^2}}\right] \tag{3.17}$$

Since the precession angle is different for the two cases, the effective permeability for the clockwise and counter-clockwise waves is also different. This constitutes the gyromagnetic effect. As explained in the previous section, the mechanism of ferromagnetism is different from that of paramagnetism. However, ferromagnetic resonances can be adequately expressed using paramagnetic classic theory and appropriate demagnetization factors.

$$\frac{d\mathbf{M}}{dt} = \gamma \mathbf{M} \times (\mathbf{B} - \mu_0 \mathbf{N} \cdot \mathbf{M}) \tag{3.18}$$

where **N** is the demagnetization factor. In practice, the static field is directed along a particular direction and is large enough to saturate the sample. Therefore, the magnetization density of a gyromagnetic material can be expressed by [39], [60]:

$$\frac{d\mathbf{M}}{dt} = \gamma \mathbf{M} \times \mathbf{B} \tag{3.19}$$

Under a strong applied field in the z direction, (3.19) is usually linearized

$$\begin{aligned} \frac{dm_x}{dt} &= \gamma(m_y B_0 - M_s b_y) & \frac{dm_z}{dt} &= -\gamma(m_x B_0 - M_s b_x) \\ B_z &= B_0 + b_z \approx B_0 & M_z &= M_s + m_z \approx M_s \end{aligned} \tag{3.20}$$

where B_0 is proportional to the saturation magnetic field, M_s is the saturation magnetiza-

tion.

3.2.6 Nonlinear phenomena

The nonlinear effect is present in all processes described above. These processes are linear in the low field approximation [39], [40], [11]. The nonlinear effect is not negligible under high fields. However, in certain conduction processes, the nonlinear effect can be dominant. In semiconductors under high fields, the drift and diffusion of carriers is nonlinear. A plasma under high fields exhibits nonlinear behavior. In the optical frequency range, certain nonlinear effects can be used to compensate for dispersive propagation.

The expression of the nonlinear effect is strongly dependent on the material and effect under study. Therefore, only a simple example of non-linear polarization is presented.

In most cases, the nonlinear behavior is expressed by nonlinear correction terms to the medium polarization equation [39]. Since in most media, the inversion (change of sign) of the electric field causes also an inversion of the polarization, the lowest-order nonlinear phenomenon results in a cubic correction term.

The expression for the nonlinear polarization density of a second-order Lorentz dielectric is [39]:

$$\frac{d^2\mathbf{P}}{dt^2} + \omega_0^2\mathbf{P} + \alpha\mathbf{P}^3 = \omega_p^2\mathbf{E} \tag{3.21}$$

where α is the nonlinear coupling factor. In most materials this factor is negligible. The nonlinear effect becomes only noticeable at high fields.

3.3 Modeling of general media in two-dimensional TLM

In the basic TLM formulation, the medium is modeled by stubs connected to the node [2]. This method is robust and efficient when these parameters are constants. However, when the material constitutive relationships are frequency dispersive and nonlinear, the model is inaccurate.

The representation of general constitutive relationships requires a modification of the medium modeling technique. The stubs can be used to model simple nonlinear relations [16], but are not suitable for representing frequency dispersive media.

In this section, two different approaches to this problem are proposed. Both techniques introduce modifications to the scattering matrix of TLM and the inclusion of a source term into the procedure. This term depends on previous values of node voltage and/or current.

The first technique is the modified scattering matrix approach. In this method, stubs are used, but the storage of previous values of the incident and reflected voltages is required in order to account for the dispersive nature of the medium. The storage is represented by a source term. The method can also be used to model nonlinear media. In this method the scattering matrix is transformed according to the medium being simulated.

The second is the nodal source approach. Here the stubs are replaced by an equivalent source connected to the node. The source is described in terms of the polarization or magnetization densities of the medium. In this method the scattering matrix is independent of the medium and the source term represents the interaction of electromagnetic fields with the medium.

3.3.1 Modified scattering matrix approach

This approach maintains the stub-loaded description of the medium. It is based on representing recursively the interaction of the frequency dependent (therefore also time dependent) stub admittance with the incident voltages at the stub as the simulation progresses. In a frequency dependent material, the initial stub admittance value is proportional to the medium constant at infinite-frequency. As the simulation time tends to infinity, the stub approaches the DC value of the medium parameter (Figure 3.6) [39].

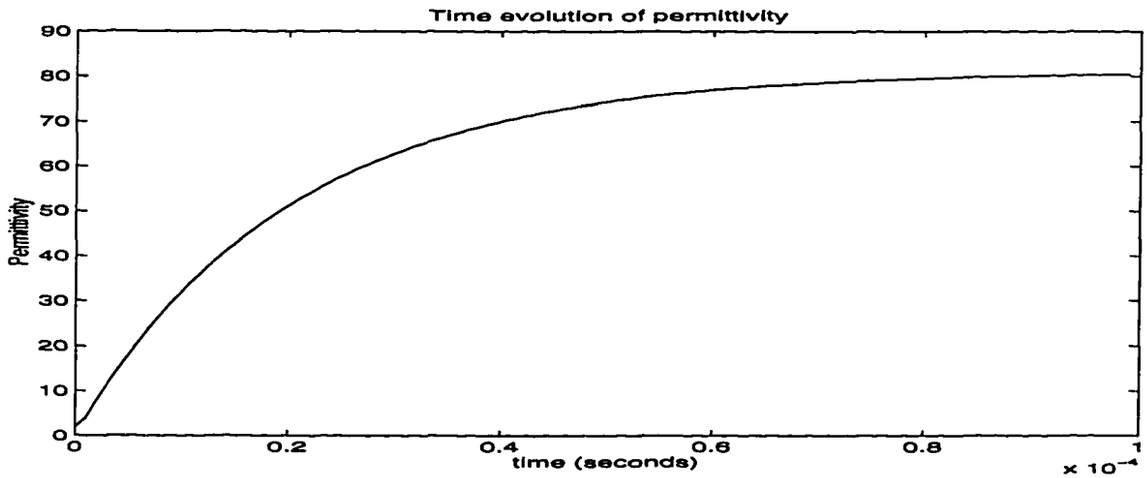

Figure 3.6 Impulse response of the relative permittivity in a first order Debye medium.

The complete description of this evolution requires the storage of previous values of the incident and reflected voltages at the stub. The number of stored voltages depends on the medium equation. In the case of a trapezoidal discretization scheme, a first-order Debye medium requires only one past value (incident and reflected), while a second-order Lorentz material requires two.

The evolution of the stub value is also dependent on the way the constitutive equation is represented in the procedure. The equations can be incorporated into the procedure using direct discretization or convolution [53]-[57]. In this thesis the convolution approach is described. The voltages incident and reflected on the stub are convolved with the impulse response of the medium. This is done recursively to minimize the storage of voltages.

The general form of the modified matrix approach is:

$$[v(k)]^r = [S]\,[v(k)]^i + \sum_{n=0}^{k} [H(n)]\,[v(n-k)]_{stubs} \tag{3.22}$$

where [H(n)[is the convolution term and [S] is the modified scattering matrix. Without loss of generality (3.22) can be expressed as:

$$_k[v]^r = [S]_k[v]^i + [J_s] \tag{3.23}$$

The technique can be illustrated by an example of a shunt node mesh modeling a first-order Debye dielectric. The resulting modified scattering matrix equation, obtained using recursive convolution is:

$$\begin{bmatrix} v_1 \\ v_2 \\ v_3 \\ v_4 \\ v_5 \end{bmatrix}_k^r = \frac{1}{y+4} \begin{bmatrix} -(2+y) & 2 & 2 & 2 & 2y \\ 2 & -(2+y) & 2 & 2 & 2y \\ 2 & 2 & -(2+y) & 2 & 2y \\ 2 & 2 & 2 & -(2+y) & 2y \\ 2 & 2 & 2 & 2 & y-4 \end{bmatrix} \begin{bmatrix} v_1 \\ v_2 \\ v_3 \\ v_4 \\ v_5 \end{bmatrix}_k^i + \frac{e^{-\frac{\Delta t}{\tau_0}}}{y+4} \begin{bmatrix} J \\ J \\ J \\ J \\ J \end{bmatrix}_{k-1} \tag{3.24}$$

$$y = 4(\varepsilon_d - 1)$$

$$\varepsilon_d = \varepsilon_s + (\varepsilon_s - \varepsilon_\infty)\, e^{-\frac{\Delta t}{\tau_0}} \qquad {}_kJ = (\varepsilon_d - \varepsilon_s)\,(v_5^i - v_5^r)_k + e^{-\frac{\Delta t}{\tau_0}}\, {}_{k-1}J$$

where Δt is the timestep. The incident and reflected voltages are shown in Figure 3.7.

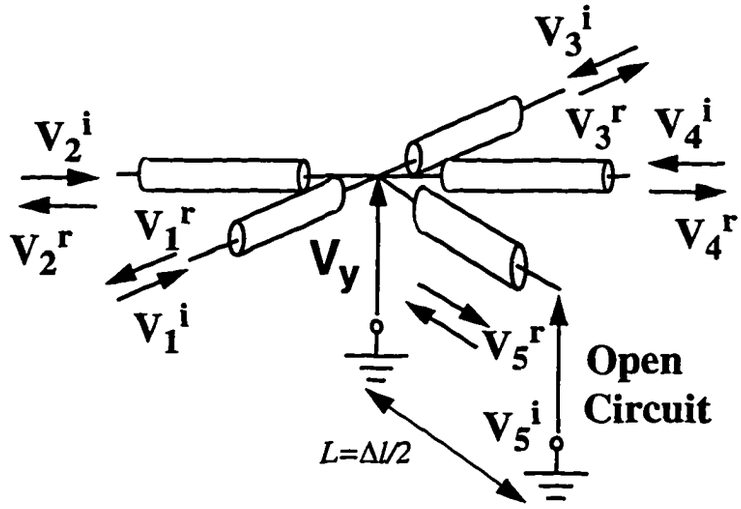

Figure 3.7 Representation of dielectric material in the shunt node. The two-dimensional shunt node is stub-loaded. In the modified matrix approach, the value of the stub admittance is frequency dependent. The length of the stub is $\Delta l/2$.

The modified scattering matrix technique has several advantages. The approach is efficient because of the short convolution. The storage is dependent on the order of the medium [53]. A second-order material needs two past values of the incident and reflected voltage at the stub.

The nonlinear effect can be incorporated with a Volterra series [11], [44]. This series is composed of the linear part and higher order correction terms. This is a very attractive feature in the modeling of certain optical nonlinearities, since they are described in this form [44].

The main disadvantage of the modified scattering matrix approach is the lack of generality. Although the source term is responsible for the storage of previous incident and reflected voltages at the stub, the scattering matrix needs to be modified according to the medium being modeled. Each dispersive or nonlinear behavior needs a different scattering matrix and correction terms.

This problem could be partially solved by using a library of node scattering matrices in a simulator. However, this is not practical. The TLM method is a general electromagnetic simulation technique, and this approach restricts its use. This disadvantage led to the development of the nodal source technique.

3.3.2 The nodal source approach

This approach does not use the stub model of dielectric and magnetic behavior. The medium is represented by a source connected to the node (Figure 3.8). The scattering matrix of the node is independent of the medium. The source is defined by the constitutive relationships of the material. The source can be represented by a lumped circuit connected to the node [61].

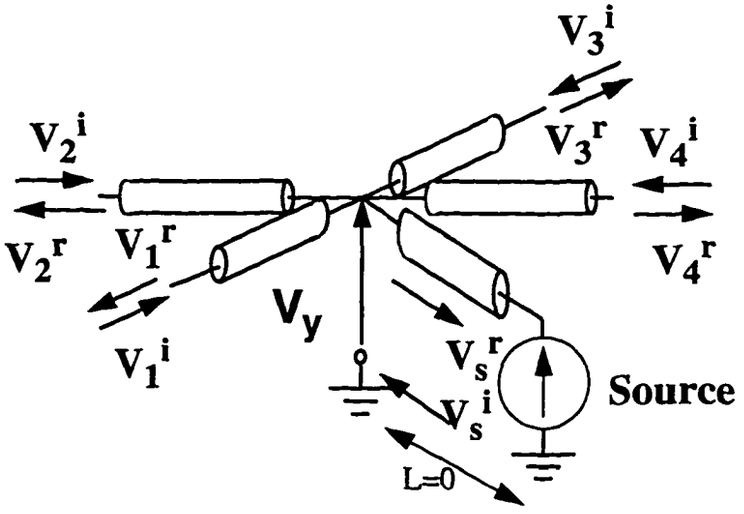

Figure 3.8 Representation of dielectric material in the shunt node. The node is connected to a nodal source representing the dielectric. The length L of the link line connecting the source to the node is infinitesimal. This line has a normalized admittance Y_r of four.

The source is connected to the node by a transmission line. In the shunt node case, this link line has a normalized characteristic admittance Y_r of four. The normalization is performed with respect to the admittance of the mesh link lines. In the series case, the link line has a normalized impedance Z_r of four (also with respect to the mesh link lines). This value is chosen to decouple the scattering matrix from the source [61].

The nodal source representation of a dispersive dielectric also requires the storage of past values of incident and reflected voltages on the link line. However, the source approach simplifies the solution of the constitutive equations. These equations are solved with circuit techniques at each timestep [12].

The circuit is defined by the constitutive relationships and the Thevenin or Norton equivalent of the node. In the shunt node case, the Norton equivalent of the node is used.

The solution of the circuit yields the total voltage at the node. In the series case, the Thevenin equivalent is used. The solution in this case is the total current at the node.

The general formulation of the nodal source approach is:

$$[\mathbf{v}]^r = [\mathbf{S}]\,[\mathbf{v}]^i + [\mathbf{J}_s] \tag{3.25}$$

where [S] is the medium independent scattering matrix, and $[\mathbf{J}_s]$ is the source vector. All rows of the source vector are linear combinations of the source function G, which is obtained from the constitutive equations.

The use of the equivalent circuit of the node simplifies the implementation of a Debye medium (3.4). In the shunt node case:

$$\begin{aligned} \mathbf{v}_n^r &= \mathbf{v} - \mathbf{v}_n^i \\ \mathbf{v} &= G\,(\mathbf{v}_1^i + \mathbf{v}_2^i + \mathbf{v}_3^i + \mathbf{v}_4^i) \end{aligned} \tag{3.26}$$

where $G(\mathbf{v}_1^i + \mathbf{v}_2^i + \mathbf{v}_3^i + \mathbf{v}_4^i)$ is the source function, n=1...4. The source function G is defined by the constitutive equations of the medium. It can usually be represented by a circuit network. In fact for most passive media, the nodal source is modeled by a passive network. The relationship described in (3.26) is solved with circuit techniques.

The network is driven by the current i and voltage v of the node. The current and voltage are defined as:

$$\begin{aligned} \mathbf{v} &= \mathbf{v}_s^r + \mathbf{v}_s^i \\ \mathbf{i} &= Y_r\,(\mathbf{v}_s^r - \mathbf{v}_s^i) \end{aligned} \tag{3.27}$$

where v^r_s and v^i_s are the reflected and incident voltages from the node seen from the nodal source (Figure 3.8). Since the incident voltage v^i_s is unknown, both current and voltage are also unknown. Therefore an equivalent circuit is used to represent the node. The transformation of the node into the equivalent circuit for the shunt node is show in Figure 3.9.

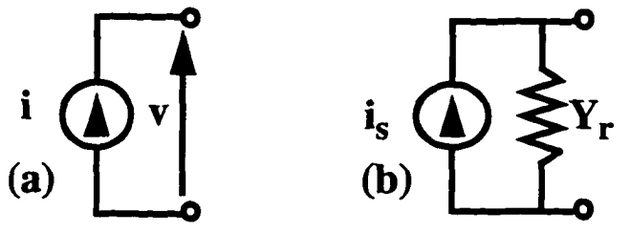

Figure 3.9 TLM node seen from the nodal source. (a) Current i and voltage v seen from the nodal source. (b) Equivalent Norton transformation with the same current and voltage. The equivalent circuit is composed by current source i_s and an admittance Y_r

The equivalent circuit transformation of the node is used to solve the circuit network that represents the medium relationship. The network is driven by a current source i_s with a equivalent admittance of Y_r. This network is solved at each timestep

The main advantage of the nodal source approach is the generality. Once the constitutive relationship is described as a circuit network, the solution procedure is straightforward. The solution procedure is not dependent on the topology of the circuit.

There is a physical interpretation to the nodal source. The source is analogous to the polarization/magnetization of the medium [39]. The electric/magnetic flux density is composed of the sum of a free space electric and a polarization/magnetization field. In this approach, the medium independent node represents the free-space part and the source represents the polarization/magnetization densities field.

Since the nodal source approach is more general than the modified scattering matrix technique, it has been chosen as the main approach to representing general constitutive relationships.

3.3.3 Nodal source in the shunt node case

In this case, the nodal source current is proportional to the derivative of the polarization of the medium. The topology of the source network is obtained from the constitutive equations [39]. The final network is obtained by connecting the source circuit with the Norton equivalent circuit for the node. In Figure 3.10, the topology of the circuit network of a generic active medium is shown. The network is connected to a TLM shunt node represented by the Norton equivalent for the node (the source i_s and shunt admit-

tance Y_r)

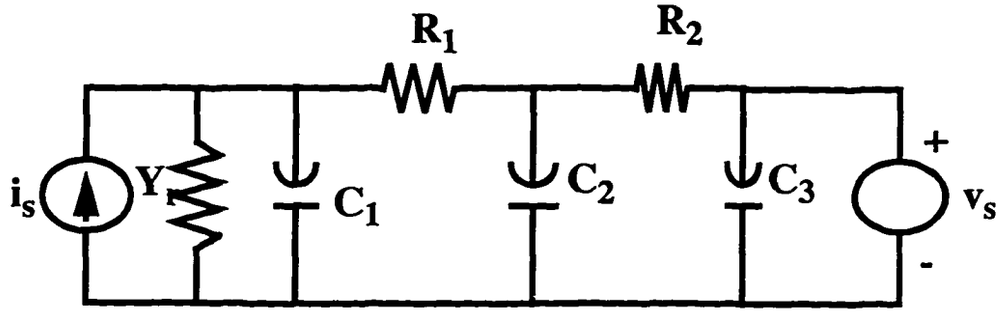

Figure 3.10 Topology of a generic nodal source and the equivalent node circuit. The resulting network is solved using circuit techniques. The admittance Y_r (normalized with respect to the admittance Y_0) is four. The elements R_1, R_2, C_1,C_2, C_3 and v_s are arbitrary.

The polarization current is:

$$i_{pol} = (2\frac{Y_0 \Delta l}{c})\frac{dp}{dt} \tag{3.28}$$

where p is the polarization density of the medium, Y_0 is the admittance of the mesh link lines. This current is responsible for the change of the total current flowing through a shunt node when a dielectric material is present (Appendix A).

The incident and reflected voltages at the line connecting node to source are decoupled [61]. The voltage reflected from the node towards the source is calculated with:

$$v_s^r = \frac{1}{4}(v_1^i + v_2^i + v_3^i + v_4^i) \tag{3.29}$$

The equivalent circuit of the shunt node seen from the nodal source yields:

$$i_s - Y_r v = 2Y_r v_s^r - Y_r v = i \tag{3.30}$$

The normalized admittance of the link line Y_r is equal to four. The Kirchoff law of current (KCL) specifies that the total current is [12]:

$$i = i_{pol} \tag{3.31}$$

The resulting network is defined by the polarization equation and the connection equation:

$$p = g(v) \tag{3.32}$$

$$2Y_r v_s^r = (2\frac{Y_0 \Delta l}{c})\frac{dp}{dt} + Y_r v \tag{3.33}$$

The voltages reflected from the node are obtained from the total voltage V by:

$$\begin{aligned} v_n^r &= v - v_n^r \\ n &= 1 \ldots 4 \end{aligned} \tag{3.34}$$

The topology of the final network is obtained from the polarization equation (3.32). For instance a first-order Debye dielectric results in the source network shown in Figure 3.11.

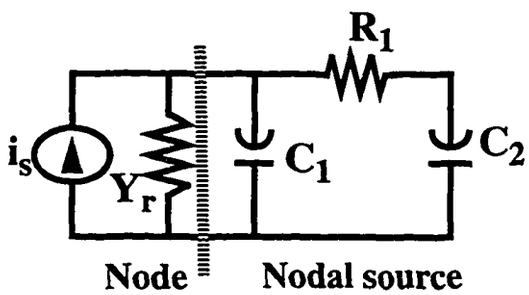

Figure 3.11 Topology of the nodal source network for the first order Debye dielectric. Since this medium is not active, only passive elements compose the network. In this particular case:

$$C_1 = 2\Delta t(\varepsilon_\infty - 1) \qquad C_2 = 2\Delta t(\varepsilon_s - \varepsilon_\infty) \qquad R = \tau_0 / 2\Delta t(\varepsilon_s - \varepsilon_\infty)$$

The resulting topology can be solved using circuit simulation techniques.

3.3.4 Nodal Source in the series node case

The analysis of the nodal source in the series case is the dual of the shunt case. The current and voltage at the node are represented by a Thevenin equivalent circuit. The voltage source is proportional to the derivative of the magnetization of the medium. The topology of the source circuit is obtained from the magnetization equation. The node equivalent is a Thevenin circuit. The final network topology is obtained by connecting the Thevenin equivalent of the node to the source circuit.

The magnetization voltage is equal to:

$$v_{mag} = (2\frac{Z_0 \Delta l}{c})\frac{dm}{dt} \tag{3.35}$$

where m is the magnetization density of the medium. This relationship (3.35) is obtained applying the same methodology described in Appendix A to the series node.

The voltage reflected from the node towards the source is calculated with:

$$v^r = (-v_1^i + v_2^i + v_3^i - v_4^i) \tag{3.36}$$

The equivalent circuit of the series node seen from the nodal source yields:

$$2Z_r v^r - Z_r i = v \tag{3.37}$$

The normalized impedance of the link line Z_r is equal to four. This value is chosen to decouple the incident and reflected voltage pulses at the network input port. The impedance is normalized with respect to the impedances of the lines connecting the nodes. The Kirchoff law of voltage (KCV) specifies that the total voltage in a closed loop is zero [12]:

$$v = v_{mag} \tag{3.38}$$

The resulting network is defined by the magnetization equation and the connection equation:

$$m = h(i) \tag{3.39}$$

$$2Z_r v^r = (2\frac{Z_0 \Delta l}{c})\frac{dm}{dt} + Z_r i \tag{3.40}$$

where h(i) is the relationship between the magnetization and the current flowing through the network. This relationship is obtained from the constitutive equations.

The voltages reflected at the nodes are obtained from the current using:

$$\begin{gathered} v_n^r = Z_r i + v_n^i \\ n = 1 \ldots 4 \end{gathered} \tag{3.41}$$

The topology of the final network is obtained from the magnetization equation (3.39).

The three-dimensional TLM node equipped with nodal sources is assembled from the decoupled series and shunt nodes.

3.4 Nodal sources in the three-dimensional case

The representation of general constitutive relationships in three dimensions is more complex than the two-dimensional case. In the most difficult case, the medium couples both magnetic and electric fields and present nonlinear and dispersive effects.

In this section the modeling of the interaction of the medium with the electromagnetic field in three-dimensional TLM is presented.

The expansion from the two-dimensional model of general constitutive equations to three dimensions is performed using the decoupled series and shunt nodes. The three-dimensional node is a combination of the nodes presented in the previous sections.

The analysis presented here is performed for the symmetrical condensed node. However, different kinds of nodes can be obtained by combining the two-dimensional nodes.

The interaction between field and medium is modeled by nodal sources. The sources are defined by the constitutive equation. The resulting scattering matrix is independent of the medium even in the case of anisotropic media. The sources act upon all field components simultaneously.

3.4.1 Assembling the three-dimensional node

The symmetrical condensed node (SCN) is composed by combining of series and shunt nodes, as presented in Figure 3.12.

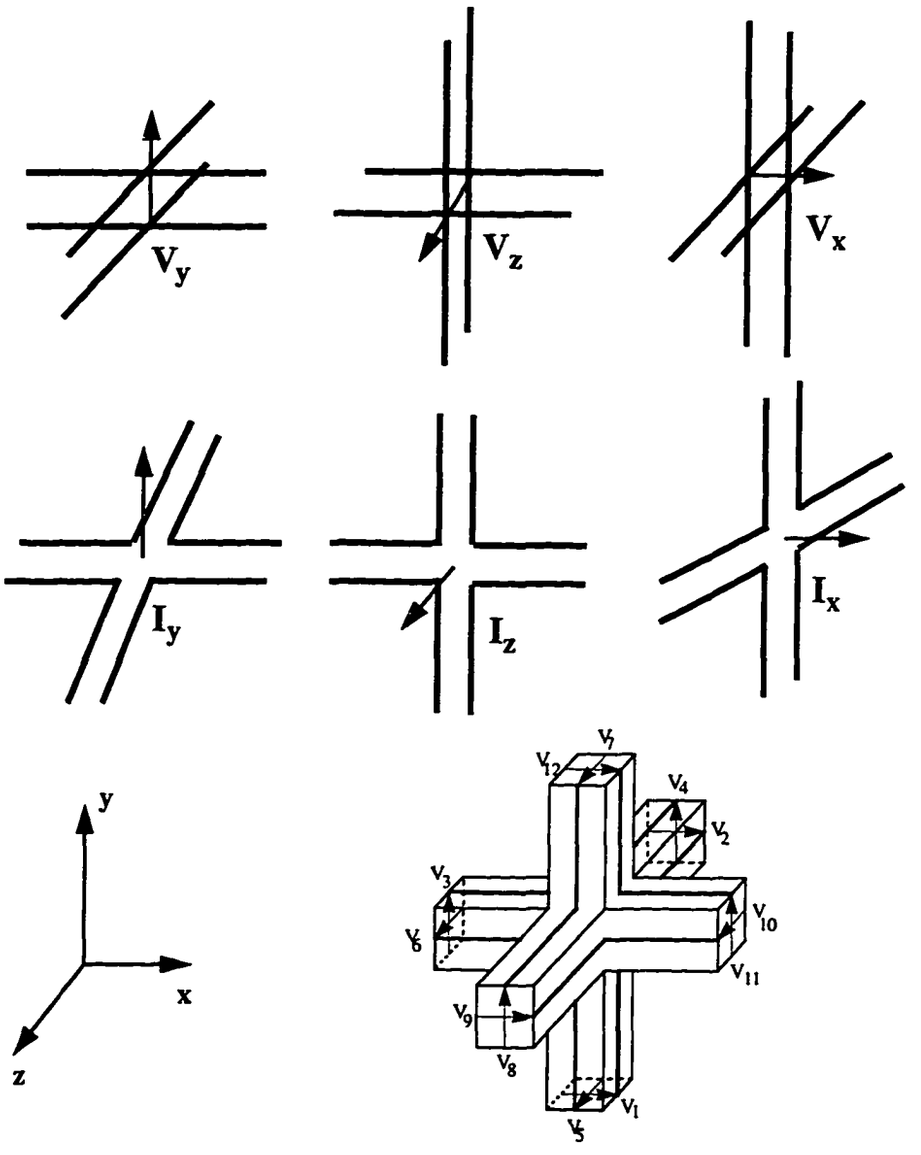

Figure 3.12 Assembling the three-dimensional node from two-dimensional shunt and series nodes. Each u-directed node (u=x,y,z) represents a field component in the u-direction (normal to the plane of the node).

The main equations that define the SCN in terms of the voltages in the shunt nodes and currents in the series nodes are [34]:

$$
\begin{aligned}
v_1^r &= v_x(t) - Z_0 i_z(t) - v_{12}^i & v_7^r &= v_z(t) - Z_0 i_x(t) - v_5^i \\
v_2^r &= v_x(t) + Z_0 i_y(t) - v_9^i & v_8^r &= v_y(t) + Z_0 i_x(t) - v_4^i \\
v_3^r &= v_y(t) + Z_0 i_z(t) - v_{11}^i & v_9^r &= v_x(t) - Z_0 i_y(t) - v_2^i \\
v_4^r &= v_y(t) - Z_0 i_x(t) - v_8^i & v_{10}^r &= v_z(t) + Z_0 i_y(t) - v_6^i \\
v_5^r &= v_z(t) + Z_0 i_x(t) - v_7^i(t) & v_{11}^r &= v_y(t) - Z_0 i_z(t) - v_3^i \\
v_6^r &= v_z(t) - Z_0 i_y(t) - v_{10}^i & v_{12}^r &= v_x(t) + Z_0 i_z(t) - v_1^i
\end{aligned}
\tag{3.42}
$$

where the voltages and currents are shown in Figure 3.12 and Z_0 is the impedance of the lines connecting the nodes (377.76 Ω).

These voltages and currents are calculated with nodal sources and equivalent node circuits. The Norton equivalent is used in the shunt case and the Thevenin equivalent in the series case. The source equations are:

$$
\begin{aligned}
v_{ex}^r &= \frac{1}{4}(v_1^i + v_2^i + v_9^i + v_{12}^i) \\
v_{ey}^r &= \frac{1}{4}(v_3^i + v_4^i + v_8^i + v_{11}^i) \\
v_{ez}^r &= \frac{1}{4}(v_5^i + v_6^i + v_7^i + v_{10}^i)
\end{aligned}
\tag{3.43}
$$

$$
\begin{aligned}
v_{mx}^r &= (v_4^i - v_5^i + v_7^i - v_8^i) \\
v_{my}^r &= (v_6^i - v_2^i + v_9^i - v_{10}^i) \\
v_{mz}^r &= (v_1^i - v_3^i - v_{12}^i + v_{11}^i)
\end{aligned}
\tag{3.44}
$$

where v_{eu}^r (u=x,y,z) is the voltage reflected from the u-directed shunt node (incident on the u-directed shunt nodal source), and v_{mu}^r (u=x,y,z) is the voltage reflected from the u-directed series node (incident on the u-directed series nodal source).

where the constitutive relationships are dependent on all currents and voltages at the node:

$$
\begin{aligned}
p_x &= p_x(v_x, v_y, v_z, i_x, i_y, i_z) \\
p_y &= p_x(v_x, v_y, v_z, i_x, i_y, i_z) \\
p_z &= p_x(v_x, v_y, v_z, i_x, i_y, i_z) \\
m_x &= m_x(v_x, v_y, v_z, i_x, i_y, i_z) \\
m_y &= m_y(v_x, v_y, v_z, i_x, i_y, i_z) \\
m_z &= m_z(v_x, v_y, v_z, i_x, i_y, i_z)
\end{aligned}
\tag{3.45}
$$

The relationship between the reflected voltages ((3.43)-(3.44)) and the constitutive equations (3.45)is:

$$
\begin{aligned}
i_{sx}(t) &= 2Y_r v^r_{ex}(t) = 8v^r_{ex}(t) = \frac{2\Delta l}{c}\frac{d}{dt}p_x(t) + 4v_x(t) \\
i_{sy}(t) &= 2Y_r v^r_{ey}(t) = 8v^r_{ey}(t) = \frac{2\Delta l}{c}\frac{d}{dt}p_y(t) + 4v_y(t) \\
i_{sz}(t) &= 2Y_r v^r_{ez}(t) = 8v^r_{ez}(t) = \frac{2\Delta l}{c}\frac{d}{dt}p_z(t) + 4v_z(t) \\
v_{sx}(t) &= 2Z_r v^r_{mx}(t) = 8v^r_{mx}(t) = \frac{2\Delta l}{c}\frac{d}{dt}m_x(t) + 4i_x(t) \\
v_{sy}(t) &= 2Z_r v^r_{my}(t) = 8v^r_{my}(t) = \frac{2\Delta l}{c}\frac{d}{dt}m_y(t) + 4i_y(t) \\
v_{sz}(t) &= 2Z_r v^r_{mz}(t) = 8v^r_{mz}(t) = \frac{2\Delta l}{c}\frac{d}{dt}m_z(t) + 4i_z(t)
\end{aligned}
\tag{3.46}
$$

The interpretation of the nodal source approach in the three-dimensional case is the same as in the two-dimensional case. The nodal sources represent the polarization and magnetization of the medium. As in the two-dimensional case the total current and voltages at the node can be obtained using circuit techniques.

Other kinds of TLM nodes can be assembled using this representation. One node of particular interest is the hybrid node [62]. The node can be used in mesh grading techniques. In this work, only the symmetrical condensed node was studied, since only the uniform mesh was used in the validation of the technique.

3.5 Conclusions

In this chapter the modeling of general constitutive relationships was presented for both two- and three-dimensional cases.

This chapter also contains a brief review of the most important interactions between the electromagnetic field and the medium. These interactions are described by the constitutive relationship of the medium. The main phenomena described here were relaxation, resonance, anisotropy, gyromagnetism and nonlinear behavior.

Each of these interactions are caused by different processes. The relaxation is associated with the orientation of the permanent dipole moment molecules with the field, and with ionic transport. The resonance is caused by the oscillation of the atoms around their equilibrium positions. Anisotropy is caused by asymmetry in the arrangement of atoms or molecules. Nonlinear phenomena are present in all cases, but becomes critical only at high fields.

In the two-dimensional case, the general medium representation was performed by modifying the scattering matrix of the node. Two basic modeling procedures were presented.

Both approaches use sources connected to the nodes to represent the medium. The first technique, based in modifications to the scattering matrix according to the medium, is not general; so the nodal source approach was chosen to represent general medium relationships.

The second approach presented a medium independent scattering matrix and has a physical interpretation. The sources connected to the node act as polarization and magnetization densities of the medium.

Together with the nodal source approach, circuit equivalents of the node were used. This allowed the solution of the resulting equations using circuit techniques. In the shunt node case an equivalent Norton circuit of the node was used. In the series case, a Thevenin equivalent was used instead.

The three-dimensional case was obtained using the combination of series and shunt nodes. This approach can be used to obtain different TLM nodes. The resulting node is connected to nodal sources representing the influence of the medium. The scattering matrix of the node is also independent of the medium.

The nodal source approach was used in all examples used to validate the procedure.

Chapter 4

Validation of the TLM Model of General Constitutive Relationships

4.1 Introduction

This chapter describes the efficient modeling of general constitutive relationships in TLM.

As seen in the previous chapter, the constitutive relationships are represented by sources connected to the TLM node. These relations describe the macroscopic effect of the interaction of fields with the medium at the microscopic level [39] in the form of differential equations describing the interaction of fields with matter.

These equations define the topology of the source network connected to the node. Since TLM is a discrete procedure, the differential equations must be discretized [63] in an efficient and general manner. The efficient solution of these equations can speed up the simulation process considerably. However, generality is the major criterion in the choice of the solution procedure.

In some cases, the components and topology of the source network can be obtained from the constitutive equations by inspection [12]. Once this is available, conventional circuit simulation techniques can be used to solve the network at each timestep, at every node.

In the general case, the constitutive equations are coupled nonlinear differential equations. In these cases, it is very difficult to obtain the topology of the network by inspection. It is easier to discretize the equations directly.

The solution of the constitutive equations using state-variable techniques can be

used in either case [64]-[65]. The state equations may be obtained from circuit equivalents or from direct inversion of the constitutive equations. The discretization of the state-variable equations is simple: several discretization schemes can be used successfully. The state-variable technique can be used in two or three-dimensional TLM without modifications to the solution procedure.

In this chapter, this technique is used to validate the modeling of general constitutive relationships in TLM. The procedure is applied in two-dimensional shunt node and to the three-dimensional symmetrical condensed node in several media. The results are compared to analytical values.

4.2 Solution of the constitutive equations

This section describes several solution procedures for the constitutive equations.

The source network can contain active and passive elements. For most media, the active elements are important only in the case of high-frequency (usually in the optical or upper microwave range) and large-amplitude (several Watts) excitation. Therefore for most media, the network will be composed by dissipative and reactive elements with no sources present (since these are usually negligible). These elements are obtained from inspection or by circuit synthesis techniques from the differential equations of the medium [12].

TLM is a discrete equivalent of a continuous process. Therefore, the source network also must be discretized. The discretization procedure affects the performance of the method. A discretization that is efficient for a particular constitutive equation may not be the best for another equation. Since there are several kinds of constitutive relationships, the best approach is to use a general discretization procedure that can represent all the possible cases.

A constitutive equation is in the form:

$$\begin{aligned} \mathbf{P} &= G(\mathbf{E}, \mathbf{H}, t) \\ \mathbf{M} &= F(\mathbf{E}, \mathbf{H}, t) \end{aligned} \tag{4.1}$$

where G and F are general functions of the **E** (electric) and **H** (magnetic) fields, and time; **P** is the polarization density, **M** is the magnetization density.

The linear medium relationships can be obtained by truncating the Taylor series of

the constitutive equations. In the linear, isotropic, time-invariant case:

$$P_u = G\left(E_u, \frac{\partial E_u}{\partial t}, \frac{\partial^2 E_u}{\partial t^2}, \ldots\right) \tag{4.2}$$

$$M_u = F\left(H_u, \frac{\partial H_u}{\partial t}, \frac{\partial^2 H_u}{\partial t^2}, \ldots\right) \tag{4.3}$$

where u indicates the direction of the field (u=x,y,z). This formulation of P and M is analogous to the description of nonlinear elements in a circuit network. In this case, the solution is obtained by the discretization of the constitutive equations. Once the discrete equations are rearranged, the solution is obtained recursively.

The constitutive equations can be discretized with any suitable discretization scheme. In this work, the following two schemes were used:

- Backwards Euler [63], [66]
- Trapezoidal [63], [66]

The direct discretization of the differential form is very efficient but cumbersome. The discretization procedure is simple, but it must be substituted into TLM. The resulting expressions are short but difficult to obtain.

The network approach can solve virtually any nonlinear circuit. The problem is to obtain the circuit components from the constitutive relationship.

The most flexible approach is the state-variable representation. It combines the advantages of the network an direct discretization approaches with very few disadvantages. The state-variables can be obtained directly from the differential equation or equivalent circuit [64]. Once, the continuous formulation is complete, the discrete formulation is simple to obtain. The disadvantage of the approach is that it is less efficient than both approaches.

4.2.1 Direct discretization

This section describes the direct discretization technique used in the solution of constitutive equations.

The procedure involves the discretization of the differential equation of the medium and substitution of incident and reflected voltages at the node. Once the substitu-

tion is performed, the equation is solved recursively.

Consider the first-order Debye medium. The differential equation of the medium is:

$$P + \tau_0 \frac{dP}{dt} = (\varepsilon_s - 1) E + \tau_0 (\varepsilon_\infty - 1) \frac{dE}{dt} \tag{4.4}$$

where τ_0 is the relaxation time constant, ε_s is the static permittivity and ε_∞ is the permittivity at infinite frequency. With the polarization relationship of the TLM node (both 2-D and 3-D cases):

$$\begin{aligned} i &= 2\Delta t \frac{dP}{dt} \\ v &= E \end{aligned} \tag{4.5}$$

The resulting medium differential equation is:

$$i + \tau_0 \frac{di}{dt} = 2\Delta t (\varepsilon_s - 1) \frac{dv}{dt} + 2\Delta t \tau_0 (\varepsilon_\infty - 1) \frac{d^2 v}{dt^2} \tag{4.6}$$

The incident and reflected voltages at the node are defined as:

$$\begin{aligned} v &= v^r + v^i \\ i &= Y_r (v^r - v^i) \end{aligned} \tag{4.7}$$

where v is the total voltage at the node, i is the current flowing through the link-line connecting the node and the source. Once the differential equation is discretized, the current and voltage are substituted by incident and reflected voltages. The resulting recursive equation is obtained with the trapezoidal discretization scheme:

$${}_{k+1}v_a^i = a ({}_{k+1}v_a^r) + b ({}_k v_a^r) + c ({}_k v_a^i) + d ({}_{k-1}v_a^r) + e ({}_{k-1}v_a^i) \tag{4.8}$$

where the coefficients are:

$$a = \frac{-(\varepsilon_s - 1 + 2\frac{\tau_0}{\Delta t}(\varepsilon_\infty - 2))}{(\varepsilon_s - 1 + 2\frac{\tau_0}{\Delta t}\varepsilon_\infty)} \qquad b = 4\frac{(1 + 2\frac{\tau_0}{\Delta t}(\varepsilon_\infty - 1))}{(\varepsilon_s - 1 + 2\frac{\tau_0}{\Delta t}\varepsilon_\infty)}$$

$$c = -4\frac{(1 - 2\frac{\tau_0}{\Delta t}(\varepsilon_\infty - 1))}{(\varepsilon_s - 1 + 2\frac{\tau_0}{\Delta t}\varepsilon_\infty)} \qquad d = \frac{(\varepsilon_s - 1 - 2\frac{\tau_0}{\Delta t}\varepsilon_\infty)}{(\varepsilon_s - 1 + 2\frac{\tau_0}{\Delta t}\varepsilon_\infty)} \tag{4.9}$$

$$e = \frac{(\varepsilon_s - 1 - 2\frac{\tau_0}{\Delta t}(\varepsilon_\infty - 2))}{(\varepsilon_s - 1 + 2\frac{\tau_0}{\Delta t}\varepsilon_\infty)}$$

This procedure results in a very efficient formulation (compared to the other possible formulations). It is efficient because the coefficients are calculated before the simulation, as part of the input file. The disadvantage is the lack of flexibility of the approach. The order of the recursive equation increases rapidly with the order of the differential equation.

4.2.2 Equivalent circuit network

An equivalent circuit network can describe the behavior of the medium. This approach has also been used in the characterization of constitutive relationships. The difficulty is to obtain the topology of the circuit network. In the case of simple medium, this is easily accomplished. The components of the network are obtained from the differential equation of the medium.

In the case of a first order Debye medium (4.4), the network can be obtained by inspection, Figure 4.1.

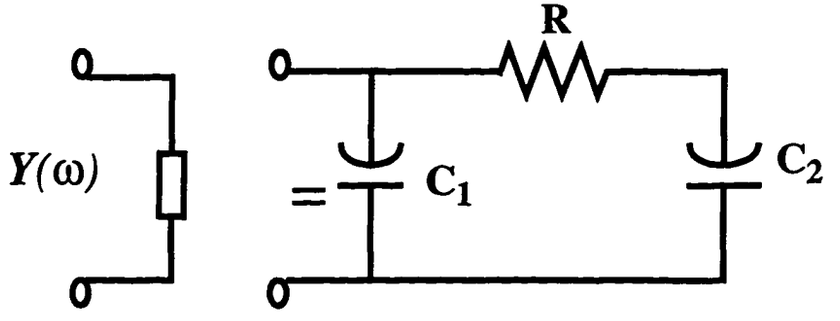

Figure 4.1 Equivalent network of a first-order Debye medium as seen from the node.

$$\text{where } C_1 = 2\Delta t(\varepsilon_\infty - 1) \qquad C_2 = 2\Delta t(\varepsilon_s - \varepsilon_\infty) \qquad R = \frac{\tau_0}{2\Delta t(\varepsilon_s - \varepsilon_\infty)}$$

The network can be solved using either Tableau or modified nodal formulation [12]. In any case, the reactive components are substituted by controlled sources.

The advantage of this approach resides in the ability to use techniques of conventional circuit simulators (SPICE, etc.). Therefore, most nonlinear behavior can be incorporated into the simulation using circuit sub-networks [12]. The sub-networks are assembled to represent the nonlinear function.

However, in the general case, the equivalent network approach works only for simple differential equations. The network synthesis procedure works well for linear one or two-port networks [12]. In the case of anisotropic materials, there can be as many as three ports in the network.

4.2.3 State-variable approach

This section describes the state-variable approach to modeling constitutive relationships.

It is a compromise between the direct discretization of the differential equation and the circuit equivalent representation. It can be obtained from equivalent circuits or directly from the differential equation [12],[65].

In the case where only the differential equation is available, the state-equations can be obtained by direct inversion of the differential equation. As an example consider the fourth-order linear differential equation

$$a\frac{d^4f}{dt^4} + b\frac{d^3f}{dt^3} + c\frac{d^2f}{dt^2} + d\frac{df}{dt} + ef = g \tag{4.10}$$

The direct inversion of the differential equation using Laplace transform results in the state variables [64]:

$$x_1(s) = f(s) = \frac{1}{a}\left(\frac{1}{s^4}(g - ef) - \frac{1}{s^3}df - \frac{1}{s^2}cf - \frac{1}{s}bf\right)$$

$$x_2(s) = \frac{1}{a}\left(\frac{1}{s}cf - \frac{1}{s^2}df + \frac{1}{s^3}(g - ef)\right) \qquad x_3(s) = \frac{1}{a}\left(\frac{1}{s^2}(g - ef) - \frac{1}{s}df\right) \tag{4.11}$$

$$x_4(s) = \frac{1}{a}\left(\frac{1}{s}(g - ef)\right)$$

The resulting system can be assembled in the form:

$$\frac{d}{dt}\begin{bmatrix} x_1(t) \\ x_2(t) \\ x_3(t) \\ x_4(t) \end{bmatrix} = \frac{1}{a}\begin{bmatrix} -b & 1 & 0 & 0 \\ -c & 0 & 1 & 0 \\ -d & 0 & 0 & 1 \\ -e & 0 & 0 & 0 \end{bmatrix}\begin{bmatrix} x_1(t) \\ x_2(t) \\ x_3(t) \\ x_4(t) \end{bmatrix} + \begin{bmatrix} 0 & 0 & 0 & 0 \\ 0 & 0 & 0 & 0 \\ 0 & 0 & 0 & 0 \\ 0 & 0 & 0 & \frac{1}{a} \end{bmatrix}\begin{bmatrix} 0 \\ 0 \\ 0 \\ g(t) \end{bmatrix} \tag{4.12}$$

The state-variable equations can be obtained directly from the equivalent circuit network using Kirchhoff's laws [12]. The state-variables are the current in inductors and voltage in capacitors.

The general form of the state-variable description is:

$$\begin{aligned} \frac{d}{dt}[\mathbf{x}] &= [\mathbf{A}]\,[\mathbf{x}] + [\mathbf{B}]\,[\mathbf{u}] \\ [\mathbf{y}] &= [\mathbf{C}]\,[\mathbf{x}] + [\mathbf{D}]\,[\mathbf{u}] \end{aligned} \tag{4.13}$$

where **[x]** is the state-vector, **[u]** is the source vector, **y** is the output vector. The matrices **[A]**, **[B]**, **[C]** and **[D]** may be a function of the state-vector.

The disadvantage of the direct inversion approach is that it may hide the physical meaning of the differential equation. This is one of the strengths of the circuit equivalent approach.

4.2.4 Discretization schemes

The discretization of the state-equations is simple. The state-equations can be discretized directly or after the solution is obtained. In the case of linear circuits, the state-equations can be solved analytically. The discretization of the analytical solution of the equations results in a discrete convolution procedure. This restricts the formulation to linear materials or to Volterra series representation. If the differential equations are discretized directly several discretization schemes can be employed.

In this thesis the backwards Euler and trapezoidal approaches [63], [66] are used together with the state-variable approach in the solution of several medium relationships.

The backwards Euler approach is unconditionally stable for physical systems modeled by TLM. It also introduces numerical losses to the system. The scheme is only first-order accurate [63], but it is very simple to implement. It is implemented as follows:

$$\begin{aligned} [\mathbf{x}(t+\Delta t)] &= [\mathbf{P}]\,[\mathbf{x}(t)] + [\mathbf{Q}]\,[\mathbf{u}(t+\Delta t)] \\ [\mathbf{y}(t+\Delta t)] &= [\mathbf{C}]\,[\mathbf{x}(t+\Delta t)] + [\mathbf{D}]\,[\mathbf{u}(t+\Delta t)] \end{aligned} \tag{4.14}$$

where:

$$[\mathbf{P}] = ([\mathbf{U}] - \Delta t[\mathbf{A}])^{-1} \qquad [\mathbf{Q}] = ([\mathbf{U}] - \Delta t[\mathbf{A}])^{-1}\Delta t[\mathbf{B}] \tag{4.15}$$

where [U] is the unit matrix.

The trapezoidal approach does not introduce numerical losses or gain to the system. In this scheme, all physically stable relationships remain numerically stable. The only problem occurs in marginally stable systems, where the modeling does not include losses. While the real system is stable, the discrete model may not be. The scheme is second-order accurate [63]. The trapezoidal approach is implemented as follows:

$$\begin{aligned} [\mathbf{x}(t+\Delta t)] &= [\mathbf{P}]\,[\mathbf{x}(t)] + [\mathbf{Q}]\,[\mathbf{u}(t+\Delta t)] + [\mathbf{R}]\,[\mathbf{u}(t)] \\ [\mathbf{y}(t+\Delta t)] &= [\mathbf{C}]\,[\mathbf{x}(t+\Delta t)] + [\mathbf{D}]\,[\mathbf{u}(t+\Delta t)] \end{aligned} \tag{4.16}$$

where:

$$\begin{aligned} [\mathbf{P}] &= ([\mathbf{U}]-\Delta t[\mathbf{A}])^{-1}([\mathbf{U}]+\Delta t[\mathbf{A}]) \\ [\mathbf{Q}] = ([\mathbf{U}] - \Delta t[\mathbf{A}])^{-1}\frac{\Delta t}{2}[\mathbf{B}] &\qquad [\mathbf{R}] = ([\mathbf{U}] - \Delta t[\mathbf{A}])^{-1}\frac{\Delta t}{2}[\mathbf{B}] \end{aligned} \tag{4.17}$$

4.3 Validation of the two-dimensional model

This section contains two examples that validate the modeling approach of general constitutive relationships in two-dimensional TLM.

Since either the shunt or series node may be used for this purpose, two shunt node examples were selected which validate the modeling procedure for frequency dependent and nonlinear dielectrics.

In the linear, frequency independent dielectric case, the accuracy of the state-variable model is the same as that of the stub-loaded approach. In fact, both approaches have the same dispersion relationship. This is shown in Chapter 5.

4.3.1 Linear frequency dependent dielectric

This section demonstrates the modeling of linear frequency dependent dielectrics in the two-dimensional case.

The frequency dependent behavior of dielectrics can be represent by suitable combinations of first-order Debye and second-order Lorentz behaviors. The second-order phenomena take into account molecular and atomic resonances, and the Debye model describe the transport of carriers or polar behavior [39].

Therefore, the modelling of frequency dependent dielectrics will be studied for both cases. These models can be represented as circuit equivalents, as shown in Figure 4.2

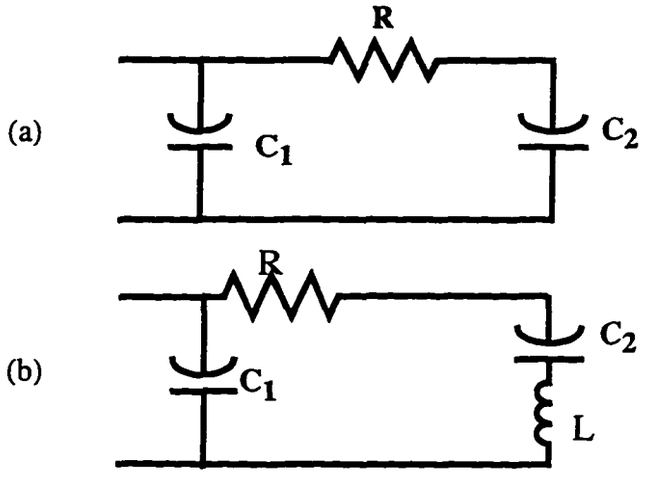

Figure 4.2 Equivalent circuit of (a) first-order Debye and (b) second-order Lorentz media.

For a dispersive dielectric medium modeled by a first-order Debye approximation, the frequency domain permittivity function is:

$$\varepsilon_r(\omega) = \varepsilon_\infty + \frac{\varepsilon_s - \varepsilon_\infty}{1 + j\omega\tau_0} \tag{4.18}$$

where τ_0 is the relaxation time constant, ε_s is the static permittivity and ε_∞ is the permittivity at infinite frequency.

The permittivity function (4.18) in this material can be modeled by the RC circuit shown in Figure 4.2.a, with the analogies:

$$C_1 = 2\Delta t(\varepsilon_\infty - 1) \qquad C_2 = 2\Delta t(\varepsilon_s - \varepsilon_\infty) \qquad R = \frac{\tau_0}{2\Delta t(\varepsilon_s - \varepsilon_\infty)}$$

The state-equations describing the circuit will be:

$$\frac{d}{dt}[v_y] = [A]\,[v_y] + [B]\,[v^r_{ey}]$$
$$\left[v^i_{ey}\right] = [C]\,[v_y] + [D]\,[v^r_{ey}] \tag{4.19}$$

with:

$$[A] = \begin{bmatrix} -\left(\frac{Y_r}{C_1} + \frac{1}{RC_1}\right) & \frac{1}{RC_1} \\ \frac{1}{RC_2} & -\frac{1}{RC_2} \end{bmatrix} \qquad [B] = \begin{bmatrix} 2\frac{Y_r}{C_1} \\ 0 \end{bmatrix} \tag{4.20}$$

$$[C] = \begin{bmatrix} 1 \\ 0 \end{bmatrix} \qquad [D] = [-1] \qquad [v_y] = \begin{bmatrix} v_y(t) \\ v_{yaux}(t) \end{bmatrix} \qquad [v^r_{ey}] = [v^r_{ey}(t)]$$

where $v_{yaux}(t)$ is an auxiliary variable used in the state-equation description of the system, Y_r is equal to 4, and v^r_{ey}, v^i_{ey} are the reflected and incident voltages at the input port of the network.

The discretization of the continuous state-variable equations was performed with trapezoidal and backwards Euler schemes. The procedure was validated by the simulation of a TEM parallel plate waveguide, partially filled by the frequency dependent dielectric, as shown in Figure 4.3.

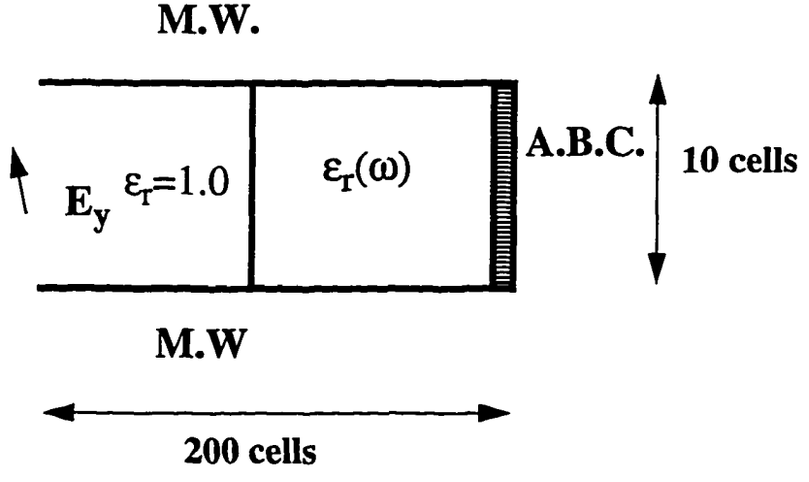

Figure 4.3 Parallel-plate waveguide used in the calculation of two-dimensional results of dispersive dielectric modeling. Legend: M.W. - Magnetic wall, A.B.C. - Absorbing boundary condition (in this case, it is a fixed reflection coefficient). The electric field Ey is normal to the plane of the device.

The frequency dependent medium was a simple model of water. The parallel plate waveguide was modeled by a mesh of 200 x 10 nodes (14.65 x 0.7325 mm) with the dielectric constant of $\varepsilon_r = 1$ as shown in Figure 4.3. The first-order Debye medium had the parameters: $\varepsilon_\infty = 1.8$, $\varepsilon_s = 81.0$ and $\tau_0 = 9.4\times10^{-12}$ seconds.

The reflection coefficient at the input port of the guide was then computed and compared to the analytical solution.

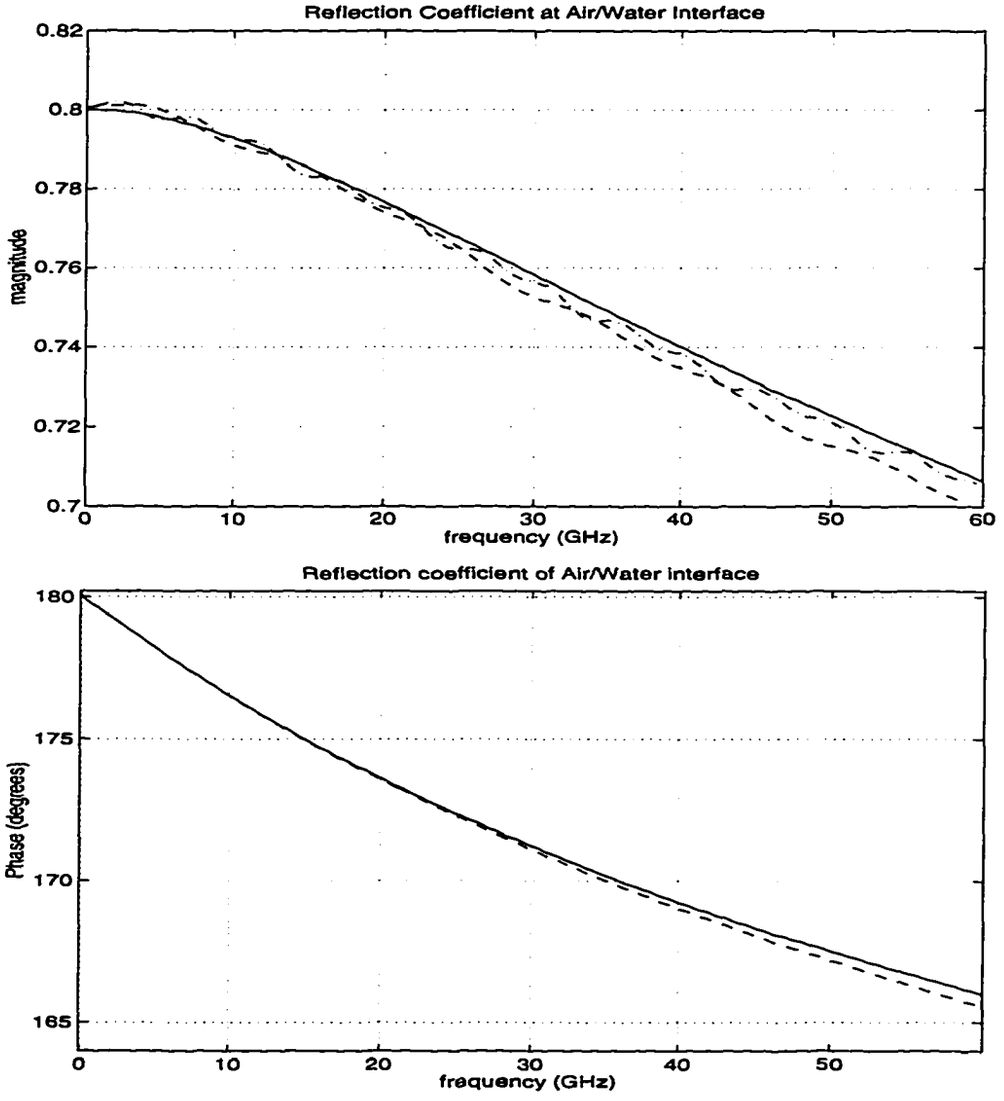

Figure 4.4 Analytically and numerically calculated magnitude and phase of the reflection coefficient of an air/water interface. The solid line is the exact result. The dashed line is the result obtained with 2048 timesteps. The dash-dotted line is the result calculated with 8192 timesteps (only with magnitude).

The validation of the model for second-order Lorentz dielectrics is similar to the first-order case. The frequency domain permittivity function is:

$$\varepsilon_r(\omega) = \varepsilon_\infty + \frac{(\varepsilon_s - 1)\,\omega_0^2}{\omega_0^2 + j\omega\delta_0 - \omega^2} \tag{4.21}$$

where ω_0 is the resonant frequency, δ_0 is the relative loss factor, ε_s is the static permittivity, and ε_∞ is the permittivity at infinite frequency.

The permittivity function (4.21) in this dispersive material has been modeled by the RLC circuit shown in Figure 4.2.b, with the analogies:

$$C1 = 2(\varepsilon_\infty - 1) \qquad C2 = 2(\varepsilon_s - \varepsilon_\infty)$$

$$R = \frac{\delta}{2\Delta t\omega_0^2(\varepsilon_s - \varepsilon_\infty)} \qquad L = \frac{1}{2(\Delta t\omega_0)^2(\varepsilon_s - \varepsilon_\infty)}$$

The equivalent circuit corresponding to (4.21) obeys the state equation:

$$\partial_t \begin{bmatrix} v(t) \\ v_n(t) \\ i_n(t) \end{bmatrix} = \begin{bmatrix} -\frac{Y_r}{C1} & 0 & -\frac{1}{C1} \\ 0 & 0 & \frac{1}{C2} \\ \frac{1}{L} & -\frac{1}{L} & -\frac{R}{L} \end{bmatrix} \begin{bmatrix} v(t) \\ v_n(t) \\ i_n(t) \end{bmatrix} + \begin{bmatrix} 2\frac{Y_r}{C1} \\ 0 \\ 0 \end{bmatrix} \left[v_{ey}^r(t)\right]$$

$$\left[v_{ey}^i(t)\right] = \begin{bmatrix} 1 \\ 0 \\ 0 \end{bmatrix} \left[v(t)\ \ v_n(t)\ \ i_n(t)\right] + \left[-1\right]\left[v_{ey}^r(t)\right] \tag{4.22}$$

where the reflected voltage from the node $v_{ey}^r(t)$ is obtained from (3.29). The voltage v_n and current i_n are auxiliary variables.

The benchmark example used in the first-order case was used here as well, the dielectric was modeled as a second order Lorentz medium with $\varepsilon_\infty = 1.0$, $\varepsilon_s = 3.056$, $f_0 = 20\text{GHz}$ and $\delta_0 = 0$, which is typical for cold plasma (collisonless plasma).

The result shown in Figure 4.5 is compared to the analytical reflection coefficient.

The simulations ran for 2048 timesteps. If the problems are simulated for a longer time, a new problem arises. As shown in Figure 4.5 reflections from the absorbing bound-

ary tend to corrupt the results.

The problem can be avoided by placing the absorbing boundaries at a sufficient distance from the measuring point, so that reflections do not reach the output point before the end of the simulation.

These effects reduced the reflections from the boundary. In these examples fixed reflection coefficients were used as absorbing conditions. If higher order absorbing boundary conditions are used, the problem becomes less critical (because of the wide-band behavior of higher-order abosrbing boundaries).

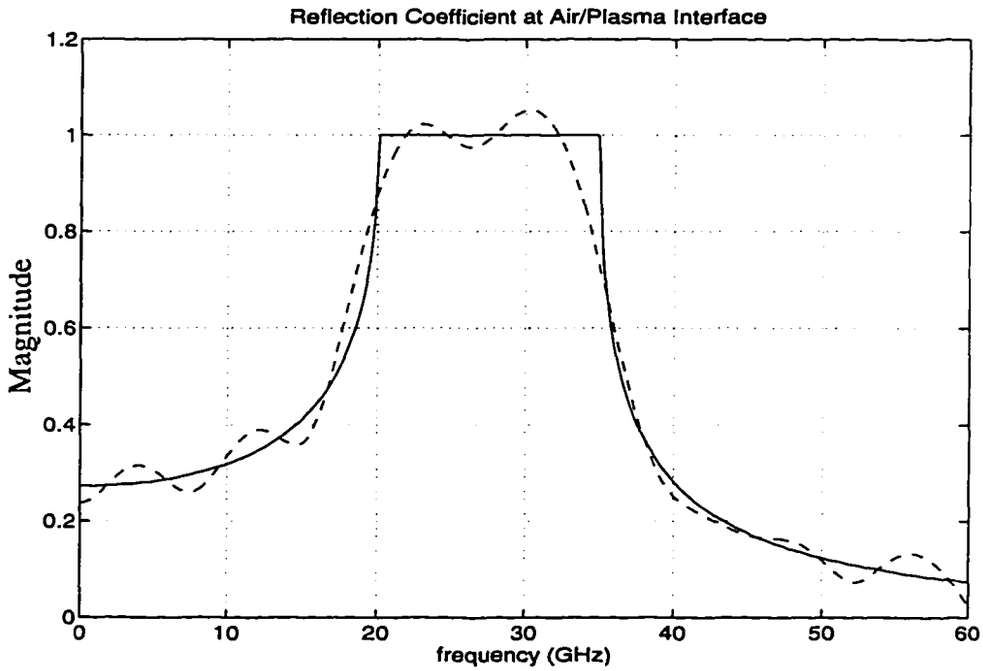

Figure 4.5 Exact and calculated results for a second-order medium interface. The dashed line result was obtained with 2048 timesteps. As the number of timesteps increase, the results can be worse due to imperfect absorbing boundary conditions. The phase behavior of second-order materials in discussed in Chapter 5.

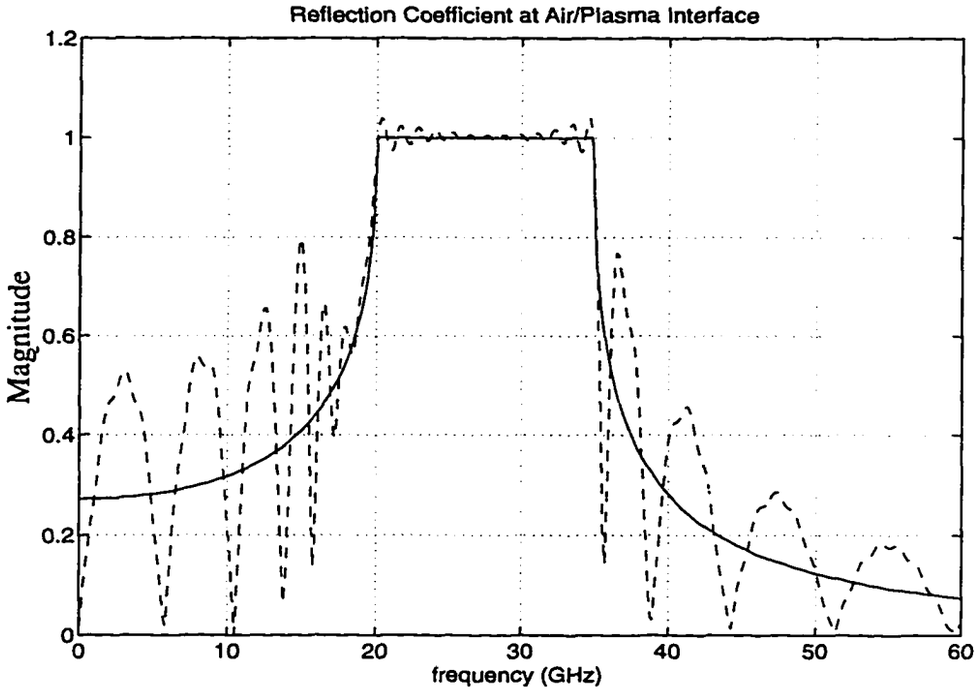

Figure 4.6 Exact and calculated results for a second-order medium interface. The dashed line result was obtained with 4096 timesteps.

The dispersion analysis of dispersive dielectrics in TLM using state-variable approach (discussed in Chapter 5) shows that the timestep should be at least $\Delta t < \tau_0/100$ to obtain accurate results. If a small frequency shift is acceptable, the limit can be decreased to $\Delta t < \tau_0/20$. This restriction applies to backwards Euler and trapezoidal discretization. In the case of second order materials, the restriction is the same for the approximate trapezoidal case and it is worse for the backwards Euler case (Chapter 5). This rule of thumb for the discretization is valid as long as $\varepsilon_r, \mu_r < 20$.

4.3.2 Nonlinear isotropic frequency dependent dielectric

This section describes the modeling and validation of nonlinear isotropic frequency dependent dielectrics.

The linear medium is generally an approximation of the material under low field assumptions [39]. The nonlinear behavior of the polarization density are usually included in the constitutive relationships by a Taylor series approximation since most macroscopic constitutive equations are phenomenological relationships (polynomial approximations).

The nonlinear behavior is included in the constitutive equations by adding odd powers of the electric field and polarization density. This is needed because of the inversion symmetry of most microscopic particles.

A first-order nonlinear approximation of the frequency dependent polarization equation can be used to describe the weak nonlinear effects. The approximation is obtained by extending the Taylor approximation of an undamped oscillator differential equation to the third order nonlinear term:

$$\frac{d^2}{dt^2}f(t) + af(t) + b(f(t))^3 + c(f(t))^5 + \ldots = g(t) \tag{4.23}$$

where g(t) is a forcing function and a, b and c are undertermined constants. These approximations usually include only odd powers of f(t).

One weak nonlinear field interaction with the medium is the inversion of the ammonia molecule [39] under a high power microwave field. The molecule has two equilibrium states. The first is a low field stable configuration. The constitutive equation that includes the second state is:

$$\frac{d^2P_y}{dt^2} + \omega_0^2 P_y + \alpha P_y^3 = \omega_p^2 E_y \tag{4.24}$$

where α is the nonlinear coupling factor.

This medium is modeled in TLM by using the relationship between the polarization current and the polarization vector, as well as the TLM field-circuit analogy,:

$$\frac{d^2 i_{pol}}{dt^2} + \omega_0^2 i_{pol} + \alpha q_{pol}^2 i_{pol} = 2\omega_p^2 \Delta t \frac{dv_y}{dt} \tag{4.25}$$

Once the differential or integral equation relating the polarization vector and the electric field is obtained, it is not difficult to derive the equivalent circuit (as shown in Figure 4.7) and the differential or integral equation relating the total voltage at the node and the nonlinear current.

Since the current and the voltage in (4.25) can be expressed in terms of the incident and reflected TLM impulse voltages at the network, a finite difference approximation is used to solve the nonlinear equation in terms of these incident and reflected voltages.

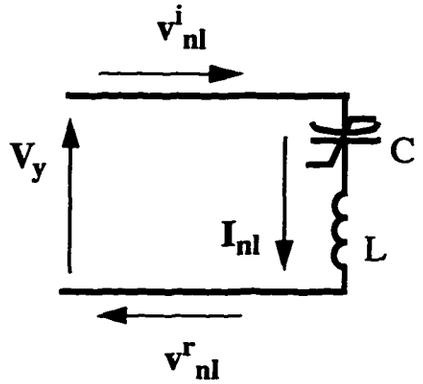

Figure 4.7 Network representation of the nonlinear differential equation.

The propagation of a soliton wave in a nonlinear dispersive medium was simulated using this model. There are several kinds of solitons [41]-[49]. The type of soliton that will propagate depends on the medium constitutive equation.

The constitutive equation described by the nonlinear oscillator (4.24) allows the propagation of self-induced-transparency (SIT) solitons [47]. In this kind of soliton propagation, once the field has a critical value the nonlinear dispersive medium behaves as transparent (no dispersion, abosrption or reflection).

The polarization in the nonlinear medium was expressed by (4.24) with the parameters of ammonia [39]:

- $\omega_p = 2\pi \times 28.7\text{GHz}$
- $\omega_0 = 2\pi \times 20.0\text{GHz}$
- $\alpha = 6.94 \times 10^{-7}$
- $E_0 = 9.33 \times 10^8$ V/m in the nonlinear case (soliton propagation)
- $E_0 = 1.0$ V/m in the linear case (mainly linear propagation)

The nonlinear coupling constant α was chosen arbitrarily. Its value was chosen to be low to show the dispersive effect in the propagation (under low field conditions $E_0 << 100$ V/m).

Equation (4.25) may be further simplified by considering that the nonlinear element

is a capacitor (Figure 4.7):

$$\frac{d^2 i_{pol}}{dt^2} + \left(\omega_0^2 + \frac{\alpha}{(\Delta t)^2}\left(v_y^{-\frac{2}{3}}\right)\right) i_{pol} = \omega_p^2 2\Delta t \frac{dv_y}{dt} \tag{4.26}$$

Resulting in the difference equation:

$${}_{k+1}v_5^i = a\,({}_{k+1}v_5^r) + b\,({}_k v_5^r) + c\,({}_k v_5^i) + d\,({}_{k-1}v_5^i) + e\,({}_{k-1}v_5^i) \tag{4.27}$$

where:

$$a = -\frac{(\omega_p^2\Delta t^2 - 4)}{(\omega_p^2\Delta t^2 + 4)}$$

$$b = \frac{2\left(\omega_0^2\Delta t^2\left(\frac{\alpha}{(\Delta t)^2}\left({}_k v_y^{-\frac{2}{3}}\right)\right) - 4\right)}{(\omega_p^2\Delta t^2 + 4)} \tag{4.28}$$

$$c = -b \qquad d = 1.0 \qquad e = -a$$

The computational domain was a rectangular box 31.25 mm long in the z-direction and 0.375 mm wide in the x direction, with a mesh parameter Δl of 31.25 μm. All the nodes inside the domain were shunt nodes, and the medium was homogeneous. The simulation was performed twice, once with a Gaussian pulse of small amplitude (1 V/m), and then with a Gaussian pulse of large amplitude(10^8V/m).

The nonlinear response is shown in Figures 4.8 to Figure 4.8.

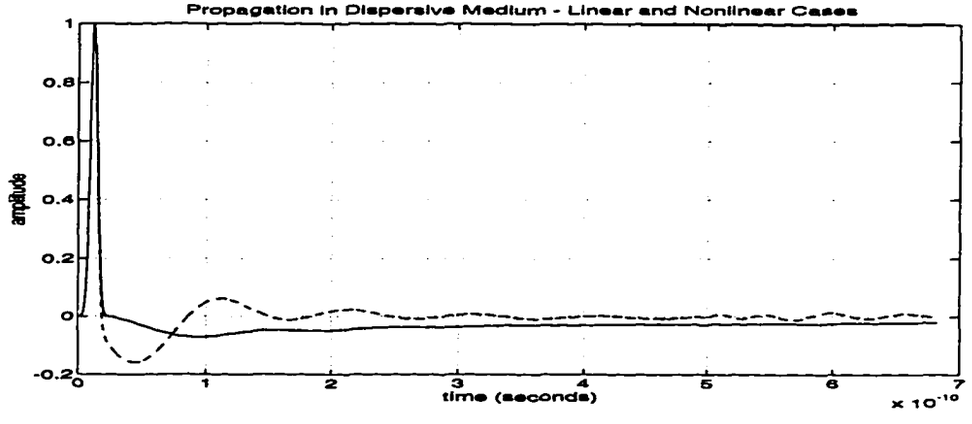

Figure 4.8 Time domain response of the nonlinear medium at the input point. Solid line: nonlinear response. Dashed line: linear response.

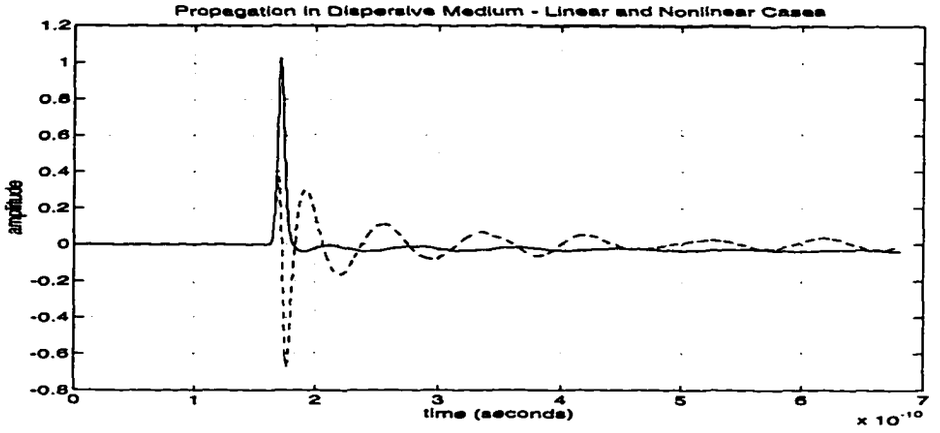

Figure 4.9 Time domain response of the nonlinear medium halfway through the line. Solid line: nonlinear response. Dashed line: linear response.

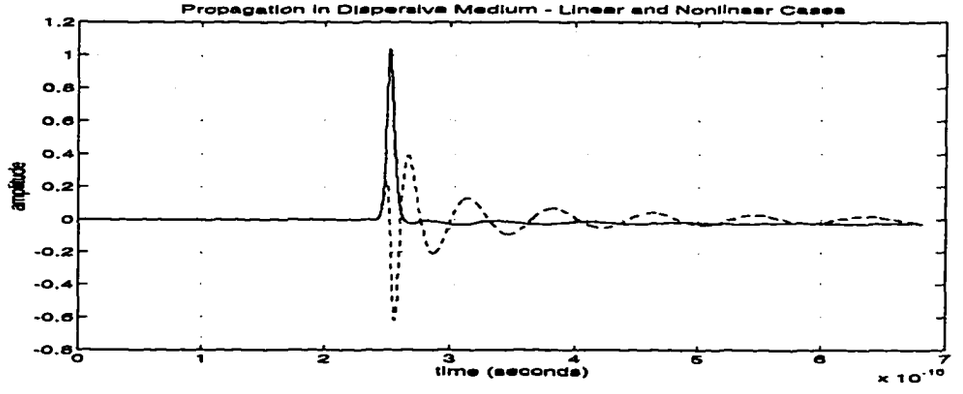

Figure 4.10 Time domain response of the nonlinear medium at the output point. Solid line: nonlinear response. Dashed line: linear response.

4.4 Validation of three-dimensional model

This section describes the validation of the three-dimensional TLM model general media.

While in two-dimensional TLM one can usually model either electric or magnetic field complex constitutive relationships, the three-dimensional model includes both. The symmetrical condensed node (SCN) was used in the three-dimensional case.

As in the two-dimensional case, spurious reflections from the absorbing boundary can occur. Since single reflection coefficient to model the absorbing boundary was used in this work, spurious reflections were avoided by making the TLM mesh very large and

truncating the time response. It may be noted here that the modeling of linear isotropic frequency independent media leads to the same results as the stub-loaded approach (if the trapezoidal discretization scheme is used).

4.4.1 Linear isotropic frequency independent medium

This section describes the SCN TLM model of linear isotropic frequency independent media and its validation.

In the case of linear isotropic frequency independent media, each field component must be associated with its own nodal source. All six source equations are generated by two equations describing the polarization current and magnetization voltage:

$$\begin{aligned} {}_u v_s(t) &= 2Z_r v^r_{mu}(t) = Z_0(\mu_r - 1)\,2\frac{\Delta l}{c}\frac{d}{dt} i_u(t) + Z_r i_u(t) \\ {}_u i_s(t) &= 2Y_r v^r_{eu}(t) = Y_0(\varepsilon_r - 1)\,2\frac{\Delta l}{c}\frac{d}{dt} v_u(t) + Y_r v_u(t) \end{aligned} \tag{4.29}$$

where u=x, y and z.

The state-variable form is:

$$\begin{aligned} \frac{d}{dt} v_u(t) &= -\frac{Y_r c}{Y_0(\varepsilon_r - 1)\,2\Delta l} v_u(t) + \frac{2Y_r c}{Y_0(\varepsilon_r - 1)\,2\Delta l} v^r_{eu}(t) \\ \frac{d}{dt} i_u(t) &= -\frac{Z_r c}{Z_0(\mu_r - 1)\,2\Delta l} i_u(t) + \frac{2Z_r c}{Z_0(\mu_r - 1)\,2\Delta l} v^r_{mu}(t) \end{aligned} \tag{4.30}$$

Resulting in:

$$\frac{d}{dt}\begin{bmatrix} [v(t)] \\ [i(t)] \end{bmatrix} = \begin{bmatrix} -\alpha[U] & [0] \\ [0] & -\beta[U] \end{bmatrix}\begin{bmatrix} [v(t)] \\ [i(t)] \end{bmatrix} + \begin{bmatrix} 2\alpha[U] & [0] \\ [0] & 2\beta[U] \end{bmatrix}\begin{bmatrix} [v^r_e(t)] \\ [v^r_m(t)] \end{bmatrix} \tag{4.31}$$

where:

[U] is the 3x3 unit matrix, [v(t)] and [i(t)] are the vectors containing the voltages and currents in x,y and z directions, $[v^r_a(t)]$ and $[v^r_n(t)]$ are the reflected voltages and:

$$\alpha = \frac{Y_r c}{Y_0(\varepsilon_r - 1)\,2\Delta l} \qquad \beta = \frac{Z_r c}{Z_0(\mu_r - 1)\,2\Delta l} \tag{4.32}$$

The approach was validated by computing the cutoff frequency results of a dielec-

tric-filled isotropic waveguide and compared with the result obtained with the stub-loaded TLM model.

The example was a WR-28 waveguide (7.112 mm by 3.556 mm, terminated by magnetic walls) using a regular mesh with a discretization of 24 x 12 x 4 cubic cells, and filled with a dielectric with ε_r of 2.22.

The first resonance of this cavity has the same frequency of the first dominant mode in a WR-28 guide filled with the same dielectric. The results are shown in Figure 4.11

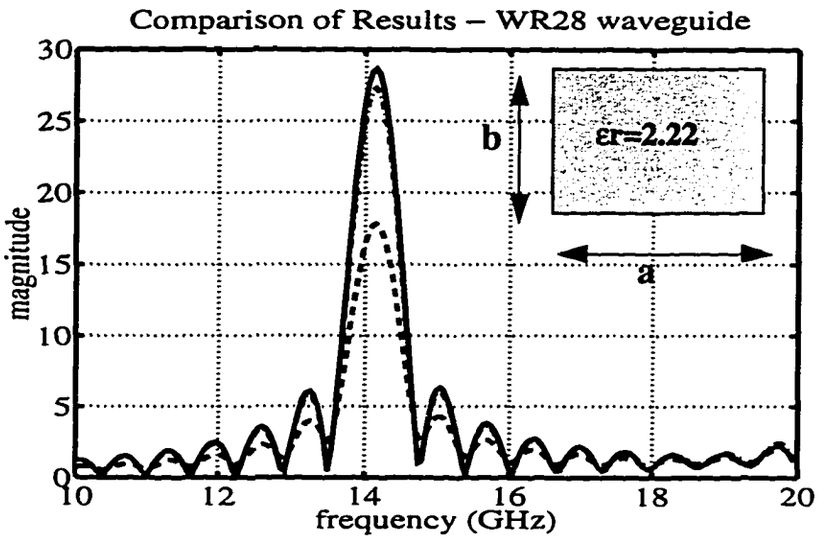

Figure 4.11 Dominant mode cutoff frequency of a WR-28 waveguide. The solid line results are obtained with stub-loaded TLM. The dashed-line results are obtained with a backwards-Euler discretization scheme. The dash-dotted lines are obtained with the trapezoidal scheme.

4.4.2 Linear isotropic frequency dependent medium

This section describes the SCN TLM model of linear isotropic frequency dependent media and its validation.

The nodal source equations are same as in the two-dimensional case, but the equations must be applied to the all electric or magnetic field components. Therefore, the necessary storage is three times as large.

The approach was validated by calculating the scattering parameters of a parallel plate waveguide partially filled with a air/dispersive material. The parallel plate waveguide was modeled by a mesh of 200 x 10 x 5 nodes (14.65 x 0.7325 x 0.36625 mm)

with the dielectric constant of $\varepsilon_r = 1$ as shown in Figure 4.12.

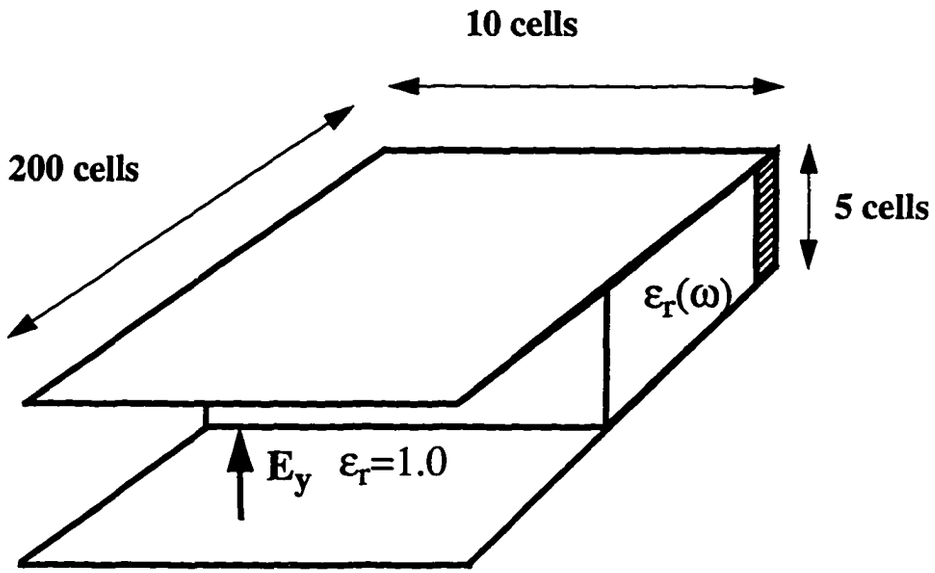

Figure 4.12 Geometry of the parallel plate waveguide.

In the first case (Figure 4.13), the dispersive dielectric was modeled as a first-order Debye medium with parameters: $\varepsilon_\infty = 1.8$, $\varepsilon_s = 10.0$ and $\tau_0 = 9.4\times10^{-12}$ seconds.

In the second case (Figure 4.13), the dielectric was modelled as a second-order Lorentz medium with $\varepsilon_\infty = 20.0$, $\varepsilon_s = 60.0$, $f_0 = 5$GHz and $\delta = 0.3$. Both results were calculated using state-space equations discretized using the backwards Euler scheme.

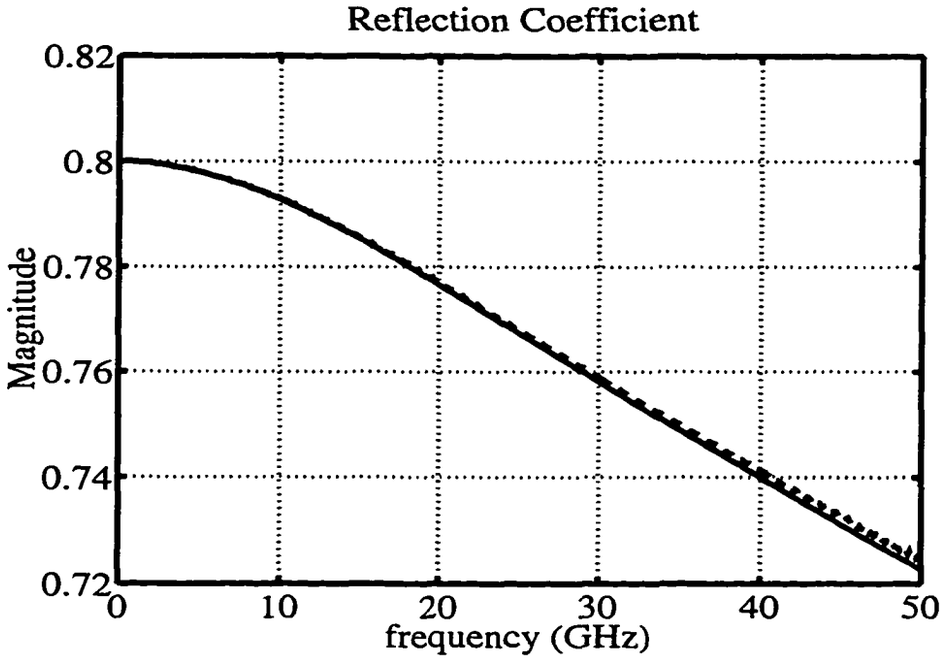

Figure 4.13 Exact and calculated magnitude of the reflection coefficients of an air-dielectric interface with a first -order dielectric.

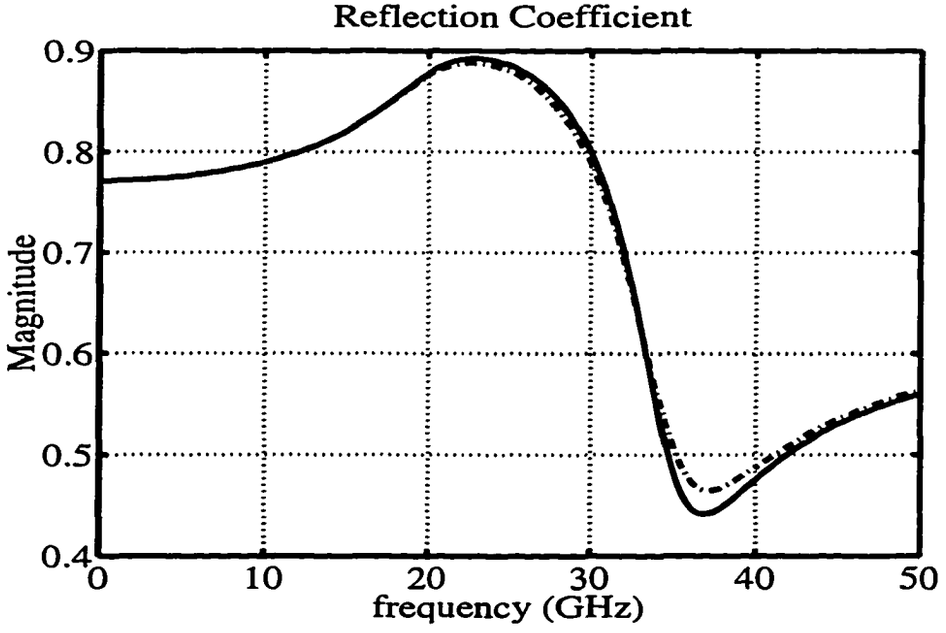

Figure 4.14 Exact and calculated reflection coefficients of an air interface with second-order dielectric.

4.4.3 Linear anisotropic frequency independent medium

This section describes the TLM SCN model of linear anisotropic frequency independent media and its validation.

In the anisotropic case, the medium model can be applied to both electric and magnetic fields simultaneously. The constitutive relationship involving both electric and magnetic fields can included by considering their tensor form. Losses can also be easily included in the relationship.

In an anisotropic material with non-diagonal tensor we have:

$$\begin{aligned} \mathbf{P} &= [F]\,\mathbf{E} = ([\varepsilon] - [U])\,\mathbf{E} \\ \mathbf{M} &= [G]\,\mathbf{H} = ([\mu] - [U])\,\mathbf{H} \end{aligned} \tag{4.33}$$

where:

$$[\varepsilon] = \begin{bmatrix} \varepsilon_{xx} & \varepsilon_{xy} & \varepsilon_{xz} \\ \varepsilon_{yx} & \varepsilon_{yy} & \varepsilon_{yz} \\ \varepsilon_{zx} & \varepsilon_{zy} & \varepsilon_{zz} \end{bmatrix} \qquad [\mu] = \begin{bmatrix} \mu_{xx} & \mu_{xy} & \mu_{xz} \\ \mu_{yx} & \mu_{yy} & \mu_{yz} \\ \mu_{zx} & \mu_{zy} & \mu_{zz} \end{bmatrix} \qquad [U] = \begin{bmatrix} 1 & 0 & 0 \\ 0 & 1 & 0 \\ 0 & 0 & 1 \end{bmatrix} \tag{4.34}$$

The constitutive state-equation is:

$$2\Delta t \frac{d}{dt} \begin{bmatrix} v_x \\ v_y \\ v_z \\ i_x \\ i_y \\ i_z \end{bmatrix} = -4 \begin{bmatrix} [F]^{-1} & [0] \\ [0] & [G]^{-1} \end{bmatrix} \begin{bmatrix} v_x \\ v_y \\ v_z \\ i_x \\ i_y \\ i_z \end{bmatrix} - 8 \begin{bmatrix} [F]^{-1} & [0] \\ [0] & [G]^{-1} \end{bmatrix} \begin{bmatrix} v^r_{ex} \\ v^r_{ey} \\ v^r_{ez} \\ v^r_{mx} \\ v^r_{my} \\ v^r_{mz} \end{bmatrix} \tag{4.35}$$

This relationship is obtained directly from (4.33) and (4.34) without the need for an equivalent circuit.

The approach was validated by the calculating the cutoff frequencies of a sapphire filled WR-28 waveguide with the same discretization used in the first example. The permittivity tensor is:

$$[\varepsilon] = \begin{bmatrix} (\varepsilon_u \cos^2\varphi + \varepsilon_v \sin^2\varphi) & \frac{1}{2}(\varepsilon_u - \varepsilon_v)\sin 2\varphi & 0 \\ \frac{1}{2}(\varepsilon_u - \varepsilon_v)\sin 2\varphi & (\varepsilon_v \cos^2\varphi + \varepsilon_u \sin^2\varphi) & 0 \\ 0 & 0 & \varepsilon_z \end{bmatrix} \tag{4.36}$$

for sapphire: $\varepsilon_u = 9.34$ and $\varepsilon_v = 11.49$, [6].

The optical axis lies on the xy plane and forms an angle φ with respect to the x axis. The problem was calculated for φ of 0°, 45° and 90° using backwards Euler discretization. The comparison between the exact and calculated results is shown in Table 4.1..

Analytical Cutoff Frequency	Axis Angle	SCN - TLM	Error (%)
6.2221 GHz	0°	6.21 GHz	0.19
6.5354 GHz	45°	6.57 GHz	0.53
6.9012 GHz	90°	6.90 GHz	0.02

Table 4.1. Comparison between analytical and computed cutoff frequencies of a sapphire-filled WR-28 waveguide for three angles between the optical axis and the x-axis.

4.4.4 Linear anisotropic frequency dependent medium

This section describes the SCN TLM model of linear anisotropic frequency dependent medium and its validation.

In a first-order approximation, magnetized ferrite is a linear anisotropic frequency dependent medium. Considering a gyromagnetic material subject to a magnetization field H_0 in the z-direction with saturation magnetization M_0 in the same direction, the linearized constitutive equations for the permeability are [7]:

$$\begin{aligned} \frac{dm_x}{dt} &= \omega_0 m_y - \omega_m m_y \\ \frac{dm_y}{dt} &= -\omega_0 m_x + \omega_m m_x \end{aligned} \tag{4.37}$$

where ω_0 and ω_m are obtained from the bias magnetic field and the saturation magnetization:

$$\begin{aligned} \omega_0 &= \Upsilon H_0 \qquad \omega_m = \Upsilon M_0 \\ \Upsilon &= 2\pi \times 2.8 \times 10^6 \ (\mathrm{Hz/Oe}) \end{aligned} \tag{4.38}$$

The constitutive equations (4.37) can be expressed in the state variable form:

$$\frac{d}{dt}\begin{bmatrix} m_x \\ m_y \end{bmatrix} = \frac{2\omega_0 Z_r}{Z_r^2 + (2\Delta t\omega_m)^2}[A]\begin{bmatrix} m_x \\ m_y \end{bmatrix} - \frac{2\omega_m Z_r}{Z_r^2 + (2\Delta t\omega_m)^2}[A]\begin{bmatrix} v_{nx} \\ v_{ny} \end{bmatrix}^r \qquad (4.39)$$

$$[A] = \begin{bmatrix} 2\Delta t\omega_m & -Z_r \\ Z_r & 2\Delta t\omega_m \end{bmatrix}$$

The technique presented in this thesis has been used to simulate an E-plane resonance isolator in a WR90 waveguide [60]. The device was designed to have a 30 dB reverse attenuation at 10 GHz. The ferrite slab was 0.5 mm wide, 24 mm long, and placed at 2.54 mm from one of the inner waveguide walls, with a saturation magnetization of 1700 Gauss and a bias magnetic field of 2840 Oersteds, (Figure 4.15). The scheme used to solve (4.39) was the backwards Euler scheme.

The results, presented in Figure 4.16, are the transmission coefficients for the forward and backward propagation (S21 and S12).

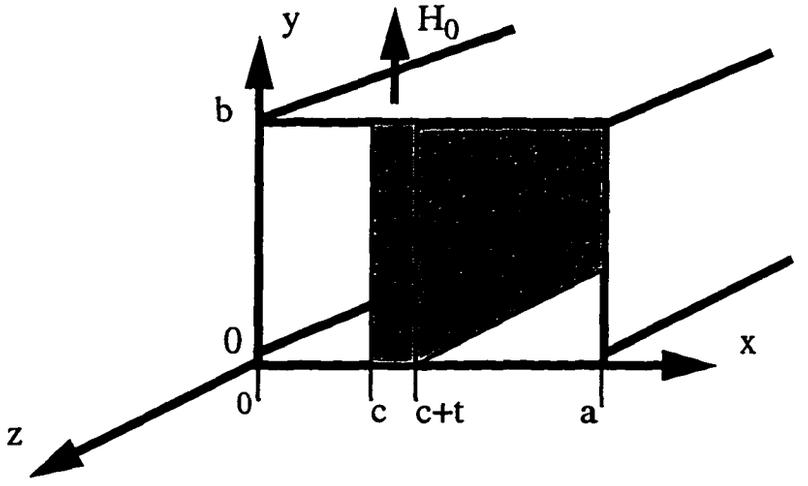

Figure 4.15 Geometry of the resonance ferrite isolator.

The results in Figure 4.16 show less reverse attenuation than expected. This was caused by the sensitivity of the results to the placement of boundaries, and the difficulty to simultaneously position the slab accurately and to discretize its thickness.

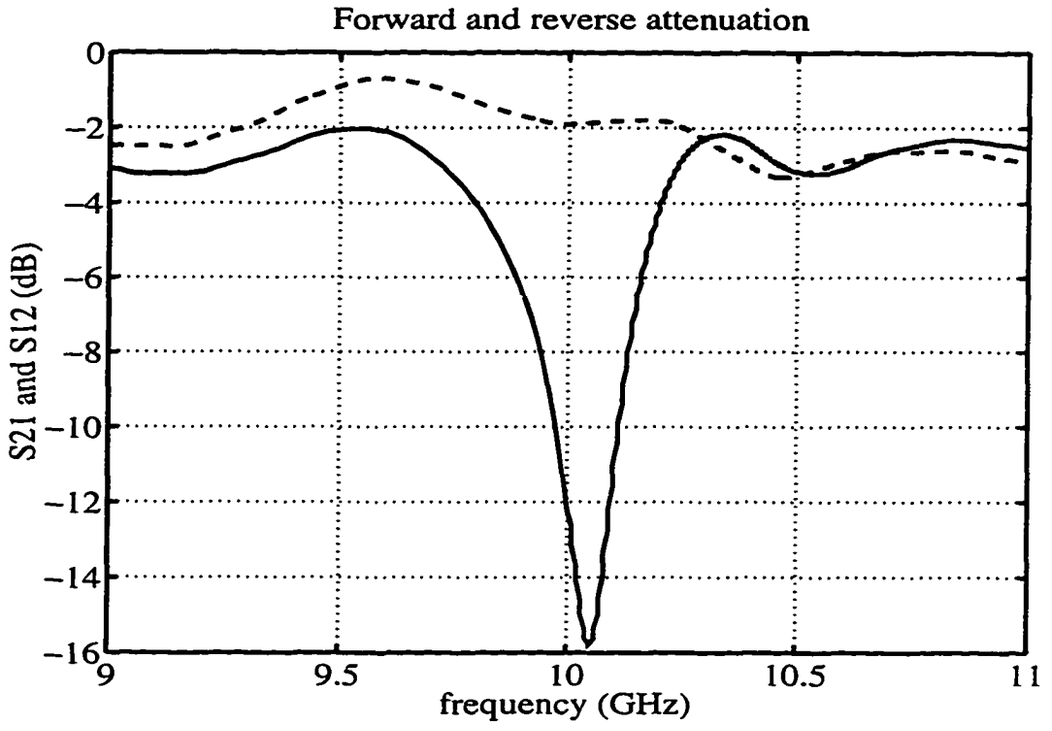

Figure 4.16 Frequency domain response of the resonance isolator. Solid line: reverse attenuation. Dashed line: forward attenuation.

4.5 Conclusions

The validation of TLM models for general constitutive relationships was presented. The modeling technique consists of decoupling the impulse scattering at the nodes from equations describing the medium by using equivalent nodal sources.

The sources are governed by differential equations. These equations are obtained from the medium constitutive relationships. The differential equations can be represented in several forms.

In this work, the equations were represented in the state-variable form. This formulation leads to simple discretization procedures. The discretization schemes used in this thesis were the backwards Euler and trapezoidal approximations. The schemes are necessary in the discretization of the differential formulation.

The procedure was validated for several kinds of medium relationships. In the modeling of frequency dependent relationships, it was observed that spurious reflections form

the absorbing boundary can affect the results unless some remedial measures are taken, such as the truncation of the time response and the use of large computational domains. The major sources of error in the simulation of frequency dependent media are discussed in Chapter 5.

In the solution of nonlinear problems, the size of the computational domain is also important when solitons are to be modeled.

The procedure was also validated for anisotropic materials. One advantage of the formulation resides ns the possibility to model materials with constitutive relationships that involve the electric and magnetic fields simultaneously.

Chapter 5

Error Analysis of the Transmission Line Matrix Method

5.1 Introduction

This chapter presents an error analysis of the TLM model for dispersive dielectrics and a new technique for quantifying errors in a simulation.

The Transmission Line Matrix (TLM) method solves a discrete approximation of a continuous problem [14]-[16]. The error analysis of TLM is the study of the differences between the numerical and exact solutions of the problem. By understanding these differences one can define and improve the accuracy of the method.

The sources of error in a TLM simulation studied in this chapter are the coarseness, velocity (or dispersion) and discretization errors [2]. The coarseness error is associated with the failure to represent rapidly varying fields or field singularities due to finite mesh size. The magnitude of this error depends on the structure being analyzed. The velocity error is related to the anisotropy of the mesh and wavelength of problem. The TLM mesh represents larger wavelengths better than shorter ones. The magnitude of the error is proportional to the square of the ratio between the wavelength and spatial step. The discretization error is related to approximation of certain shapes, like circles and spheres, by a stepwise rectangular contour.

The principal method to quantify errors in TLM is dispersion analysis [22]-[27]. In this analysis, the mesh is uniform and infinite. In this case, the field can be obtained analytically (the solution is an infinite number of propagating and evanescent modes present in the mesh). These modes are represented by complex exponentials (the exponent is the propagation constant). The substitution of these exponentials into the TLM scheme

results in an eigenvalue problem. The solution of the eigenvalue problem is the dispersion relation of the method. This relation shows the accuracy of the method. The dispersion analysis shows that TLM is a second-order accurate method. A numerical method is second-order accurate if the numerical solution approaches the continuous one with the square of the discretization step [67]-[69].

The error analysis of dispersive dielectrics in TLM is done using the same procedure. In the case of dispersive dielectrics, the accuracy of the method depends on the ratio between the timestep chosen and the relaxation time of the medium. The accuracy also depends on the values of the loss, and the permittivities.

This thesis also presents a new technique for error analysis. The method is based in the analytical solution of TLM difference equations. The solution procedure can be applied in inhomogeneous bounded meshes with or without absorbing boundary conditions (ABC). The error bounds of the field solutions are obtained analytically by comparing the continuous and discrete solution of the problem.

The dispersion analysis shows the geometry independent, general characteristics of the method (quantifies the velocity error). It provides the relationship between the wavenumbers (eigenvalues) of the modes propagating in the mesh and spatial step. It characterizes the velocity error in TLM using a homogeneous, unbounded mesh for the analysis. The dispersion analysis presents the minimum error in a simulation.

Since the dispersion analysis is performed in infinite homogeneous space it does not include coarseness and discretization errors. The dispersion relation shows the effect of representing the space as a mesh of nodes. However, it can adapted to characterize the coarseness error of certain field singularities in an infinite mesh.

The solution of the TLM difference equations includes specific features of the geometry in the characterization of the numerical solution. It also provides the amplitudes of the modes (eigenvectors) or features such as the impedance of discontinuities or number of modes propagating. Therefore, the new technique characterizes also the coarseness and discretization errors of the problem. In certain cases, it can provide the maximum error in a simulation.

This solution procedure for TLM difference equations was developed in this thesis. Two important results were obtained using the analytical solution of difference equations in selected problems: positive and negative frequency shifts in the presence of dielectrics

and first order convergence.

The first result was obtained by calculating the TLM solution of a partially filled waveguide. Using the dispersion analysis, one can prove that TLM and FDTD introduce a positive shift in the calculation of the cutoff wavenumbers of homogeneous cavities. However, the results for the difference equations show that both methods can have positive or negative frequency shifts in inhomogeneous cavities (with several dielectrics). The reason is due to an interface effect which introduces another source of error.

The second result was obtained with the analytical solution of TLM for a capacitive diaphragm in a TEM waveguide. Usually, TLM solutions of irises and diaphragms (and filters composed by these elements) present a frequency shift in the calculated response. It was observed that in these cases the numerical solution converged linearly to the actual result. The analytical solution of the discrete problem showed the reason. In the numerical solution, a first-order error term in the form of a stray reactance is in shunt with the exact reactance. This stray reactance causes the linear convergence to the exact result.

5.2 Sources of error in TLM

The TLM method solves a discrete approximation of a continuous problem. Therefore, the solution of the discrete problem may have some features that are not present in the continuous one [22], [69].

The differences between the solutions are caused by the discretization of space and time. As mentioned before, there are three main sources of spatial error: dispersion, coarseness, and discretization errors [2]. The next sections will discuss each of them.

There are also other sources of error in TLM. These usually occur in the processing of the data before or after a simulation. This thesis will only present the analysis of the error caused by spatial discretization.

5.2.1 Dispersion or velocity error

The velocity error is a result of the discretization of the problem. This error can be reduced by refining the mesh, but it will always be present. The dispersion analysis of the TLM method quantifies the minimum error present in a simulation.

The dispersion analysis is performed in free-space with an infinite mesh [22]. However, this mesh is composed of discrete points. Wavelengths of the order of two spatial

discretization step (or smaller) cannot be represented in the mesh.

In the free space case, if the minimum wavelength is much larger than the spatial discretization, the error is substantially reduced. Since the dispersion erroris the minimum error present in any simulation, the total error in any given problem will always be equal or greater than the velocity erro

5.2.2 Coarseness error

The coarseness is also a result of the discretization of the problem. The coarseness error is present when edges are simulated, Figure 5.1.

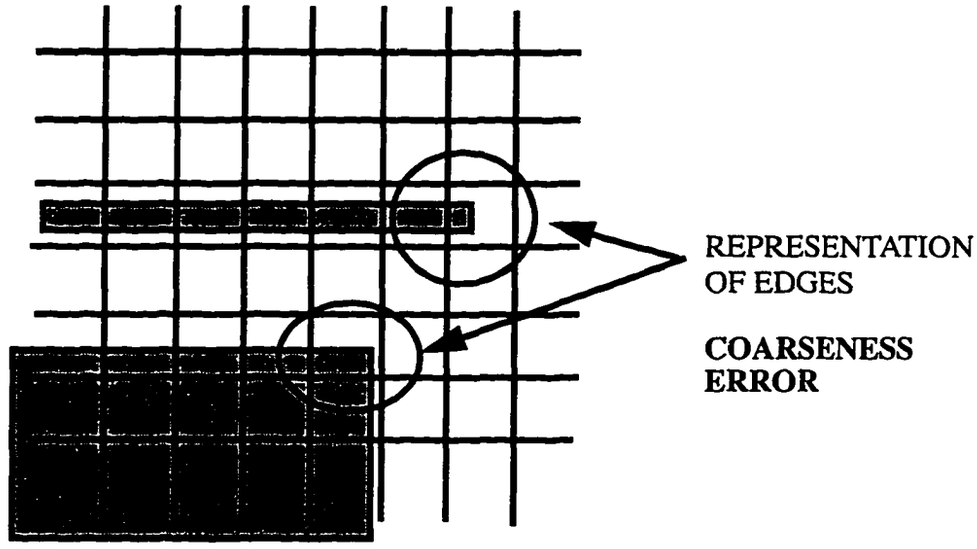

Figure 5.1 Coarseness error in a two-dimensional TLM mesh. In both cases presented here, only a very fine discretization will be able to represent the features of the problem. The field at the edge is not properly represented in the mesh and the position of the object is changed because its boundary must lie between adjacent transmission lines

In the solution of problems with fine features such as infinitesimally thin wedges or wires the coarseness error is the dominant source of error.

In these cases, the coarseness error is caused by the finite number of modes present in the mesh. The main effect is a reduction of the convergence rate of TLM from second-order to first-order. Therefore if the discretization of the mesh is doubled, the error is reduced by a factor of two instead of four, as in the second-order case.

The coarseness error can be reduced by using special nodes to represent fine features.

5.2.3 Discretization error

The discretization problem is caused by errors in the placement of boundaries in TLM. This error arises when solving problems containing circles, ellipses, spheres and ellipsoids. The problem is caused by the rectangular nature of the mesh.

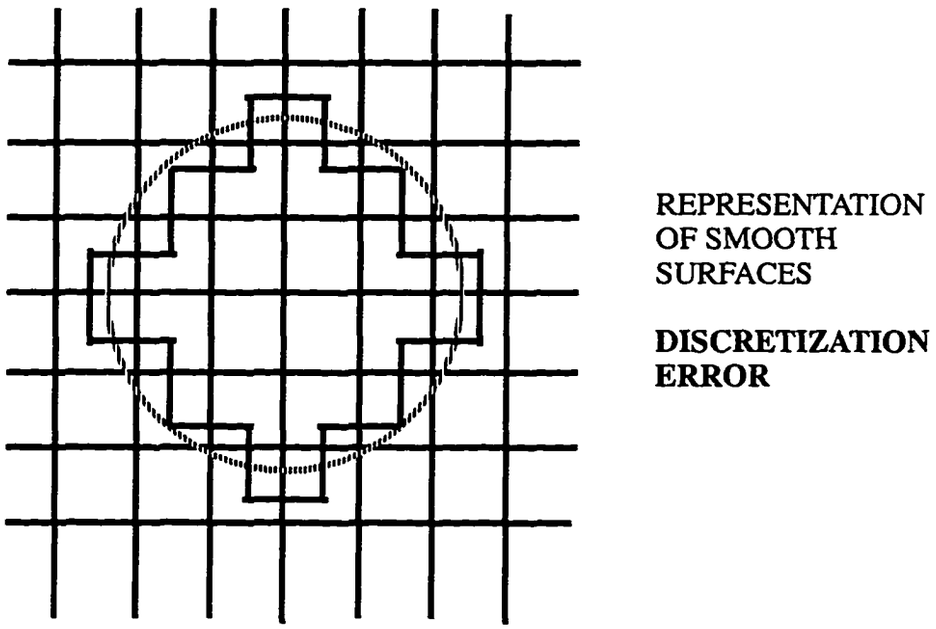

Figure 5.2 Discretization error in a two-dimensional mesh. The circle is represented by a combination of rectangular areas.

The dispersion analysis can be used to quantify the effect of discretization and coarseness errors in the propagation constant. When this analysis is performed in homogeneous unbounded space, it cannot provide information regarding the error in the placement of boundaries. However, by connecting the nodes at an open or short-circuited boundary, it is possible to quantify the coarseness and discretization error of the problem.

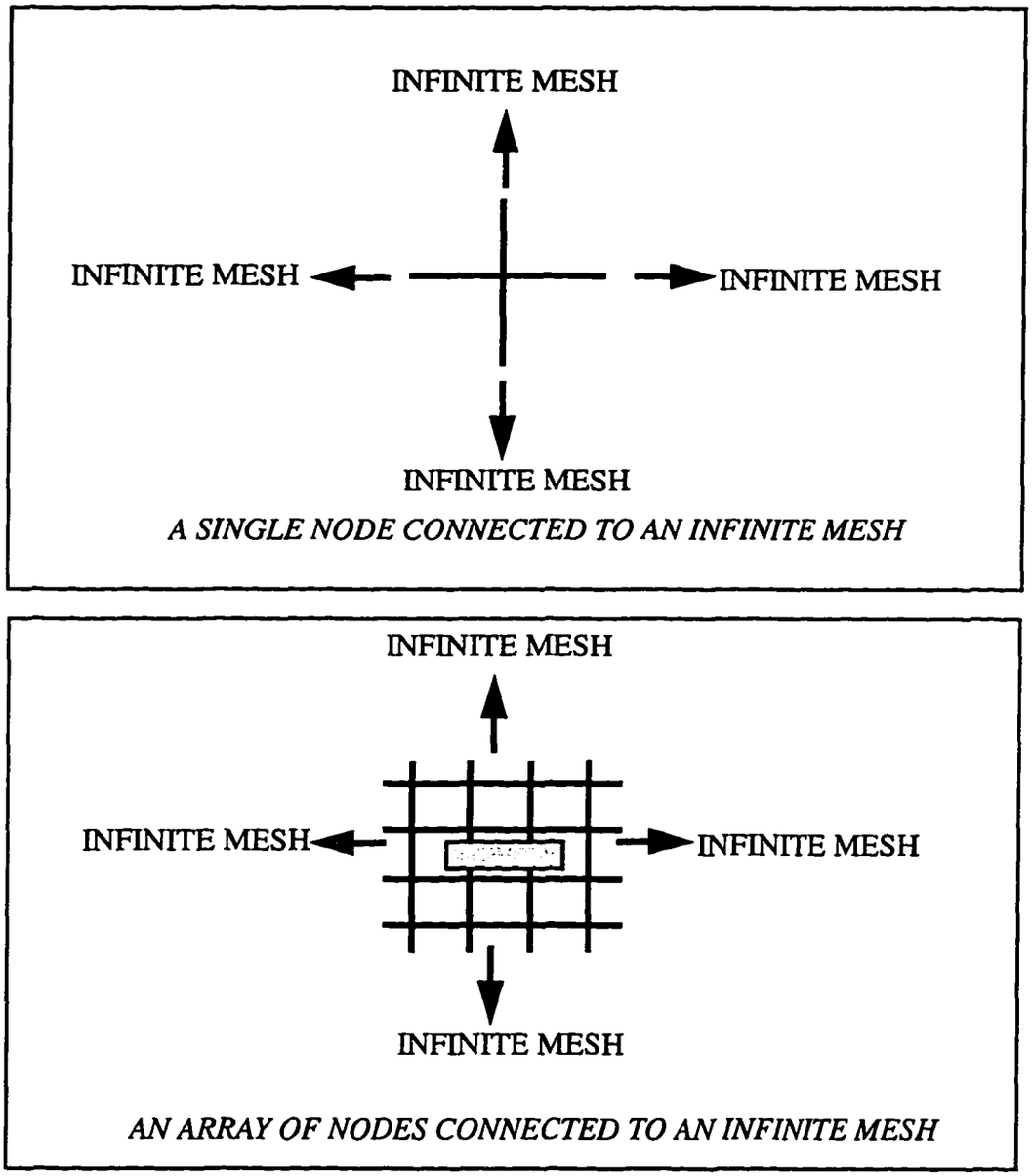

Figure 5.3 The dispersion of an array of nodes enclosing the discontinuity can be used to quantify the coarseness and discretization errors.

The main problem is that this approach leads to large matrices.

The discretization error can be eliminated by using special schemes in the placement of the boundaries.

5.3 Error analysis in TLM

The objective of error analysis in TLM is to identify and quantify the sources of error in TLM. In the previous section, three major sources of error in TLM were presented. These were the coarseness, dispersion and discretization errors. The velocity error can be quantified with dispersion analysis. The actual error caused by the discretization and coarseness is problem dependent. It is difficult (if not impossible) to obtain error bounds for a general case.

The main technique to quantify the velocity error in TLM is the dispersion analysis [22]. It is the solution of a TLM mesh in the frequency domain assuming Floquet modes in the mesh. These modes are complex exponentials with unknown propagation constants. The propagation constants are obtained by transforming the TLM algorithm into an eigenvalue problem. The solution of the eigenvalue equations yields the dispersion relation of the method. This analysis is performed in the homogeneous free-space case.

A second analysis technique was developed in this thesis. The procedure relies on the solution of the difference equation of TLM. Its solution can be obtained not only for the free-space case, but also for various boundary value problems. This technique can quantify the discretization, dispersion and coarseness errors in each of these cases.

The technique employs the separation of variables in a rectangular coordinate system. Once the wave equation is separated, the solution is obtained for each coordinate direction. As in the continuous case, the total solution is the product of the solutions in each direction [31]-[33].

5.3.1 Dispersion analysis

The generalized dispersion analysis of two- and three-dimensional TLM networks was presented in 1993 by Nielsen and Hoefer [22]. The authors derived closed-form dispersion relations for the two-dimensional shunt and series nodes and the three-dimensional expanded node.

The solution procedure considers steady-state solutions of the form:

$$f(x, y, z, t) = A\exp(j(k_x x + k_y y + k_y z + \omega t)) \tag{5.1}$$

The substitution of these modes into the TLM scheme will result in an eigenvalue equation:

$$[\mathbf{P}]\,[\mathbf{S}] = [\mathbf{T}] \tag{5.2}$$

The solution of the eigenvalue equation:

$$\det\left([\mathbf{I}] - [\mathbf{T}]\,[\mathbf{P}]\,[\mathbf{S}]\right) = 0 \tag{5.3}$$

is the dispersion relationship. The matrices [**T**], [**P**] and [**S**] depend on the type of the node [22].

The number of solutions of dispersion relation will be equal to the order of the matrix. In the vacuum, the two-dimensional node will have four solutions: two are static and two are propagating. The propagating solutions are characterized by the equation [23]:

$$2\cos(k_0\Delta l) = \cos(k_x\Delta l) + \cos(k_z\Delta l) \tag{5.4}$$

In free space a three-dimensional node will have 12 solutions, four are static and eight are propagating. In the case of the symmetrical condensed node, two of these solutions will be spurious. The propagating and spurious solutions are given by the equation [23], [25]:

$$\begin{aligned} \cos(k_0\Delta l) &= \frac{1}{2}(XY + XZ + YZ - 1) \\ X &= \cos(k_x\Delta l) \\ Y &= \cos(k_y\Delta l) \\ Z &= \cos(k_z\Delta l) \end{aligned} \tag{5.5}$$

These equations result from the discretization of the continuous problem. The relations are periodic in space as well as in time. This causes the presence of passbands and stopbands in the solution spectra.

The relations are also anisotropic. The dispersion in the axial directions is different from that in the diagonal directions. Finally, the relations are frequency dependent. The phase and group velocities of the waves propagating through a TLM mesh change with frequency.

Since the phase and group velocities are frequency dependent, a simulation of a cavity will result in a frequency shift effect [2]. This is characteristic of the discretization of space. The discrete solution is a mapping of the continuous frequency spectrum into periodic frequency bands. This effect could be corrected if the scheme was not anisotropic. This means that the frequency mapping is also direction dependent [22].

The TLM provides accurate results only in the range where the wavelength is at least 10 times larger than the spatial step.

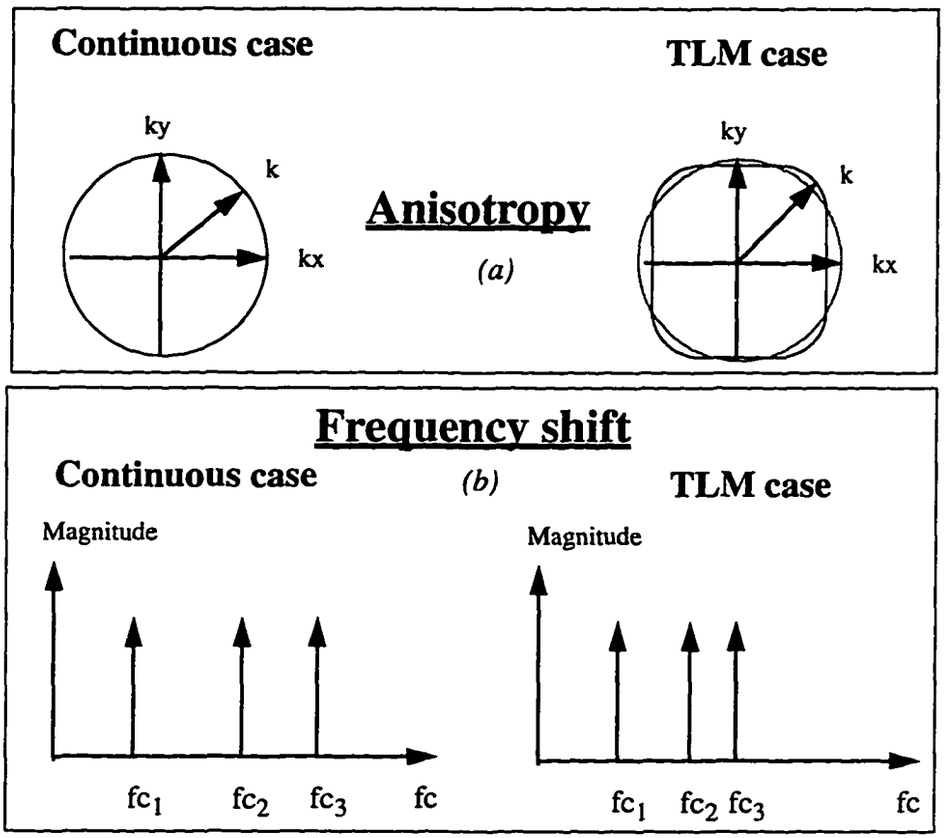

Figure 5.4 The effect of anisotropy and frequency shift in TLM (These effects were exaggerated for the sake of clarity). (a) The relationship between the wavenumbers kx and ky in the continuous case describe a circle with radius k. In TLM, the circle is transformed into a distorted circle. (b) The shorter the wavelength (high frequencies), the greater the frequency shift (caused by the frequency mapping).

Since the node is anisotropic, the dispersion is not equal in all directions. The direction of maximum dispersion is a characteristic of a particular node. In the two-dimensional case, this is the axial direction. In the three-dimensional symmetric condensed node, it is the main diagonal direction.

5.3.2 Solution of difference equations

This procedure consists of solving the difference equation of the scheme with the boundary conditions of the discrete problem. The result can be used to quantify the effects of the discretization and coarseness errors in specific problems.

This technique is problem dependent. While dispersion analysis provides a general picture of the behavior of TLM, the solution of difference equations is problem specific. However, the solution of some specific problems allows to draw some conclusions regarding the behavior in a general case.

Using this procedure, it was verified that TLM and FDTD are second-order accurate only if logarithmic singularities are not present. In the case of wedges, both methods are only first-order accurate.

The application of this technique to inhomogeneous problems revealed a dielectric interface effect in TLM. An error in the positioning of the interface between two dielectrics in TLM can have substantial impact on the accuracy of a simulation. The higher the difference between dielectric constants, the greater this effect can be.

The first-order convergence and dielectric interface effect cannot be verified by dispersion analysis. In these cases, the solution of difference equations can be used to quantify coarseness and discretization errors of a general simulation. The general procedure is based in the solution of the difference wave equation (which is the difference equation for the electric field in two-dimensional shunt TLM):

$$\Phi^{k+1}_{(m,n)} = c\frac{\Delta t}{\Delta l}\left[\Phi^{k}_{(m+1,n)} + \Phi^{k}_{(m-1,n)} + \Phi^{k}_{(m,n+1)} + \Phi^{k}_{(m,n-1)}\right] - \Phi^{k-1}_{(m,n)} \qquad (5.6)$$

The partial difference equation is transformed into a set of one-dimensional difference equations. This is done using separation of variables:

$$\begin{aligned} X(x+\Delta l) &= (2-(k_x\Delta l)^2)\,X(x) - X(x-\Delta l) \\ Z(z+\Delta l) &= (2-(k_z\Delta l)^2)\,Z(z) - Z(z-\Delta l) \\ E_y(x,z) &= X(x)\,Z(z) \\ k_x^2 + k_z^2 &= \frac{2}{(c\Delta t)^2}\sin^2\left(\frac{\omega\Delta t}{2}\right) \end{aligned} \qquad (5.7)$$

where X(x) and Z(z) are only functions of x and z, respectively, and k_x and k_z are the separation constants.

The solution of each of these equations is performed using the z-transform [66] or assuming a finite series solution. Usually, the finite series formulation is used in space, since the mesh size is not infinite.

In theory, any series that satisfies the boundary conditions can be used. However, there is an advantage to using finite Fourier series. Each term of the series can be considered as a natural solution mode of problem. The solution of the discrete problem can be also expressed as a sum of natural modes. These discrete modes have the same mathematical representation as continuous modes.

The difference equations can also be used to solve inhomogeneous problems. In these cases, the problem is divided into several homogeneous problems. These problems are connected using boundary conditions.

The boundary conditions and mesh size of the simulated problem are the same as those imposed upon the difference equations. The result is a natural inclusion of the coarseness and discretization errors in the solution of the difference equations.

5.4 Dispersion analysis of dispersive dielectrics

This section describes the dispersion analysis of frequency dependent dielectrics. The analysis is performed by reducing the order of the TLM matrix to the free-space case. This is possible by assuming harmonic excitation of the mesh. In this case, the nodal source of a passive medium can be included in the scattering matrix of the node, which reduces the order of the TLM matrix. In the stub-loaded node case, the procedure is equivalent to the elimination of the stub by changing the impedance of the remaining transmission lines.

The dispersion characteristic of TLM is obtained by solving (5.3). This equation can be used in the two and three-dimensional cases [22]. In the case of the two-dimensional node with stub, the order of these matrices is four for the free-space case. In the stub-loaded case the matrices are of order five. In the three-dimensional SCN case the free space node is of order twelve and the stub-loaded node is of order eighteen.

The order of the scattering matrix is reduced to the free-space case by using frequency domain transformations. This reduces the analytical effort involved in the solution of the dispersion equation. It also establishes the equivalence between the stub-loaded and nodal source models of constitutive relationships.

The reduction of the order of the matrix is performed by obtaining the relationship between the incident and reflected voltages at the stub (or at the source) and the total voltage and current at the node.

The analysis will be presented for the two-dimensional shunt node. The procedure is similar for other kinds of nodes. The relationship between incident and reflected voltages at the stub-port and the total voltage at the node are:

$$v^i_{stub}(t+k\Delta t) = v^r_{stub}(t) \qquad v^r_{stub}(t) + v^i_{stub}(t) = v_{node}(t) \tag{5.8}$$

where Δt is the timestep and v_{node} is the voltage across the node. Using the Fourier Transform of (5.8) and combining the two equations results in:

$$V^i_{stub}(\omega) = \frac{V_{node}(\omega)}{1+\exp(j\omega\Delta t)} \tag{5.9}$$

The substitution of this relationship into the scattering matrix of the two-dimensional shunt node reduces the order of the matrices to four.

The same procedure can be applied to the nodal source where the relationship is:

$$8v^i_{ay}(t) = 4v_y(t) - 2\Delta t(\varepsilon_r - 1)\frac{d}{dt}v_y(t) \tag{5.10}$$

5.4.1 The two-dimensional case

The matrix is reduced by substituting the voltage incident from the stub (or the source) in the expression of the total voltage across the node:

In the stub-loaded shunt node case:

$$v_y(t) = \frac{2}{4+y}\left(v^i_1(t) + v^i_2(t) + v^i_3(t) + v^i_4(t)\right) + \frac{2y}{4+y}v^i_5(t) \tag{5.11}$$

In the nodal source case the total voltage is:

$$v_y(t) = \frac{1}{4}\left(v^i_1(t) + v^i_2(t) + v^i_3(t) + v^i_4(t)\right) + v^i_s(t) \tag{5.12}$$

These equations can be used to assemble the scattering matrix of the node:

$$[S] = \frac{1}{\upsilon}\begin{bmatrix} 1-\upsilon & 1 & 1 & 1 \\ 1 & 1-\upsilon & 1 & 1 \\ 1 & 1 & 1-\upsilon & 1 \\ 1 & 1 & 1 & 1-\upsilon \end{bmatrix} \tag{5.13}$$

where in the stub-loaded case:

$$\upsilon = 2\,(1 - j\,(\varepsilon_r - 1)\tan(\omega\Delta t/2))$$
$$\omega\Delta t = k_0\Delta l \tag{5.14}$$

and in the nodal source case:

$$\upsilon = 2\,(1 - j\omega\Delta t\,(\varepsilon_r - 1)) \tag{5.15}$$

The derivative in time needs to be represented with some discretization scheme. The main discretization schemes used in this case are:

Backwards Euler:

$$j\omega = j\frac{\sin(\omega\Delta t/2)}{\Delta t}\exp(-j\frac{\omega\Delta t}{2}) \tag{5.16}$$

Trapezoidal

$$j\omega = j\frac{2}{\Delta t}\tan(\frac{\omega\Delta t}{2}) \tag{5.17}$$

In the case of the trapezoidal approximation of the derivative, the stub-loaded and nodal source approaches are equal.

The substitution of the scattering matrix into the dispersion relation results in the closed form dispersion equation:

$$2\cos(k_0\Delta l) + j\,(2 - \upsilon)\sin(k_0\Delta l) = \cos(k_x\Delta l) + \cos(k_z\Delta l) \tag{5.18}$$

The stub-loaded model is a particular case of the nodal source approach. Therefore only the nodal source approach will be studied in this section.

A useful way to visualize the dispersion relationship is to use an equivalent dielectric constant. In the characterization of dispersive dielectrics, this is perhaps the best form to quantify the dispersion error.

The equivalent dielectric constant is defined with respect to a particular propagation direction. The definition in the u (u= x,z) direction is:

$$\varepsilon_r(\omega) = \frac{k_0^2}{k_u^2} \tag{5.19}$$

This result is compared to the dielectric relationship of the dielectric.

The dispersion relationship for the two-dimensional case for the linear non-disper-

sive dielectric was calculated considering two discretization schemes: backwards Euler and trapezoidal. The solution for various values of the dielectric constant is shown in Figure 5.5.

The backwards Euler approach introduces numerical losses to the solution. In the low frequency range, the loss is independent of the dielectric being modeled. In this discretization scheme the concept of cutoff frequencies is not well defined.

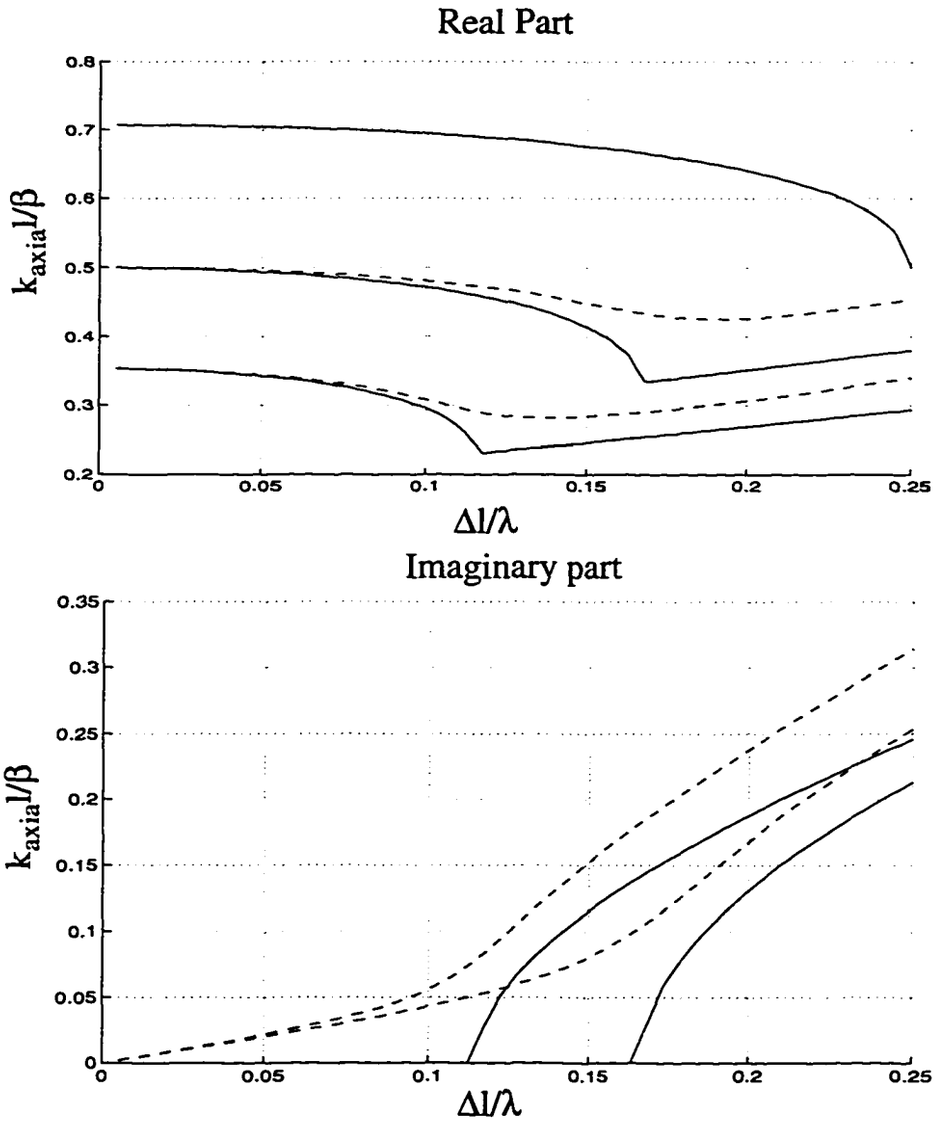

Figure 5.5 Dispersion of the two-dimensional TLM node. The solid line was obtained with trapezoidal discretization. The dashed line was obtained with backwards Euler discretization.

In the case of a first-order Debye representation of dielectric behavior:

$$\varepsilon_r(\omega) = \varepsilon_\infty + \frac{\varepsilon_s - \varepsilon_\infty}{1 + j\omega\tau_0} \tag{5.20}$$

The dielectric behavior was studied only in the direction of maximum dispersion. In this case it is the axial direction (x or z). Using the trapezoidal discretization scheme results in the propagation vector

$$k_{10}\Delta l = \operatorname{acos}\left[1 - 4\sin^2\left(\frac{\omega\Delta t}{2}\right)\frac{\varepsilon_s\cos\left(\frac{\omega\Delta t}{2}\right) + j\frac{2\tau_0}{\Delta t}\varepsilon_\infty\sin\left(\frac{\omega\Delta t}{2}\right)}{\cos\left(\frac{\omega\Delta t}{2}\right) + j\frac{2\tau_0}{\Delta t}\sin\left(\frac{\omega\Delta t}{2}\right)}\right] \tag{5.21}$$

Another way to represent the dispersive behavior is to compare the equivalent dielectric constant. with the dielectric relationship. In the case corresponding to (5.20), the equivalent dielectric constant is:

$$\varepsilon_r(\omega) = \frac{\left(\operatorname{asin}\left[\sqrt{2}\sin\left(\frac{\omega\Delta t}{2}\right)\sqrt{\varepsilon_\infty + \frac{\varepsilon_s - \varepsilon_\infty}{1 + j\frac{2\tau_0}{\Delta t}\tan\left(\frac{\omega\Delta t}{2}\right)}}\right]\right)^2}{(\omega\Delta t)^2} \tag{5.22}$$

Comparing (5.20) with (5.22) shows a shift in the material relaxation frequency. The maximum relaxation frequency shift introduced by TLM in the dielectric behavior is given by:

$$\frac{\Delta\omega}{\omega} = 1 - \frac{2\tau_0}{\Delta t}\operatorname{atan}\left(\frac{\Delta t}{2\tau_0}\right) \tag{5.23}$$

The shift is of the order of:

$$\frac{\Delta\omega}{\omega} \approx 1 - 2\frac{\tau_0}{\Delta t}\operatorname{atan}\left(\frac{\Delta t}{2\tau_0}\right) \approx \left(\frac{\Delta t}{2\tau_0}\right)^2 \tag{5.24}$$

where $\Delta t/\tau_0$ is the relative time constant of the medium.

The dispersion relation was plotted with respect to the variation of the relative time constant. The best results are obtained with relatively large time constants (as expected from (5.23)). The analysis shows no problems with the representation in the low fre-

quency range. The results are shown in Figure 5.6.

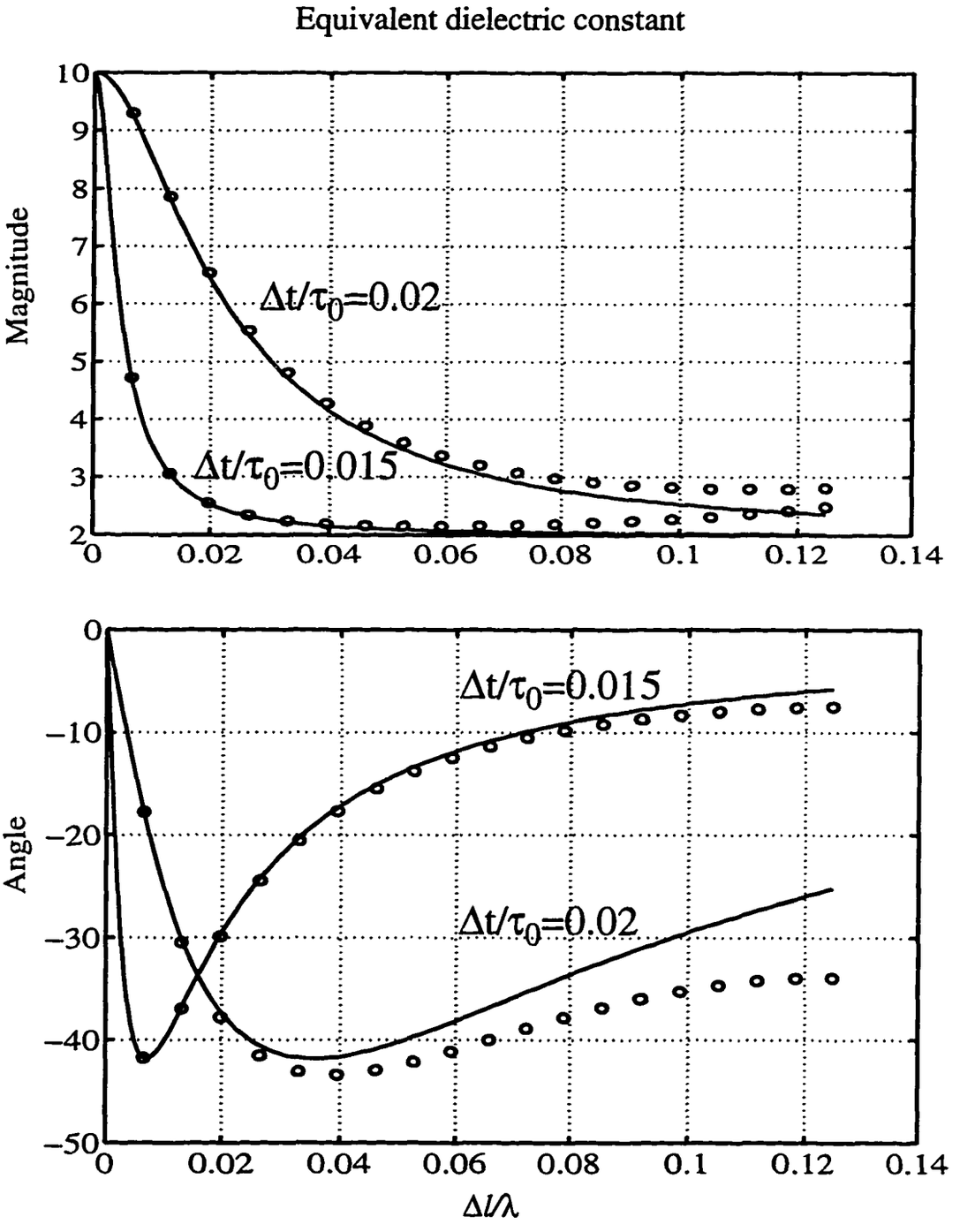

Figure 5.6 Dispersion of the two-dimensional TLM node. Solid line - exact relative permittivity, o - TLM equivalent relative permittivity. The medium is a first-order Debye dielectric represented with the trapezoidal discretization scheme. The graph shows the magnitude and phase angle of the equivalent dielectric constant of the medium.

The second-order Lorentz representation of dielectrics is:

$$\varepsilon_r(\omega) = \varepsilon_\infty + \frac{(\varepsilon_s - \varepsilon_\infty)\,\omega_0^2}{\omega_0^2 + j\omega\delta_0 - \omega^2} \tag{5.25}$$

Using the equivalent dielectric representation for the axial direction results in:

$$\varepsilon_r(\omega) = \frac{\left(\operatorname{asin}\left[\sqrt{2}\sin\left(\frac{\omega\Delta t}{2}\right)\sqrt{\varepsilon_\infty + \zeta}\right]\right)^2}{(\omega\Delta t)^2}$$

$$\zeta = \frac{(\varepsilon_s - \varepsilon_\infty)\,(\Delta t\omega_0)^2}{(\Delta t\omega_0)^2 + j\left(2\tan\left(\frac{\omega\Delta t}{2}\right)\right)\delta_0\Delta t - \left(2\tan\left(\frac{\omega\Delta t}{2}\right)\right)^2} \tag{5.26}$$

There is also a resonant frequency shift present in this representation. The error is:

$$\frac{\Delta\omega}{\omega} \approx \left(\frac{(\omega_0\Delta t)^2 - (\delta_0\Delta t)^2}{4}\right) \tag{5.27}$$

where $\omega_0\Delta t$ is the relative resonant frequency and $\delta_0\Delta t$ is the relative loss of the medium.

The dispersion relation was plotted with respect to the change in the relative resonant frequency. The equivalent dielectric constant results are in good agreement with the analytical ones. The expression (5.27) is valid for relative resonant frequencies lower than 0.25. The frequency shift increases with the relative resonant frequency.

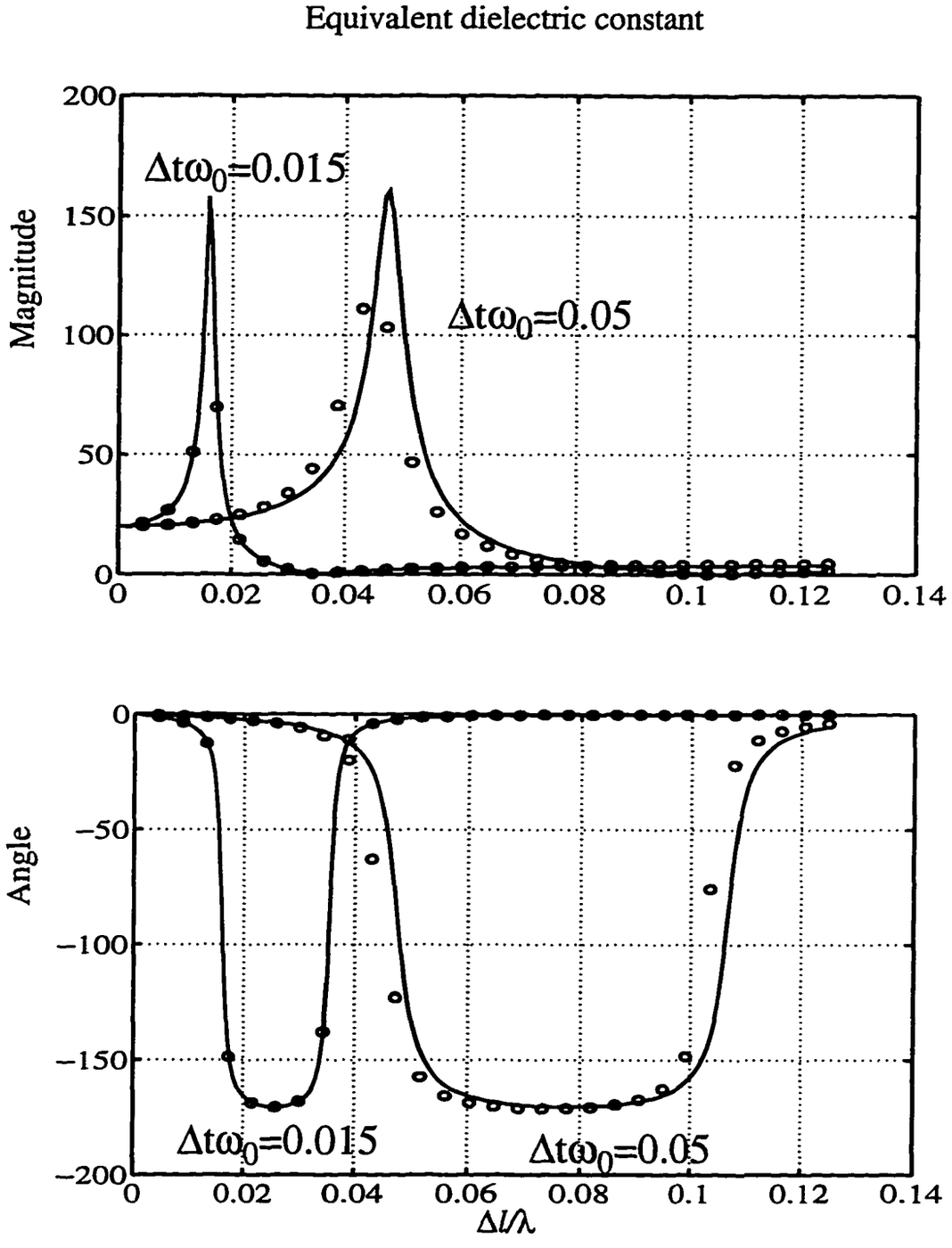

Figure 5.7 Dispersion of the two-dimensional TLM node. Solid line - exact relative permittivity, o - TLM equivalent relative permittivity. The medium is a second-order Lorentz dielectric represented with the trapezoidal discretization scheme. The graph shows the equivalent dielectric constant for two resonant frequency values.

5.4.2 The three-dimensional case

The study of the three-dimensional case will be restricted to the symmetrical condensed node [16]. The results are obtained using the same procedure as in the two-dimensional case. The major problems associated with the calculations are the size of the mesh and the complexity involved. The scattering matrix is of order twelve. In this analysis the relative permeability was considered to be unity.

The final expression is a fifth-order polynomial. There is no closed-form solution possible in this case [26], [27]. The solution can be obtained only for particular directions of propagation: axial, secondary and main diagonals. In the SCN the main diagonal is the direction of maximum dispersion.

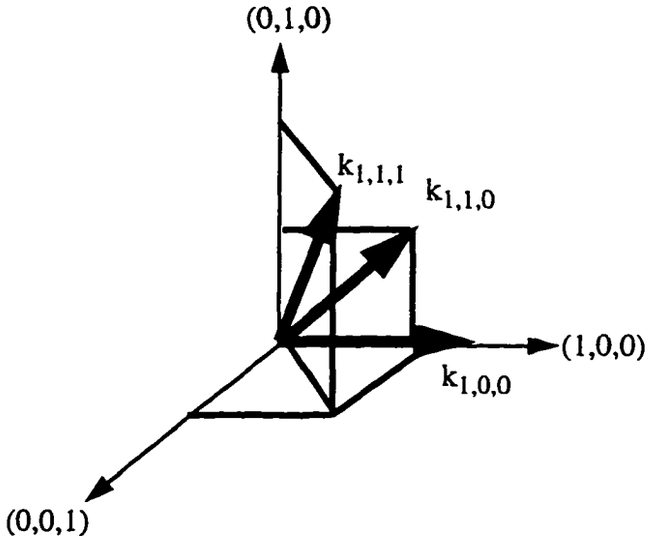

Figure 5.8 Main directions of propagation in three-dimensions. The axial (1,0,0), secondary diagonal (1,1,0) and main diagonal (1,1,1) are represented in the figure.

The expressions for the normalized propagation constant of propagating modes for the linear isotropic non-dispersive dielectric case are for:

Axial propagation:

$$k_{100}\Delta l = \text{acos}\left[\frac{\sqrt{\varepsilon_r}\sin(\omega\Delta t)}{\sqrt{\varepsilon_r + \cos(\omega\Delta t) - \varepsilon_r\cos(\omega\Delta t)}}\right] \tag{5.28}$$

Secondary diagonal propagation:

$$k_{110}\Delta l = \operatorname{acos}\left[1 - 4\varepsilon_r \sin^2\left(\frac{\omega\Delta t}{2}\right)\right] \tag{5.29}$$

Main diagonal propagation:

$$k_{111}\Delta l = \operatorname{acos}\left[\frac{1}{3}\left(8\left(\varepsilon_r - 1\right)\sin^2\left(\frac{\omega\Delta t}{2}\right) + \sqrt{R}\right)\right]$$
$$R = 16\left(\varepsilon_r^2 + \varepsilon_r + 1\right)\cos^2\left(\frac{\omega\Delta t}{2}\right)\cos\omega\Delta t + 1 - 8\varepsilon_r - 8\varepsilon_r^2\cos\omega\Delta t \tag{5.30}$$

There is also a second mode in the main diagonal direction. This is the spurious mode of propagation with the normalized propagation constant:

$$k_s\Delta l = \pi - \operatorname{acos}\left[\frac{1}{3}\left(8\left(\varepsilon_r - 1\right)\sin^2\left(\frac{\omega\Delta t}{2}\right) + \sqrt{R}\right)\right] \tag{5.31}$$

In the low frequency range the dielectric constant of the spurious mode is very high. Therefore, this mode propagates much slowly than the physical modes. This is a feature of the spurious mode which is independent of the value of the dielectric.

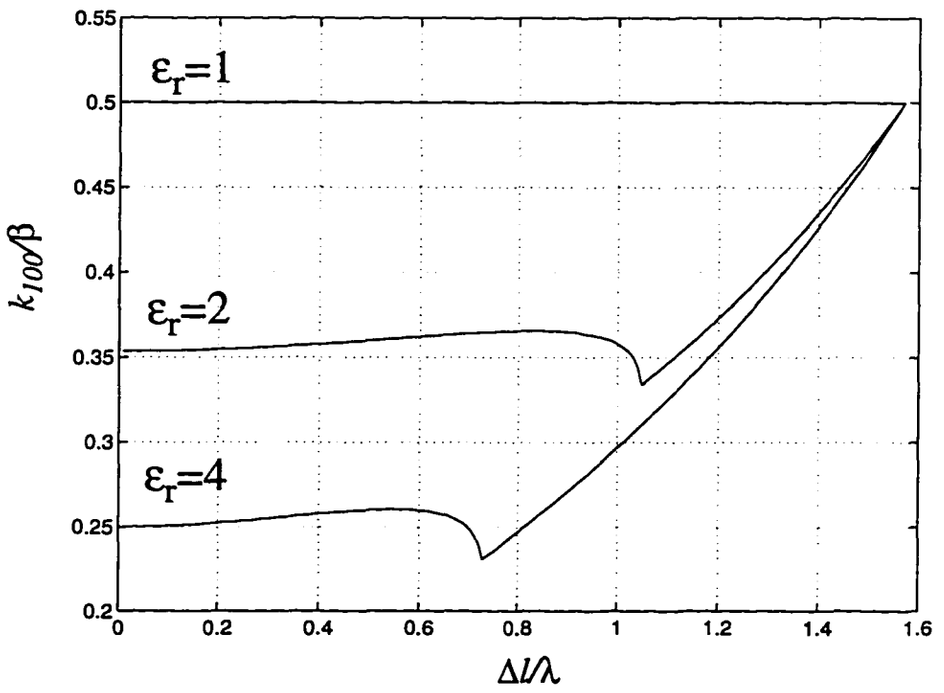

Figure 5.9 Dispersion of the symmetrical condensed node along the 100 direction of propagation. The propagation along the axial planes is less dispersive than that in the FDTD method [23].

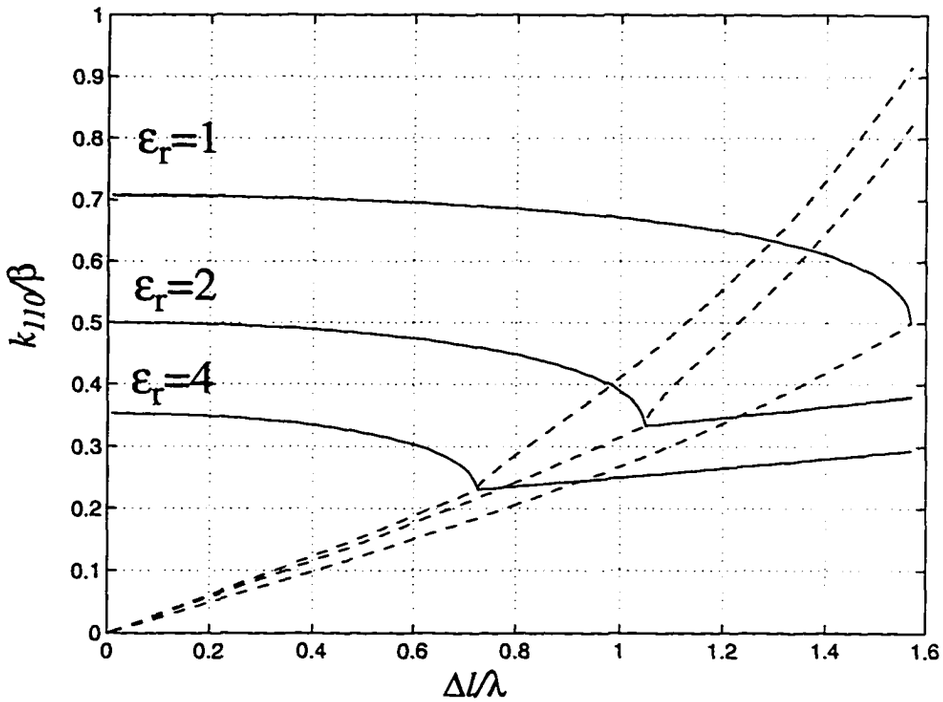

Figure 5.10 Dispersion of the symmetrical condensed node along the 110 direction of propagation.

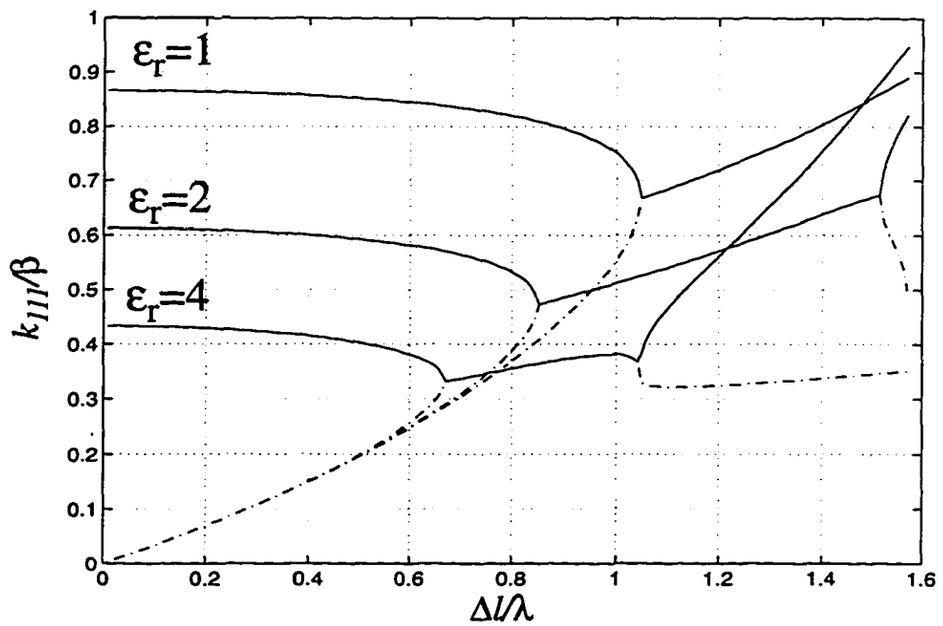

Figure 5.11 Dispersion of the symmetrical condensed node along the 111 direction of propagation. The worst dispersion occurs along this direction (main diagonal). It is also along this direction that spurious modes are supported.

The main problem in the study of linear dispersive media in the SCN is anisotropy. The equivalent dielectric constant is different depending on the direction of propagation. However, in the low frequency range the node can be considered approximately isotropic. Therefore, all the calculations can be performed considering only one particular direction.

A comparison between the equivalent dielectric constants in all directions was performed. The conclusion is that in the low frequency range, the results obtained with the two-dimensional analysis can be used in the symmetrical condensed node scheme.

The results for the first-order and second order dielectrics are presented for the main diagonal direction (worst dispersion error).

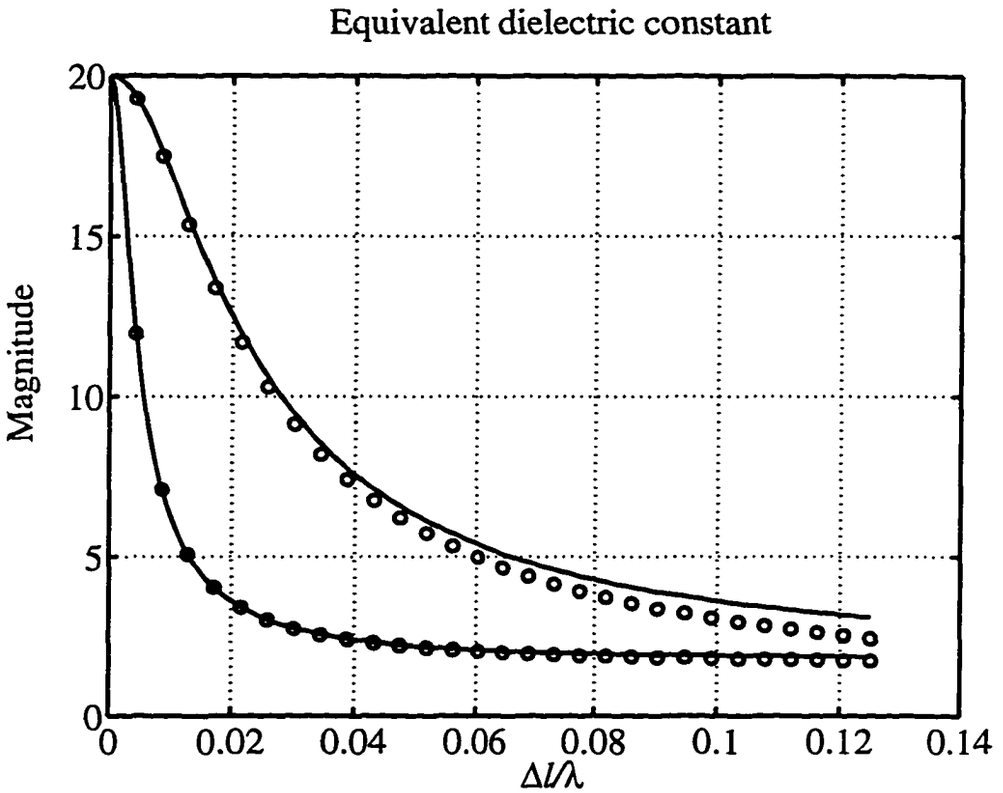

Figure 5.12 Dispersion of the symmetrical condensed node for a first-order Debye dielectric along the (111) direction for two values of $\Delta t/\tau_0$ ($\Delta t/\tau_0$=0.01 and $\Delta t/\tau_0$=0.02)The equivalent dielectric constant is compared to the analytical value of the constant. Solid line - exact relative permittivity, o - TLM equivalent relative permittivity.

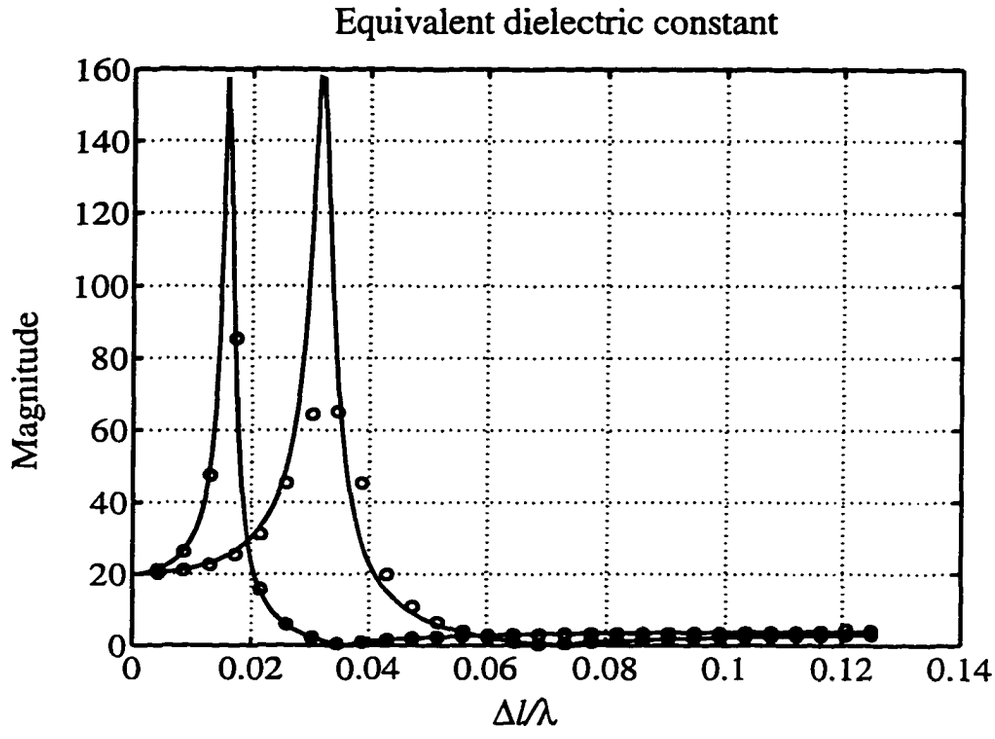

Figure 5.13 Dispersion of the symmetrical condensed node with a second-order Lorentz dielectric along the main directions of propagation for two relative resonant frequencies $\Delta t\omega_0$ ($\Delta t\omega_0$ =0.01 and $\Delta t\omega_0$ =0.02). The equivalent dielectric constant is compared to the analytical value of the constant. Solid line - exact relative permittivity, o - TLM equivalent relative permittivity.

5.5 Difference equations

This section describes the solution of TLM difference equations. The solution of difference equations of a numerical method is different from a dispersion analysis. The dispersion analysis solves the numerical scheme in an infinite homogeneous mesh [22]. The difference equation of the method can be solved in a finite inhomogeneous case.

The dispersion analysis provides general, geometry independent features of the method. The solution of difference equations is geometry dependent and accounts for specific features of the problem.

The solution of TLM difference equations requires some transformations to the scheme. Once the scattering and propagation parts of the method are combined, the electric and magnetic field difference equations can be obtained.

In the three-dimensional case, the equations will be coupled. The uncoupled equations are obtained with the formulation of discrete electric and magnetic potentials.

However, in the two-dimensional shunt node case, the electric field difference equation is not coupled to the other components. Therefore, in the shunt node case, the electric field equation can be used to characterize the scheme.

The solution procedure for the wave difference equation is similar to the continuous counterpart [31]-[33]. The partial difference equation is transformed into a set of one-dimensional difference equations using the separation of variables.

Each of these equations is solved, and the combination of all solutions is subject to the boundary conditions. Since the mesh is finite, all spatial solutions are usually expressed as a finite Fourier series. As in the continuous case, the solution is also a combination of modes.

In some cases, the quasi-static approximation of the solution is sufficient to verify some of TLM properties. The quasi-static solution of TLM can also be obtained by using the discrete Laplace equation.

In the characterization of TLM convergence this is a useful result. In the general characterization of discontinuities, the sum of higher-order modes is in general converging fast. The convergence of the method in these cases is determined by the convergence of the static solution.

5.5.1 The wave difference equation

In the case of TLM, the scattering and propagation of voltages represent the difference equations that describe the electric and magnetic fields. The procedure relies on the transmission line analogy, describing the propagation and scattering of voltage pulses through an array of transmission lines. During a simulation, the field components can be obtained from the stream of voltage pulses. In the two-dimensional shunt node case, the voltages scattered at each node are obtained from the incident voltages by:

$$\begin{bmatrix} v_1 \\ v_2 \\ v_3 \\ v_4 \end{bmatrix}^{r}_{k+1} = \frac{1}{2}\begin{bmatrix} -1 & 1 & 1 & 1 \\ 1 & -1 & 1 & 1 \\ 1 & 1 & -1 & 1 \\ 1 & 1 & 1 & -1 \end{bmatrix}\begin{bmatrix} v_1 \\ v_2 \\ v_3 \\ v_4 \end{bmatrix}^{i}_{k} \tag{5.32}$$

These reflected pulses are transferred to the neighboring nodes by:

$$\begin{aligned} v_1^i(m,n) &= v_3^r(m+1,n) & v_4^i(m,n) &= v_2^r(n+1) \\ v_3^i(m,n) &= v_3^r(m-1,n) & v_2^i(m,n) &= v_4^r(n-1) \end{aligned} \tag{5.33}$$

The field components are obtained using the voltage-to-field mapping:

$$\begin{bmatrix} E_y \\ Z_0 H_x \\ Z_0 H_z \end{bmatrix} = \frac{1}{2} \begin{bmatrix} 1 & 1 & 1 & 1 \\ \sqrt{2} & 0 & -\sqrt{2} & 0 \\ 0 & -\sqrt{2} & 0 & \sqrt{2} \end{bmatrix} \begin{bmatrix} v_1 \\ v_2 \\ v_3 \\ v_4 \end{bmatrix}^i \tag{5.34}$$

However, there is no unique field-to-voltage mapping [70]. Considering the fourth eigenvector solution of the dispersion relationship as an additional field component W results in a unique mapping. The component obtained from the null space of (5.34) has the dimensions of an electric field [65]. The unique field-to-voltage mapping is:

$$\begin{bmatrix} v_1 \\ v_2 \\ v_3 \\ v_4 \end{bmatrix}^i = \frac{1}{2} \begin{bmatrix} 1 & \sqrt{2} & 0 & 1 \\ 1 & 0 & -\sqrt{2} & -1 \\ 1 & -\sqrt{2} & 0 & -1 \\ 1 & 0 & \sqrt{2} & 1 \end{bmatrix} \begin{bmatrix} E_y \\ Z_0 H_x \\ Z_0 H_z \\ W \end{bmatrix} \tag{5.35}$$

The additional field component completes the bijective mapping. Using this mapping, the TLM algorithm is transformed into a set of difference equations. The electric field is not coupled to any other components.

The electric field difference equation is:

$$E_{y(m,n)}^{k+1} = \frac{1}{2}\left[E_{y(m+1,n)}^{k} + E_{y(m-1,n)}^{k} + E_{y(m,n+1)}^{k} + E_{y(m,n-1)}^{k}\right] - E_{y(m,n)}^{k-1} \tag{5.36}$$

The remaining equations for other field components are:

$$\begin{aligned} H_{x(m,n)}^{k+1} &= H_{x(m+1,n)}^{k} + H_{x(m-1,n)}^{k} - H_{x(m,n)}^{k-1} + \frac{1}{2Z_0}\left[W_{(m+1,n)}^{k} - W_{(m-1,n)}^{k}\right] \\ H_{z(m,n)}^{k+1} &= H_{z(m,n+1)}^{k} + H_{z(m,n-1)}^{k} - H_{z(m,n)}^{k-1} + \frac{1}{2Z_0}\left[W_{(m,n-1)}^{k} - W_{(m,m+1)}^{k}\right] \\ W_{(m,n)}^{k+1} &= A^k + B^k - W_{(m,n)}^{k-1} \end{aligned} \tag{5.37}$$

$$A^k = \frac{1}{2}\left[W^k_{(m,n+1)} + W^k_{(m,n-1)} - W^k_{(m+1,n)} - W^k_{(m-1,n)}\right]$$
$$B^k = Z_0\left(H^k_{z(m,n+1)} - H^k_{z(m,n-1)} - H^k_{x(m+1,n)} + H^k_{x(m-1,n)}\right) \tag{5.38}$$

The independence of the electric field from other components allows the solution of most problems by solving only one partial difference equation. The equation is solved with boundary and initial conditions for the electric field.

This is also the case in FDTD. In a two-dimensional problem, the results obtained with TLM and FDTD must be equal provided that both have the same field initial conditions (only Ey(t=0) is non-zero), discretization, and timestep.

The next sections describe the procedure for solving two-dimensional difference equations. The first example is the solution of a static problem. The result will show that there is only a finite number of modes in a bounded discrete problem.

The second example is the solution of a partially dielectric loaded waveguide. The results show a dielectric interface effect when two or more dielectrics are present in a simulation. This effect is not predicted by the dispersion analysis.

The last example shows the first order convergence of logarithmic discontinuities in TLM. The convergence rate is reduced because of the finite number of modes.

5.5.2 The two-dimensional Laplace equation

The Laplace equation can be used to obtain static solutions of the wave equation. In the case of TEM wave propagation, the Laplace equation can be used to calculate the impedance of the line or to characterize a discontinuity.

The main result presented in this section is the finite number of modes in characterization of any discrete bounded problem. In the continuous bounded problem, the solution is expressed as an infinite sum of modes. In the discrete bounded problem, this sum is finite.

The problem under study is the solution of the discrete Laplace equation of the potential box problem, Figure 5.14.

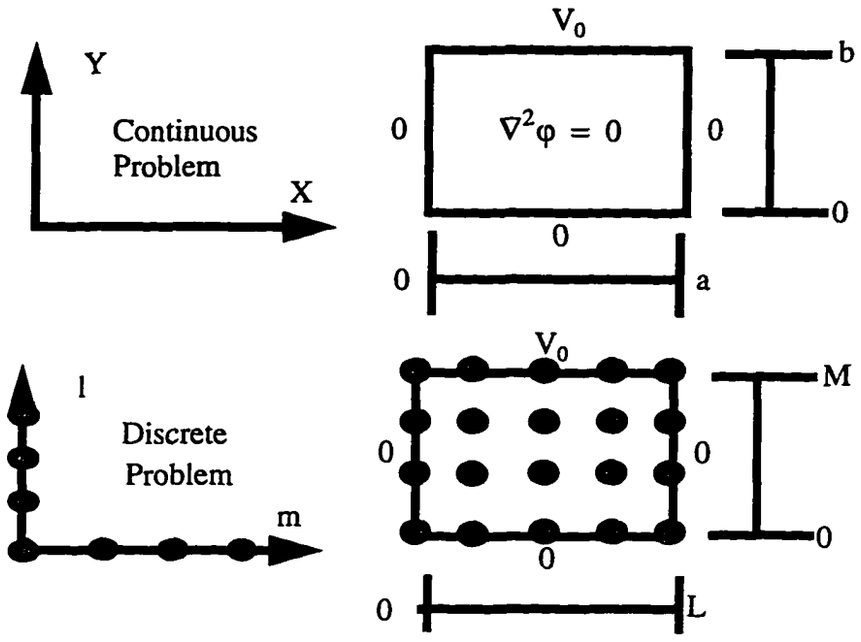

Figure 5.14 The potential box problem. The solutions are obtained by solving the continuous and discrete Laplace equations

The continuous Laplace equation is:

$$\nabla^2\phi = 0 \tag{5.39}$$

Subject to the boundary conditions:

$$\begin{aligned} \varphi(0, y) &= 0 \\ \varphi(a, y) &= 0 \\ \varphi(x, 0) &= 0 \\ \varphi(x, b) &= V_0 \end{aligned} \tag{5.40}$$

The solution of the problem is [31]:

$$\varphi(x, y) = \frac{4Vo}{\pi} \sum_{n=1,3}^{\infty} \frac{1}{n} \frac{\sin(n\frac{\pi}{a}x)\sinh(n\frac{\pi}{a}y)}{\sinh(n\pi\frac{b}{a})} \tag{5.41}$$

The discrete Laplace equation is:

$$\varphi(m,l) = \frac{1}{4}(\varphi(m+1,l) + \varphi(m-1,l) + \varphi(m,l+1) + \varphi(m,l-1)) \tag{5.42}$$

Subject to the boundary conditions:

$$\begin{aligned} \varphi(0,l) &= 0 \\ \varphi(M,l) &= 0 \\ \varphi(m,0) &= 0 \\ \varphi(m,L) &= V_0 \end{aligned} \tag{5.43}$$

The solution of the discrete problem is (Appendix C):

$$\varphi(m,l) = \sum_{n=1,3}^{M-1} \left[\frac{2Vo}{M \sin\left(\frac{n\pi}{2M}\right)} \right] \frac{\sin\left(n\frac{\pi}{M}m\right) \sinh\left(2l \operatorname{asinh}\left(\sin\left(\frac{n\pi}{2M}\right)\right)\right)}{\sinh\left(2L \operatorname{asinh}\left(\sin\left(\frac{n\pi}{2M}\right)\right)\right)} \tag{5.44}$$

The comparison between (5.41) and (5.44) shows a perfect correspondence between the mathematical expressions, but not between the number of modes.

While the continuous problem involves an infinite number of modes, the discrete one involves a finite set. In the numerical scheme, there are only as many modes as there are free points on the mesh. This can be visualized in Figure 5.15.

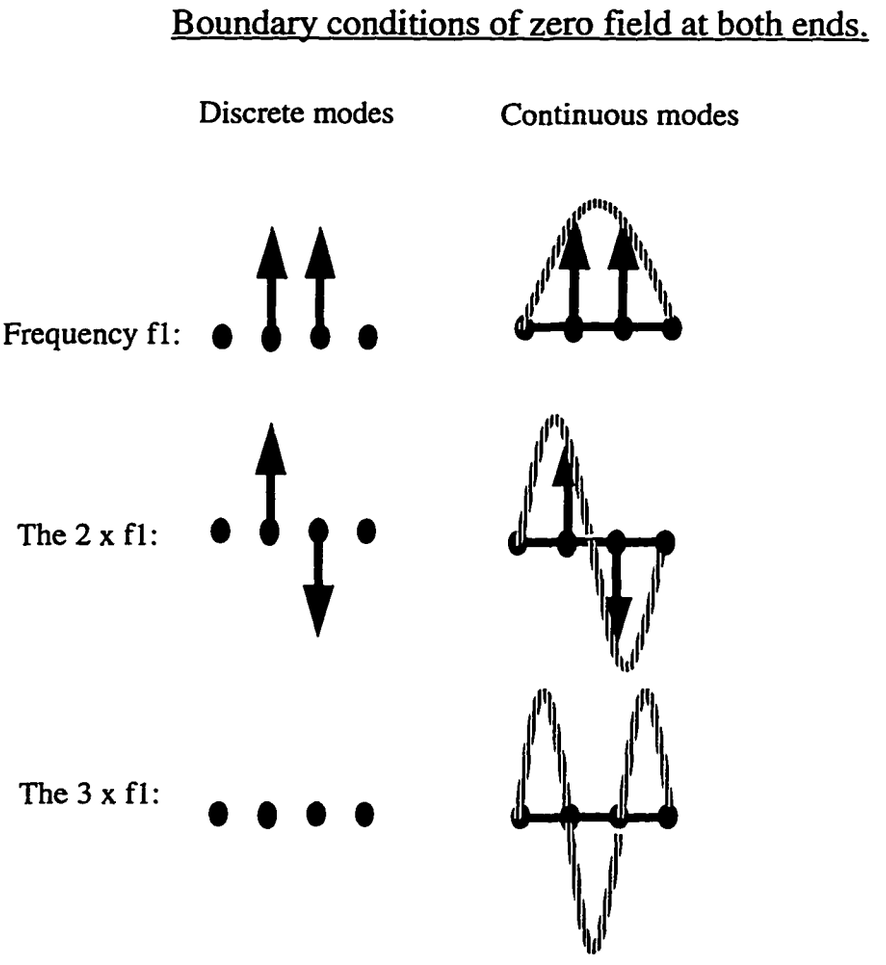

Figure 5.15 Number of modes in a discrete structure. The number of allowed modes is equal to the number of free nodes. The natural consequence is that any infinite sum of modes is truncated to the number of free nodes is the discrete problem.

The importance of the finite number of modes resides in the truncation of the infinite series. The convergence of the method is dependent not only on the dispersion relationship, but also on the series of modes. If the series has only first order convergence so does the solution [71].

A comparison between results obtained with (5.41), (5.44) and (5.42) for a voltage of 100V and M=L=5 is shown in Table I. The difference between the numerical solution and the numerical and analytical solutions of the difference equation is caused by round-

off error [67]-[69].

X,Y point	ϕ analytical	ϕ numerical	ϕ discrete
(a/4,b/4)	6.7972	7.14286	7.14285713
(a/4,b/2)	18.2028	18.75000	18.74999999
(a/4,3b/4)	43.2028	42.85714	42.85714281

Table 5.1. Results for the potential box

5.5.3 TLM solution of partially filled waveguide

The partially filled waveguide was solved for the electric field discrete wave equation. The eigenvalues of the problem for the dominant mode were obtained and compared to simulations and analytical values.

The calculated eigenvalues for the dominant mode were obtained by subdividing the waveguide into two homogeneous regions, and by enforcing the continuity of the field at the dielectric interface. The resulting transcendental equation was used to obtain the analytical eigenvalues of the discrete problem.

The eigenvalue equation for the discrete problem is:

$$A + B = 0$$

$$A = \sin\left(2\operatorname{asin}\left[\sqrt{2\varepsilon_r}\sin\left(\frac{\beta a}{2N\sqrt{2}}\right)\right]\right)\tan\left(2N\frac{t}{a}\operatorname{asin}\left[\sqrt{2\varepsilon_r}\sin\left(\frac{\beta a}{2N\sqrt{2}}\right)\right]\right) \tag{5.45}$$

$$B = \varepsilon_r\sin\left(2\operatorname{asin}\left[\sqrt{2}\sin\left(\frac{\beta a}{2N\sqrt{2}}\right)\right]\right)\tan\left(2N\left(1-\frac{t}{a}\right)\operatorname{asin}\left[\sqrt{2}\sin\left(\frac{\beta a}{2N\sqrt{2}}\right)\right]\right)$$

The eigenvalue equation for the continuous problem is [31]:

$$\beta a\sqrt{\varepsilon_r}\tan\left(\beta a\sqrt{\varepsilon_r}\frac{t}{a}\right) + \varepsilon_r\beta a\tan\left(\beta a\left(1-\frac{t}{a}\right)\right) = 0 \tag{5.46}$$

The comparison between results for a 10 point discretization is shown in Figure 5.16. This results shows that the main source of discrepancy between the continuous and discrete results is not dispersion. The cause is a surface effect in the interface between air and dielectric. The error tends to decrease with small dielectric fillings and increase with

large ones.

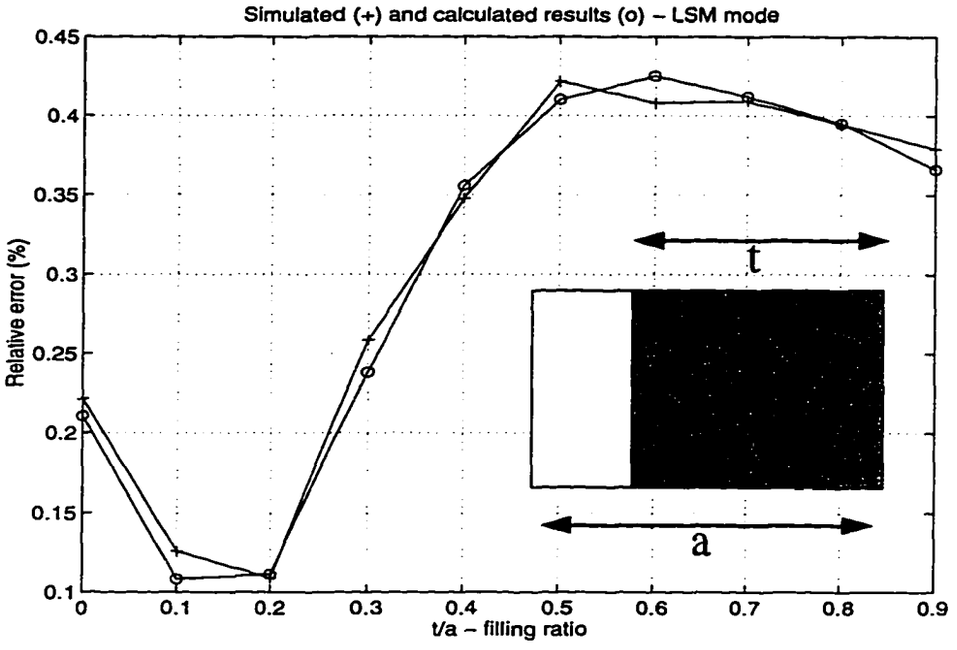

Figure 5.16 Relative error of the partially filled waveguide for a 10 point discretization. The graph shows the error of the TLM simulated results and the exact result (+) and the error of the analytical TLM results and the exact result (o).

This result is confirmed by TLM simulations of a dielectric filled cavity. The reduction of error cannot be explained by dispersion analysis. Additional analytical results show that the resonant frequencies may have positive shift with certain dielectric fillings or for higher order mode resonances.

Therefore, TLM does not have only negative frequency shifts in inhomogeneous problems, This is only the case for homogeneous media. If two or more dielectrics are present in the simulation the frequency shift may be positive or negative.

5.5.4 TLM solution of a capacitive diaphragm

This section presents the solution of the electric field discrete wave equation for the capacitive diaphragm in a TEM waveguide [31]. The result is the susceptance of the diaphragm in the discrete case.

The result shows that the frequency shifts observed in several TLM simulations are not caused by spurious modes. The reason for the shift is the finite number of modes in

the solution of the difference equation. However, due to the complexity involved in the solution of the difference equations for this problem, a closed form result for all frequencies is very difficult to obtain. In spite of this, the static solution can be obtained with the convergence bounds.

The summation of an infinite number of modes yields the analytical low frequency solution in the continuous case. The numerical solution is obtained with a finite sum of modes. The result is bounded by:

$$B_{exact} - \frac{4k_0\Delta x}{\pi}\alpha \le B_{discrete} \le B_{exact} + \frac{4k_0\Delta x}{\pi}\alpha \tag{5.47}$$

where α is a constant dependent on the number of cells in the discretized domain.

These results show that the discrete solution has a different convergence behavior (from quadratic to linear) in the presence of certain discontinuities. The reason, which is valid for other logarithmic discontinuities, is the slow convergence of the mode series. Figure 5.17 shows the convergence error of the method versus the number of cells.

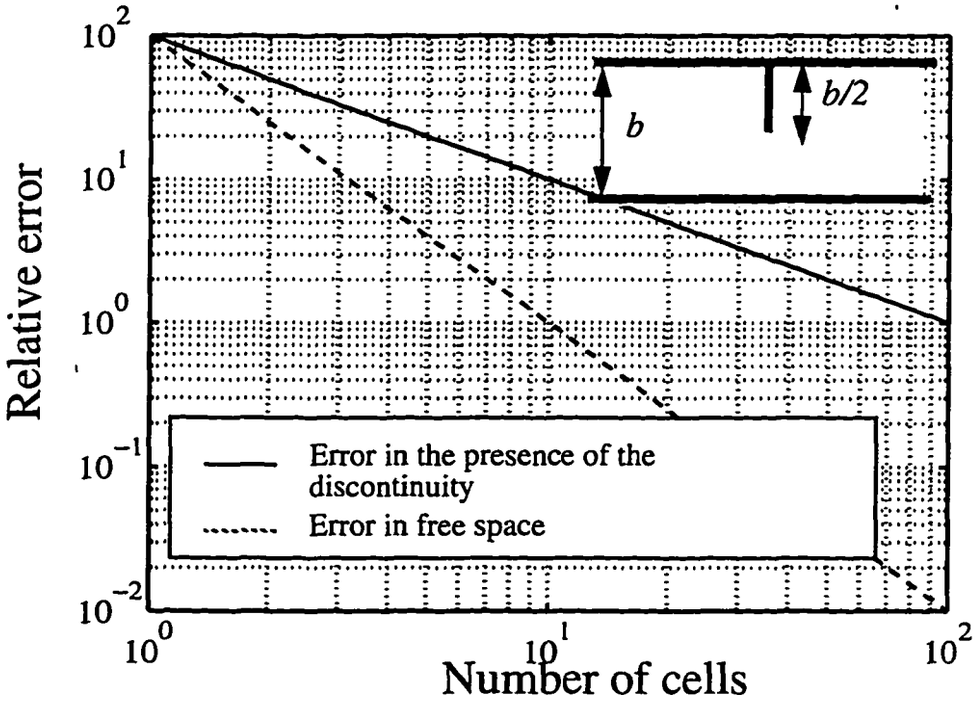

Figure 5.17 Error in the susceptance of the capacitive diaphragm as a function of the number of cells along the waveguide height.

The rate of convergence of the susceptance is dependent on the number of modes of the mesh. The number of cells determines the number of modes allowed by the TLM difference equation. Therefore, the frequency shift observed in TLM simulations of this kind of discontinuity is a natural result of the difference equation.

The result can be improved by local modifications in the TLM mesh that include the static field behavior near the edge [72]-[73]. The total effect is the improvement of the convergence of the series.

5.6 Conclusions

This chapter presented a dispersion analysis of frequency dependent dielectric and a new procedure to quantify errors in a simulation.

The dispersion relations for the two- and three-dimensional TLM nodes were presented. An analysis for frequency dependent dielectrics was performed. The results were obtained for the Debye and Lorentz models of medium behavior. In the non-dispersive case, the source model leads to the same results as the stub-loaded representation, if the trapezoidal discretization scheme for the derivative is used.

In the two-dimensional case, it was verified that the relative time constant of the medium is the main factor in the accuracy of the simulation. The frequency shift created by the resonant frequencies of the medium is inversely proportional to the square of the relative time constant.

The SCN analysis was performed only in particular directions of propagation. The reason is the complexity of the equations involved in the solution for all directions. The existence of spurious modes was verified for the propagation in the main diagonal direction. These modes are independent of the dielectric being modeled.

The solution of the difference equation of TLM was presented. The new procedure was used to quantify some of the sources of error in a TLM simulation. The use of the technique explained the frequency shifts in TLM simulation of structures with infinitesimally thin wedges. The reason is the reduction of the convergence rate of the method. The finite number of modes supported by the mesh causes this effect.

The first-order term of the susceptance of this kind of wedge discontinuities appears as a stray capacitance in the problems. Therefore, the calculated results shift down or up in frequency. The direction of the shift depends on whether the boundary con-

dition is situated between nodes or at a node. This shift is a natural feature of the discrete scheme and is also present in FDTD.

The solution of the discrete wave equation also revealed an interface effect in the representation of heterogeneous structures (more than one dielectric). The effect can be the main source of error in these cases. In the presented example, the effect caused a reduction of the error for small dielectric fillings. Additional analysis suggests that positive frequency shifts may be present in inhomogeneous structures.

Chapter 6

Conclusions and Future Work

6.1 Modeling and the real world

Theory is an approximation of reality.

The same can be said regarding the accuracy of numerical modeling techniques. While the use of numerical packages expands the knowledge of the world around, it presents the same problems that affect every approximation. The numerical solution can be close to the reality, but it is not reality.

The continuous development of more accurate, more efficient and powerful numerical methods is necessary. The purpose of engineering is to understand the world and use its laws to the benefit of humankind. At least, that is the belief of the author.

This benefit may be achieved by developing new products and technologies at a very fast rate. In this world, numerical packages are a necessity. The development of faster processors, new wireless technology, new data processing methods could not happen without numerical techniques.

These technical breakthroughs have one common denominator: computers. It was with the development of computers that the design process became more efficient. The manufacturing became more accurate. Now most of the design is performed with computer models. The rate of change reached the point where no engineer could solve today's design problems without numerical techniques.

The new engineer faces now an interesting challenge. The electromagnetic systems designer sometimes must also be able to deal with biological interactions, electromagnetic interference, quantum effects and coupled problems in general.

The solution of new problems is no longer a problem of a particular field expert. The new simulation packages must also be able to include new features to model these problems. At least this is true for general purpose numerical methods.

The Transmission Line Matrix (TLM) method is in this class of numerical methods. The purpose of this thesis was to extend the TLM to a wider range of applications. The major part of this work shows the successful extension of the method to more complex interactions between media and fields.

6.2 Modeling general constitutive relationships

This thesis presented a novel approach to the modeling of general electromagnetic medium behavior with the Transmission Line Matrix (TLM) method. The proposed technique is based on the definition of equivalent sources connected to the nodes. The equivalent sources are defined by the constitutive relationships of the medium.

However, several topics remain to be studied. The most important is the modeling of coupled transport and electromagnetic phenomena [10]. The extension to this kind of problems lies in the definition of the equivalent sources that are modeling the medium behavior. These sources could depend on other factors than the electric field, such as temperature, moisture concentration or charge carrier concentration.

The process coupled to the electromagnetic problem to be solved together with TLM could also be solved using a TLM mesh, or by finite differences in the time domain. The TLM mesh that models the electromagnetic field would be represented by a source term in the other problem. The solution of the coupled problem can rely on the equivalent source to represent the dielectric behavior. This idea is clarified in Fig.6.1.

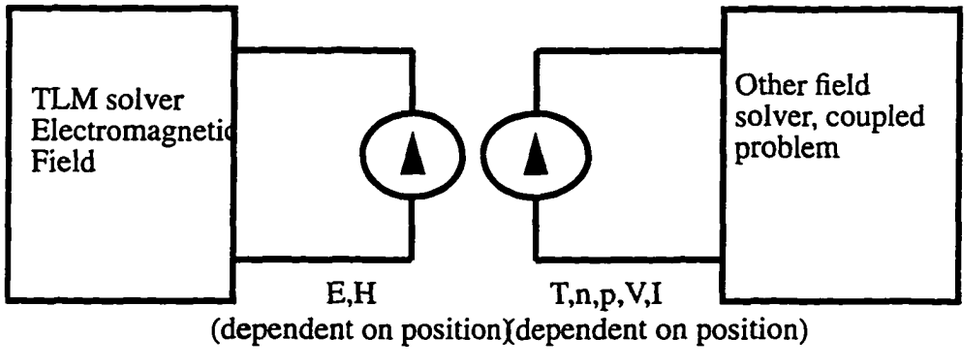

Figure 6.1 Solution of the coupled problem. The TLM solver provides a source term for the other field solver, and the results of the other field solver provides a TLM source term.

The flexibility of the equivalent source approach allows the coupling of TLM electromagnetic field solution to study temperature effects in semiconductors, full wave analysis of semiconductor devices, heating, and diffusion effects in the wave propagation through semiconductor substrates.

6.3 Error analysis in TLM

Numerical results are approximations of analytical results.

The solution of general constitutive relationships in TLM is the major topic of this thesis. However, during the development of the modeling procedure, several questions regarding the accuracy of TLM arose.

These questions ranged from the presence of spurious modes to the explanation of frequency shifts in numerical results. Because of those questions and many more, the author decided to examine closely the TLM method. In this investigation the numerical solution of dispersion analysis of frequency dependent dielectrics in TLM was performed.

However, dispersion analysis seldom provides all the information needed to characterize the accuracy of a TLM result. The dispersion analysis yields the minimum error present in a simulation. The use of the analysis in the Symmetrical Condensed Node (SCN) TLM shows the existence of spurious modes. These modes have high spatial variation and propagate at low frequencies [22].

However, the analysis cannot quantify these modes or predict any coupling between real and spurious modes. The limitations of dispersion analysis were overcome by the analytical solution of difference equations. This procedure was based on one-dimensional cases.

The use of this new tool provided a different picture of the accuracy of numerical methods. Although both TLM and FDTD are considered second-order accurate methods, this does not hold in the presence of certain discontinuities. It was also verified that the frequency shift of results in both methods could be positive or negative if inhomogeneous dielectrics are present.

This is not caused by spurious modes. This is caused by the discretization of a continuous problem. In the past these effects were assumed to be caused by spurious modes or discretization errors. However, these problems are natural to discrete solutions of par-

tial differential equations. One way of eliminating these effects is to implement local corrections to the mesh.

A more difficult challenge is the study of spurious modes in the SCN case. The high-spatial wavelength, low frequency solutions suggest also a consistency problem of these equations. During the development of this thesis, the difference equation technique was applied to the solution of the three-dimensional case. However, the solution of this problem proved to be very complex and limited to specific directions of propagation.

6.4 Overall conclusions

With the help of the theory developed in this work, the modeling of general medium interactions in the TLM method has become a reality. The use of equivalent nodal sources avoids the need to change the scattering matrix if a new medium is simulated. The method can be used to analyze frequency dependent, nonlinear, anisotropic materials. The solution of the medium equations can be performed using any general circuit analysis technique.

The study of the accuracy of the TLM method led to the development of a new tool in the characterization of numerical methods. Although, this technique was used in TLM and FDTD, it can be extended to other methods as well.

Appendix A

Modification of the Scattering Matrix

The main objective of this appendix is to demonstrate the equivalence between the stub loaded and the equivalent source models. Consider these two representations of the node, Figure A.1.

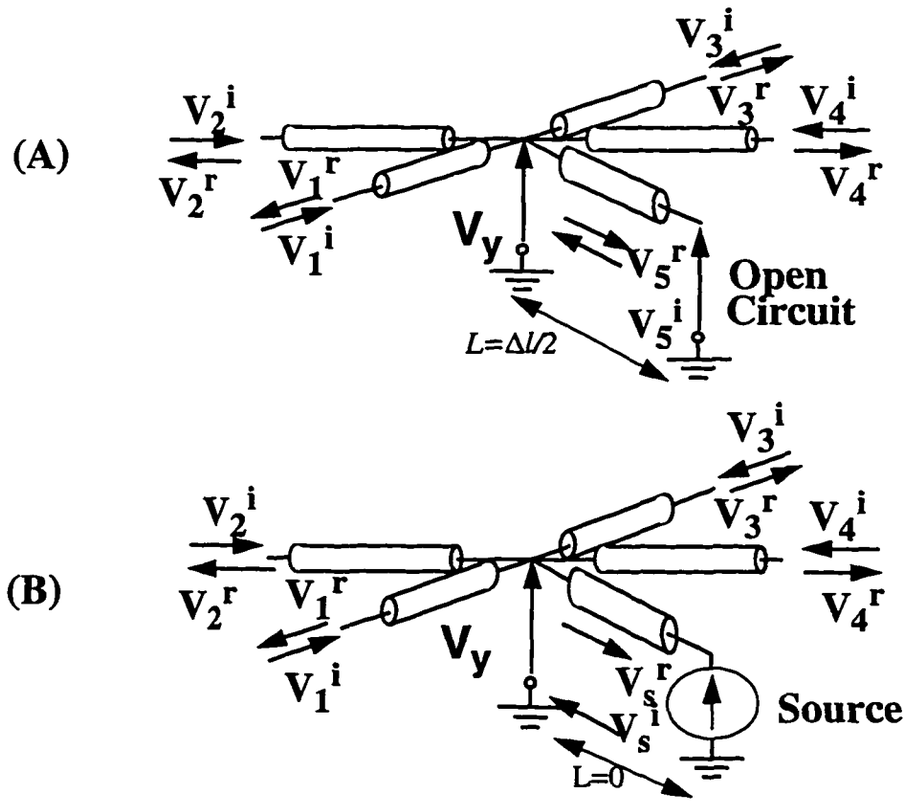

Figure A.1 Representation of a Dispersive Dielectric in the TLM

The purpose of this appendix is to demonstrate the equivalence between the stub-loaded (Figure A.1.a) and nodal source (Figure A.1.b) representations of the node.

In this development a frequency dependent dielectric is considered. In the stub-loaded case, the dielectric is modeled by a frequency dependent stub. The representation of this node is easily achieved in the frequency domain. To this end, consider that all quantities shown in Figure A.1 are transformed to the frequency domain.

The frequency dispersive linear dielectric is characterized by the complex permittivity:

$$\varepsilon_r(\omega) = \varepsilon_\infty + \chi(\omega) \tag{A.1}$$

Then the constitutive relationship in the frequency domain is:

$$\vec{D}(\omega) = \varepsilon_0 \vec{E}(\omega) + \varepsilon_0 ((\varepsilon_\infty - 1) + \chi(\omega)) \vec{E}(\omega) = \varepsilon_0 \vec{E}(\omega) + \vec{P}(\omega) \tag{A.2}$$

Therefore, the frequency dependent effect could be represented, in a two-dimensional TLM shunt network, by the inclusion of a source P(ω) in parallel with the shunt node, as shown in Figure A.1.b

In order to obtain the TLM formulation of this new shunt node, it is necessary to perform a change of variables from the incident and reflected voltages at the open-circuited stub of Figure A.1.a ($v_5^i(\omega)$ and $v_5^r(\omega)$) to the incident and reflected voltages at the source of Figure A.1.b ($v_s^i(\omega)$ and $v_s^r(\omega)$) from the TLM node.

This change of variables can be accomplished by expressing the incident and reflected voltages at the source as a linear combination of the incident and reflected voltages at the stub. However, since the dielectric behavior is totally modeled by the source, the stub-loaded node must undergo a change of relative dielectric constant.

Since the incident and reflected nodal source voltages ($v_s^i(\omega)$ and $v_s^r(\omega)$) are linear combinations of the incident and reflected stub voltages ($v_5^i(\omega)$ and $v_5^r(\omega)$), the change of dielectric constant does not change the energy at the node. The energy "lost" by changing the dielectric constant of node must be supplied by a source connected to the node.

The change of relative dielectric constant of the node is accomplished by add-

ing and subtracting a certain dielectric constant to the relative permittivity of the node. The value of this constant ε_1 will be determined later. The frequency domain permittivity may be expressed as:

$$\varepsilon_r(\omega) = (\varepsilon_1 - \varepsilon_1 + \varepsilon_r(\omega)) \tag{A.3}$$

In order to reduce the size of the expressions, we introduce the auxiliary variable:

$$V_{aux}(\omega) = \frac{1}{2}(V_1^i(\omega) + V_2^i(\omega) + V_3^i(\omega) + V_4^i(\omega)) \tag{A.4}$$

The total node voltage across the stub-loaded node, Figure A.1, is:

$$V_y(\omega) = \frac{2}{4+y}(V_1^i(\omega) + V_2^i(\omega) + V_3^i(\omega) + V_4^i(\omega) + 2yV_5^i(\omega)) \tag{A.5}$$

where:

$$y = 4(\varepsilon_r(\omega) - 1) \tag{A.6}$$

The total voltage at the node (A.5) can be expressed as:

$$\varepsilon_r(\omega)\, V_y(\omega) = V_{aux}(\omega) + 2\varepsilon_r(\omega)\, V_5^i(\omega) - 2V_5^i(\omega) \tag{A.7}$$

substituting (A.3) in the node voltage (A.7):

$$(\varepsilon_1 - \varepsilon_1 + \varepsilon_r(\omega))\, V_y(\omega) = V_{aux}(\omega) + 2(\varepsilon_1 - \varepsilon_1 + \varepsilon_r(\omega))\, V_5^i(\omega) - 2V_5^i(\omega) \tag{A.8}$$

At this point, we change the relative permittivity of the node. We can define:

$$y_1 = 4(\varepsilon_1 - 1) \tag{A.9}$$

then, (A.3) will now be represented as:

$$V_y(\omega) = \frac{4}{y_1+4}V_{aux}(\omega) + \frac{2(\varepsilon_r(\omega) - \varepsilon_1)}{y_1+4}(2V_5^i(\omega) - V_y(\omega)) \tag{A.10}$$

which is in fact the expression of the nodal source:

$$V_y(\omega) = \frac{4}{y_1+4}V_{aux}(\omega) + g_s(\omega) \tag{A.11}$$

using the identity:

$$V_y(\omega) = V_5^i(\omega) + V_5^r(\omega) \tag{A.12}$$

then (A.10) may be rewritten as:

$$V_y(\omega) = \frac{4}{y_1+4} V_{aux}(\omega) + \frac{2(\varepsilon_r(\omega)-\varepsilon_1)}{y_1+4}(V_5^i(\omega) - V_5^r(\omega)) \tag{A.13}$$

The difference between the incident and reflected voltages indicate that the source is current source, since the voltage and current at the node input port are given by:

$$\begin{aligned} V_{stub} &= V_5^r(\omega) + V_5^i(\omega) \\ I_{stub} &= y(V_5^i(\omega) - V_5^r(\omega)) \end{aligned} \tag{A.14}$$

We will consider the node in Figure A.1.b. The source is connected to the node by a link-line of admittance y_1. The total voltage at this node is:

$$V_y(\omega) = \frac{2}{y_1+4}(V_1^i(\omega) + V_2^i(\omega) + V_3^i(\omega) + V_4^i(\omega) + y_1 V_s^i(\omega)) \tag{A.15}$$

The link-line transmits the incident and reflected voltages from to node to the source. Since the two nodes must have the same total voltage (both are modeling the same dielectric):

$$V_s^i(\omega) + V_s^r(\omega) = V_y(\omega) = V_5^i(\omega) + V_5^r(\omega) \tag{A.16}$$

Comparing (A.13) with (A.15) results in the equivalence equation:

$$\frac{y_1}{y_1+4} V_s^i(\omega) = \frac{y_1}{y_1+4} V_5^i(\omega) + \frac{2(\varepsilon_r(\omega)-\varepsilon_1)}{y_1+4}(V_5^i(\omega) - V_5^r(\omega)) \tag{A.17}$$

Using the voltage conservation law (A.16), a similar equation is obtained for the reflected voltage. Rewriting (A.17):

$$V_s^i(\omega) = V_5^i(\omega) - \frac{(\varepsilon_r(\omega)-\varepsilon_1)}{2(\varepsilon_1-1)}(V_5^r(\omega) - V_5^i(\omega)) \tag{A.18}$$

the use of (A.16) in (A.18), results in;

$$V_s^r(\omega) = V_5^r(\omega) + \frac{(\varepsilon_r(\omega)-\varepsilon_1)}{2(\varepsilon_1-1)}(V_5^r(\omega) - V_5^i(\omega)) \tag{A.19}$$

subtracting (A.18) from (A.19), the relationship is derived:

$$\begin{aligned} V_s^i(\omega) &= V_5^i(\omega) - \frac{(\varepsilon_r(\omega) - \varepsilon_1)}{2(\varepsilon_r(\omega) - 1)} (V_s^r(\omega) - V_s^i(\omega)) \\ V_s^r(\omega) &= V_5^r(\omega) + \frac{(\varepsilon_r(\omega) - \varepsilon_1)}{2(\varepsilon_r(\omega) - 1)} (V_s^r(\omega) - V_s^i(\omega)) \end{aligned} \tag{A.20}$$

The source function can be completely specified using the condition of total reflection at the stub. The frequency domain relationship between the incident and reflected voltages at the stub is:

$$v_5^i(t) = v_5^r(t - \Delta t) \leftrightarrow V_5^i(\omega) = V_5^r(\omega) e^{j\omega\Delta t} \tag{A.21}$$

The substitution of (A.21) into (A.20) yields the first equation of the source:

$$V_s^i(\omega) = V_s^r(\omega) e^{-j\omega\Delta t} - \frac{(\varepsilon_r(\omega) - \varepsilon_1)}{(\varepsilon_r(\omega) + (\varepsilon_1 - 2))} (V_s^r(\omega) - V_s^i(\omega) e^{-j\omega\Delta t}) \tag{A.22}$$

The second equation of the source is obtained by substituting (A.16) into (A.15):

$$V_s^r(\omega) = \frac{2}{y_1 + 4} (V_1^i(\omega) + V_2^i(\omega) + V_3^i(\omega) + V_4^i(\omega) + (y_1 - 2) V_s^i(\omega)) \tag{A.23}$$

However, these equations (A.22) and (A.23), have a problem: the coupling between the incident and reflected voltages. The coupling can be avoided in the same way shown in [4], by specifying ε_1. The choice of a suitable value results in a link line admittance y_1 of 4 (therefore ε_1 of 2). This value will decouple the incident and reflected voltages ($v_s^i(\omega)$ and $v_s^r(\omega)$) in the scattering matrix:

$$\begin{bmatrix} v_1 \\ v_2 \\ v_3 \\ v_4 \\ v_a \end{bmatrix}^r = \frac{1}{4} \begin{bmatrix} -3 & 1 & 1 & 1 & 4 \\ 1 & -3 & 1 & 1 & 4 \\ 1 & 1 & -3 & 1 & 4 \\ 1 & 1 & 1 & -3 & 4 \\ 1 & 1 & 1 & 1 & 0 \end{bmatrix} \begin{bmatrix} v_1 \\ v_2 \\ v_3 \\ v_4 \\ v_a \end{bmatrix}^i \tag{A.24}$$

and the relationship expressed in (A.22) will change to:

$$V_s^i(\omega) = V_s^r(\omega)\, e^{-j\omega\Delta t} - \frac{\varepsilon_r(\omega) - 2}{\varepsilon_r(\omega)} \left(V_s^r(\omega) - V_s^i(\omega)\, e^{-j\omega\Delta t}\right) \tag{A.25}$$

Since the behavior of the source is best characterized by its current and voltage, it is necessary to develop (A.25) further. The current and the voltage at input port of the source:

$$\begin{aligned} V_y(\omega) &= V_s^r(\omega) + V_s^i(\omega) \\ I_{pol}(\omega) &= 4\left(V_s^r(\omega) - V_s^i(\omega)\right) \end{aligned} \tag{A.26}$$

and the relationship between the current and the voltage is:

$$I_{pol}(\omega) = Y(\omega)\, V_y(\omega) \tag{A.27}$$

where the I_{pol} is the current at the input terminals of the source.

The further development of (A.25) will results in:

$$V_s^r(\omega) - V_s^i(\omega) = (\varepsilon_r(\omega) - 1)\left(V_s^r(\omega) + V_s^i(\omega)\right) \frac{1 - e^{-j\omega\Delta t}}{1 + e^{-j\omega\Delta t}} \tag{A.28}$$

combining (A.28) with (A.26) results in:

$$I_{pol}(\omega) = \left(4j\,(\varepsilon_r(\omega) - 1)\tan\left(\omega\frac{\Delta t}{2}\right)\right) V_y(\omega) \tag{A.29}$$

For a small timestep, or for infinitesimal link line length, (A.29) may be approximated by:

$$I_{pol}(\omega) = j\omega 2\Delta t\,(\varepsilon_r(\omega) - 1)\, V_y(\omega) \tag{A.30}$$

Since the analogy between fields and circuit quantities states that:

$$E_y(\omega) = V_y(\omega) = V_a^r(\omega) + V_a^i(\omega) \tag{A.31}$$

and the polarization vector P may be expressed as:

$$P_y(\omega) = \varepsilon_0\,(\varepsilon_r(\omega) - 1)\, E_y(\omega) \tag{A.32}$$

Therefore, combining (A.32) with (A.30) the current flowing through the admittance is:

$$I_{pol}(\omega) = j\omega\frac{2\Delta t}{\varepsilon_0} P_y(\omega) \tag{A.33}$$

Transforming (A.33) back to the time domain:

$$i_{pol}(t) = \frac{2\Delta t}{\varepsilon_0}\frac{d}{dt}P_y(t) \qquad \text{(A.34)}$$

Appendix B

Discrete State-Variable Formulation of RC and RLC Circuits

This appendix describes the discretized state equations obtained by using the equivalent circuits for the Debye and Lorentz media.

The discrete state-variable equations are represented in Chapter 4, Section 4.2.4 on page 51

The backward Euler formulation of the state-variable description of a first order Debye medium will result in the following matrices:

$$[A'] = \alpha\begin{bmatrix} C1\,(1+C2R) & C2 \\ C1 & C2\,(1+C1R+RY_r) \end{bmatrix} \qquad \alpha = \frac{1}{C1+C2+C1C2R+Y_r+C2RY_r} \tag{B.1}$$

$$[B'] = 2Y_r\alpha\begin{bmatrix} (1+C2R) \\ 1 \end{bmatrix} \tag{B.2}$$

with $C_1 = 2\,(\varepsilon_\infty - 1)$ $\qquad R = \dfrac{\tau_0}{2\Delta t\,(\varepsilon_s - \varepsilon_\infty)}$ $\qquad C_2 = 2\,(\varepsilon_s - \varepsilon_\infty)$

The approximate trapezoidal formulation will lead to:

$$[A'] = \beta\begin{bmatrix} C1 - C2\,(1-C1R) - Y_r\,(1+C2R) & 2C2 \\ 2C2 & -C1 + C2\,(1+C1R) - Y_r\,(1-C2R) \end{bmatrix} \tag{B.3}$$

$$\beta = \frac{1}{C1 + C2 + C1C2R + Y_r + C2RY_r}$$

$$[B'] = 2Y_r\beta\begin{bmatrix} (1+2C2R) \\ 1 \end{bmatrix} \tag{B.4}$$

The following equivalence is valid:

$$C_1 = 4\,(\varepsilon_\infty - 1) \qquad R = \frac{\tau_0}{2\Delta t\,(\varepsilon_s - \varepsilon_\infty)} \qquad C_2 = 4\,(\varepsilon_s - \varepsilon_\infty)$$

The backward Euler formulation of the state-variable description of a Lorentz medium will result in the following matrices:

$$[A'] = \alpha\begin{bmatrix} C1\,(1+C2L+C2R) & C2 & -C2L \\ C1 & C2\,(1+C1L+C1R+Y_rL+RY_r) & L\,(C1+Y_r) \\ C1C2 & -C2\,(C1+Y_r) & C2L\,(C1+Y_r) \end{bmatrix}$$

$$\alpha = \frac{1}{C1 + C2 + C1C2L + C1C2R + Y_r + C2LY_r + C2RY_r} \tag{B.5}$$

$$[B'] = 2Y_r\alpha\begin{bmatrix} (1+C2L+RC2) \\ 1 \\ C2 \end{bmatrix}$$

with: $C1 = 2\,(\varepsilon_\infty - 1) \qquad C2 = 2\,(\varepsilon_s - \varepsilon_\infty)$

$$R = \frac{\delta}{2\Delta t\omega_0^2\,(\varepsilon_s - \varepsilon_\infty)} \qquad L = \frac{1}{2\,(\Delta t\omega_0)^2\,(\varepsilon_s - \varepsilon_\infty)}$$

Appendix C

Solution of the Discrete Laplace Equation for the Potential Box

Consider the two-dimensional solution of the Laplace equation in a potential box [31] in Chapter 5.

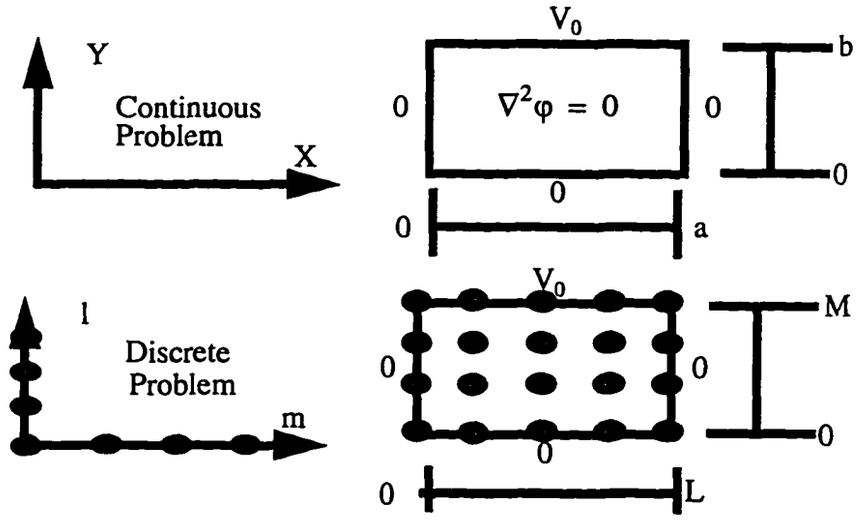

The Laplace equation describes the continuous problem:

$$\nabla^2\phi = 0 \tag{C.1}$$

subject to the boundary conditions:

$$\varphi(0, y) = 0 \qquad \varphi(a, y) = 0 \qquad \varphi(x, 0) = 0 \qquad \varphi(x, b) = V_0 \tag{C.2}$$

The solution is:

$$\varphi(x, y) = \frac{4Vo}{\pi} \sum_{n=1,3}^{\infty} \frac{1}{n} \frac{\sin(n\frac{\pi}{a}x)\sinh(n\frac{\pi}{a}y)}{\sinh(n\pi\frac{b}{a})} \tag{C.3}$$

Consider now the discrete equivalent of the potential box characterized by the five-point finite-difference scheme:

$$\varphi(m, l) = \frac{1}{4}(\varphi(m+1, l) + \varphi(m-1, l) + \varphi(m, l+1) + \varphi(m, l-1)) \tag{C.4}$$

The discrete problem is subject to the same boundary conditions as the continuous case. The box is discretized into a rectangular mesh of M by L points. The discretization step is such that:

$$\begin{aligned} a &= M\Delta s \\ b &= L\Delta s \end{aligned} \tag{C.5}$$

The five point difference scheme (C.4) can be rewritten as:

$$\begin{aligned} \delta_m\varphi + \delta_l\varphi &= 0 \\ \delta_m\varphi &= \frac{\varphi(m+1, l) - 2\varphi(m, l) + \varphi(m-1, l)}{\Delta s} \\ \delta_l\varphi &= \frac{\varphi(m, l+1) - 2\varphi(m, l) + \varphi(m, l-1)}{\Delta s} \end{aligned} \tag{C.6}$$

This set of equations represents the sampling of a continuous field over a domain, at discrete points. Since the field is defined at each sampling point, the separation of variables is possible at these points:

$$\varphi(m, l) = X(m)\,Y(l) \tag{C.7}$$

Substituting the solution (C.7) into (C.6) results in:

$$\left(\frac{X(m+1) - 2X(m) + X(m-1)}{X(m)}\right) + \left(\frac{Y(l+1) - 2Y(l) + Y(l-1)}{Y(l)}\right) = 0 \tag{C.8}$$

which can be expressed as two one-dimensional equations:

$$\begin{aligned} X(m+1) &= (2 - k_x^2)X(m) - X(m-1) \\ Y(l+1) &= (2 - k_y^2)Y(l) - Y(l-1) \end{aligned} \tag{C.9}$$

with the dispersion relationship:

$$k_x^2 + k_y^2 = 0 \tag{C.10}$$

The solutions of (C.9) are in the form:

$$\begin{aligned} X(m) &= A_1 e^{-j\alpha m} + A_2 e^{j\alpha m} \\ Y(l) &= B_1 e^{-j\beta l} + B_2 e^{j\beta l} \end{aligned} \tag{C.11}$$

The solution in the m-direction is readily obtained by applying the boundary conditions of the discrete problem together with the dispersion relationship:

$$\varphi(0, l) = 0 \qquad \varphi(M, l) = 0 \qquad a = M\Delta s \tag{C.12}$$

Resulting in the function:

$$X(m) = A\sin\left(\frac{n\pi}{M}m\right) \qquad k_x = 2\sin\left(\frac{n\pi}{2M}\right) \tag{C.13}$$

The solution in the l-direction is obtained by applying the boundary condition in the l direction:

$$\varphi(m, 0) = 0 \qquad b = L\Delta s \tag{C.14}$$

The solution in the l-direction is:

$$Y(l) = B\sin(\beta l) \qquad \beta = 2\,\mathrm{asin}\left(\frac{k_y}{2}\right) \tag{C.15}$$

Using the dispersion relationship:

$$k_z = 2j\sin\left(\frac{n\pi}{2M}\right) \tag{C.16}$$

results in the solution:

$$\begin{aligned} X(m) &= A\sin\left(\frac{n\pi}{M}m\right) \\ Y(l) &= B\sinh\left(2l\,\mathrm{asinh}\left(\sin\left(\frac{n\pi}{2M}\right)\right)\right) \end{aligned} \tag{C.17}$$

Using the remaining boundary condition:

$$\varphi(m, L) = V_0 \tag{C.18}$$

The solution in the m-direction involves the use of a finite Fourier series in the form:

$$\sum_{n=0}^{M-1} a_n \sin\left(\frac{n\pi}{M}m\right) \sinh\left(2L\,\mathrm{asinh}\left(\sin\left(\frac{n\pi}{2M}\right)\right)\right) = V_0 \qquad \text{(C.19)}$$

The Fourier sum (instead of integral) is used to obtain the coefficients of the series:

$$\sum_{k=0}^{M-1} A_k = \sum_{k=0}^{M-1} B_k$$

$$A_k = \left[\sum_{n=0}^{M-1} a_n \sin\left(\frac{n\pi}{M}m\right) \sinh\left(2L\,\mathrm{asinh}\left(\sin\left(\frac{n\pi}{2M}\right)\right)\right)\right] \sin\left(\frac{\pi k}{M}m\right) \qquad \text{(C.20)}$$

$$B_k = [V_0] \sin\left(\frac{\pi k}{M}m\right)$$

The series coefficients are:

$$a_n = \frac{V_0\left(\cos(n\pi) - 1\right) \sin\left(\frac{n\pi}{M}\right)}{M\left(\cos\left(\frac{n\pi}{M}\right) - 1\right) \sinh\left(2L\,\mathrm{asinh}\left(\sin\left(\frac{n\pi}{2M}\right)\right)\right)} \qquad \text{(C.21)}$$

which result in the solution:

$$\varphi(m, l) = \sum_{n=1,3}^{M-1} \left[\frac{2Vo}{M \sin\left(\frac{n\pi}{2M}\right)}\right] \frac{\sin\left(n\frac{\pi}{M}m\right) \sinh\left(2l\,\mathrm{asinh}\left(\sin\left(\frac{n\pi}{2M}\right)\right)\right)}{\sinh\left(2L\,\mathrm{asinh}\left(\sin\left(\frac{n\pi}{2M}\right)\right)\right)} \qquad \text{(C.22)}$$

Bibliography

[1] Sadiku, M.N.O., *Numerical Techniques in Electromagnetics*, CRC Press, 1992.

[2] T. Itoh, Ed. *Numerical Techniques for Microwave and Millimeter Wave Passive Structures*, New York, Wiley, 1989, pp.469-591.

[3] Booton Jr., R.C., *Computational Methods for Electromagnetics and Microwaves*, John Wiley & Sons, New York, 1992

[4] Bui, M.D., Stuchly, S.S. and Costache, G.I., "Propagation of transients in dispersive dielectric media", *IEEE Transactions on Microwave Theory and Techniques*, vol. 39, no.7, pp. 1165-1171, Jul, 1991.

[5] Sullivan, D.M, "A frequency dependent FDTD method for biological applications", *IEEE Transactions on Microwave theory and Techniques*, vol. 40, no. 3, pp.532-539, Mar. 1992.

[6] Alexopoulos, N.G. "Integrated circuits structures on anisotropic substrates", *IEEE Transactions on Microwave Theory and Techniques*, vol. 33, no. 10, pp. 847-881, Oct. 1985.

[7] Baden Fuller, A.J., *Ferrites at Microwave Frequencies*, Peter Peregrinus Ltd., London, 1987.

[8] Huang, J. and Wu, K "A unified TLM model for wave propagation of electrical and optical structures considering permittivity and permeability tensors", *IEEE Transactions on Microwave Theory and Techniques*, vol. 43, no.10, pp. 2472- 2477, Oct. 1995.

[9] Young, J.L. and Brueckner, F.P., "A time domain numerical model of a warm plasma", *Radio Science*, vol.29, no. 2, pp. 451-463, Mar-Apr 1994.

[10] Alsunaidi, M.A. and El Ghazaly, S.M., "High frequency time domain modeling of GaAs FETs using hydrodynamic model coupled with Maxwell's equations", *IEEE MTT-S International Symposium Digest*, pp. 397-400, 1994.

[11] Goorjian, P.M., Taflove, A., Joseph, R.M. and Hagness, S.C., "Computational modeling of femtosecond optical solitons from Maxwell's equations", *IEEE Journal of Quantum Electronics*, vol. 28, no. 10, pp. 2416-2422, Oct. 1992.

[12] Chua, L.O., Desoer, C.A. and Kuh, E.S. *Linear and Nonlinear Circuits*, Mc-Graw Hill, 1987

[13] Yee, K.S. "Numerical solution of initial boundary value problems involving Maxwell's equations in isotropic media", *IEEE Transactions on Antennas and Propagation*, vol. 14, pp. 302-307, May, 1966.

[14] Johns, P.B. and Beurle, R.L., "Numerical Solution of 2 Dimensional Scattering Problems using a Transmission Line Matrix", *Proc. IEE*, vol. 118, no. 9, pp. 1203-1208, Sep. 1971.

[15] Christopoulos, C., *The Transmission-Line Modeling Method* - TLM, IEEE Press, 1995.

[16] Hoefer, W.J.R. "The transmission-line matrix method - theory and applications", *IEEE Transactions on Microwave Theory and Techniques*, vol. 33, no. 10, pp. 882-893, Oct. 1985.

[17] Krumpholz, M. and Katehi, L.P.B., "New FDTD scheme based on orthonormal wavelet expansions", *PIERS Proceedings*, pp. 411, 24-28th Jul. 1995.

[18] Sabet, K.F. and Kathehi, L.P.B., "On the use of multidimensional wavelet expansions with the 3-D method of moments", *PIERS Proceedings*, pp. 412, 24-28th Jul. 1995

[19] Berenger, J.P. "A perfectly matched layer for the absorption of electromagnetic waves", *Journal of Computational Physics*, vol. 114, no. 2, pp. 185-200, Oct. 1994.

[20] Eswarappa, C. and Hoefer, W.J.R., "Bridging the gap between TLM and FDTD", *IEEE Microwave and Guided Waves Letters*, vol. 6, no. 1, pp. 1-3, Jan. 1996.

[21] Choi, D.H., "A comparison of the dispersion characteristics associated with the TLM and FD-TD methods", *International Journal of Numerical Modelling*, vol.2, pp. 203-214, 1989.

[22] Nielsen and W.J.R. Hoefer, "Generalized dispersion analysis and spurious modes of 2 D and 3 D TLM formulations", *IEEE Transactions on Microwave Theory and Techniques*, vol. 41, pp.1375-1384, Aug. 1993.

[23] Krumpholz, M. and P. Russer, "On dispersion of TLM and FDTD", *IEEE Transactions on Microwave theory and techniques*, vol.42, pp. 1275-1279, Jul. 1994.

[24] Celuch Marcysiak, M. and W.K. Gwarek, "On the effect of bilateral dispersion in inhomogeneous symmetrical condensed node modeling", *IEEE Transactions on Microwave Theory and Techniques*, vol. 42, pp. 1069-1073, Jun. 1994.

[25] Trenkic, V. , T.M. Benson and C. Christopoulos, "Dispersion analysis of a TLM mesh using a new scattering matrix formulation", *IEEE Microwave and Guided Wave Letters*, vol.5, no.3, pp.79-80, Mar. 1995.

[26] Berini, P. and Wu, K. "A comprehensive study of numerical anisotropy and dispersion in 3D TLM meshes" *IEEE Transactions on Microwave Theory and Techniques*, vol.43, no. 5, pp.1173-1181, may 1995.

[27] Morente, J.A, Gimenez, G. Porti, J.A. and Khalladi, M. "Dispersion analysis for a TLM mesh of symmetrical condensed nodes with stubs", *IEEE Transactions on Microwave Theory and Techniques*, vol.43, no.2, pp.452-456, Feb. 1995.

[28] Johns, P.B. "A symmetrical condensed node for the TLM method", *IEEE Transactions on Microwave Theory and Techniques*, vol. 35, no. 4., pp.370-377, 1987.

[29] Righi, M., Eswarappa, C. Hoefer, W.J.R. and Russer, P.,"An alternative way of computing S-parameters via impulsive analysis without using absorbing boundary conditions", *IEEE MTT-S International Symposium Digest*, pp. 1203-1206, 1995.

[30] Russer, P., Righi, M., Eswarappa, C. and Hoefer, W.J.R., "Lumped element equivalent circuit parameter extraction of distributed microwave circuits via TLM simulation", *IEEE MTT-S International Symposium Digest*, pp. 887-890, 1994.

[31] Collin, R.E. , *Field Theory of Guided Waves*, (2nd ed.) IEEE Press, Piscataway N.J. 1991.

[32] Harrington, R.F., *Time-Harmonic Electromagnetic Fields*, Mc-Graw Hill, New York, 1961.

[33] Balanis, C.A., *Advanced Engineering Electromagnetics*, John Wiley & Sons, New York, 1989.

[34] Naylor, P., and Ait. Sadi, R. "Simple method for determining 3 D TLM nodal scattering parameters in nonscalar problems", *IEE Electronic letters*, vol.28, pp.2353-2354, Dec. 3, 1992.

[35] Jin, H., Huang, J., Vahldieck, R. and Russer, P. "Rigorous analysis for mixed transmission line interconnects using the frequency domain TLM method", *IEEE Transactions on Microwave Theory and Techniques*, vol. 41, no. 12, pp. 2248-2255, Dec. 1993.

[36] Buchwald, J.Z. *The rise of the wave theory of light* University of Chicago Press, Chicago, 1989.

[37] Hunt, B.J. *The Maxwellians* Cornell University Press, Ithaca, 1991.

[38] Eswarappa, C. and Hoefer, W.J.R., " One-way absorbing boundary conditions for 3-D TLM analysis of planar and quasi-planar structures", *IEEE Transactions on Microwave Theory and Techniques*, vol 42, no. 9, pp. 1669-1677, Sep. 1994.

[39] Portis, A.M., *Electromagnetic Fields Sources and Media*, John Wiley & Sons, New York, 1978

[40] Elmore, W.C. and Heald, M.A., *Physics of Waves*, Dover publications Inc., 1985.

[41] Boardman, A.D. and Xie, K., "Theory of spatial solitons", *Radio Science*, vol.28, no.5, 891-899, Sep. Oct. 1993.

[42] Hasegawa, A. and Tappert, F., "Transmission of stationary nonlinear optical pulses in dispersive dielectric fibers. I. Anomalous dispersion", *Applied Physics Letters*, vol.23, no.3, 142-144, 1st Aug., 1973.

[43] Ma, J.G and Wolff, I., "Propagation characteristics of TE waves guided by thin films bounded by nonlinear media", *IEEE MTT-S International Symposium Digest*, pp. 465-468, 1994.

[44] Hasegawa, A., "Numerical study of optical soliton transmission amplified periodically by the stimulated Raman process", *Applied Optics*, vol.23, no.19, pp. 3302-3309, 1st Oct. 1984.

[45] Kodama, Y. and Hasegawa, A., "Nonlinear pulse propagation in a monomode dielectric guide", *IEEE Journal of Quantum Electronics*, vol. 23, no. 5, pp. 510-524, May 1987.

[46] Zabusky, N.J. and Kruskal, M.D., "Interaction of solitons in a collisionless plasma and recurrence of initial states", *Physical Review Letters*, vol. 15, no. 6, pp. 240-243, 9th Aug. 1965.

[47] McCall, S.L. and Hahn, "Self induced transparency by pulsed coherent light",*Physical Review Letters*, vol. 18, no. 21, pp.908-911, 22nd May 1967.

[48] Gardner, C.S., Greene, J.M., Kruskal, M.D. and Miura, R.M., "Method for solving the Korteweg deVries equation", *Physical Review Letters*, vol. 19, no. 19, pp. 1095-1097, 6th Nov 1967.

[49] Zakharov, V.E. and Shabat, A.B., "Exact theory of two dimensional self focusing and one dimensional self modulation of waves in nonlinear media", *Soviet Physics JETP*, vol. 43, no.1, pp.62-69, Jan. 1972.

[50] Ghatak, A.K. and Kothari, L.S., *An Introduction to Lattice Dynamics*, Addison Wesley, London, 1972.

[51] Brillouin, L., *Wave Propagation in Periodic Structures*, (2nd ed.) Dover Publications Inc., USA, 1953.

[52] Perelomova, N.V. and Tagieva, N.M., *Problems in Crystal Physics with Solutions*, Mir Publishers, Moscow, 1983.

[53] Luebbers, R.J, Hunsberger, F. "FDTD for Nth order dispersive media" *IEEE Transactions on Antennas and Propagation*, vol.40, no. 11, pp.1297-1301. Nov. 1991.

[54] Sullivan, D.M. "Frequency dependent FDTD methods using z transforms", *IEEE Transactions on Antennas and Propagation*, vol.40, no.10, pp.1223-1230, Oct. 1992.

[55] Luebbers, E. Steich, D. and Kunz, K., "FDTD calculation of scattering from frequency dependent materials", *IEEE Transactions on Antennas and Propagation*, vol.41, no.9, 1249-1257, Sep. 1993.

[56] Luebbers R. , F.P. Hunsberger, K.R. Kunz, R.B. Standler and M. Schneider, " A frequency dependent finite difference time domain formulation for dispersive materials", *IEEE Transactions on Electromagnetic Compatibility*, vol. 32, pp. 222-227, Aug, 1990.

[57] Ghandi, O.P., Gao, B.Q, Chen, J.Y, "Frequency dependent finite difference time domain formulation for general dispersive media", *IEEE Transactions on Microwave Theory and Techniques*, vol. 41. pp. 658-665, Apr. 1993.

[58] Brillouin, L., *Wave Propagation and Group Velocity*, Academic Press, New York 1962.

[59] Doniach, S. and Sondheimer, E.H., *Green's Functions for Solid State Physicists*, W.A. Benjamin, Inc., Massachusetts, 1974.

[60] Pozar, D.M., *Microwave Engineering*, Addison-Wesley, 1990.

[61] Russer, P., So, P.M., Hoefer, W.J.R., "Modeling of nonlinear active regions in TLM", *IEEE Microwave and Guided Wave Letters*, vol. 1, no. 1, pp. 10-13, Jan 1991.

[62] Scaramuzza, R. and Lowery, A.J. "Hybrid symmetrical condensed node for the TLM method", *IEE Electronic Letters*, vol.26, no.23, 1947-1948, 8th Nov., 1990

[63] Gladwell, I. And Sayers, D.K. (ed.) *Computational Techniques for Ordinary Differential Equations*, Academic Press, London, 1980

[64] DeCarlo, R., *Linear Systems- A State Variable Approach with Numerical Implementation*, Prentice Hall, 1989

[65] Chen, C.T. *Linear System Theory and Design*, Holt, Rinehart and Wiston, New York, 1984.

[66] Oppenheim, A.V., *Discrete Time Signal Processing*, Prentice Hall Inc., 1989.

[67] McCormick, S.F. (ed.), *Multigrid Methods*, Society for Industrial and Applied Mathematics, Michigan, 1987

[68] Southwell, R.V., *Relaxation Methods in Theoretical Physics*, Oxford University Press, London, 1952.

[69] Smith, G.D., *Numerical Solution of Partial Difference Equations, Finite Difference Methods*, (2nd ed.) Oxford Applied mathematics and computing series, Oxford University Press, Oxford, 1978.

[70] Krumpholz, M. and Russer, P. "Field theoretical derivation of TLM", *IEEE Transactions on Microwave Theory and Techniques*, vol. 42, no. 9, pp.1660-1668, Sep. 1994.

[71] Abramowitz, M. and Stegun, I. (ed.), *Handbook of mathematical functions*, Dover publications, Inc. New York, 1972.

[72] Cascio, L., Tardioli, G., Rozzi, T. and Hoefer, W.J.R., "Quasi-static correction of a knife edge corner in 2D TLM algorithm", *Proceedings of the 12th ACES*, pp.317-324, 1995.

[73] Herring, J.L. and Hoefer, W.J.R., "Compensation of coarseness error in TLM modeling of microwave structures with the symmetrical condensed node", *IEEE MTT-S International Symposium Digest*, pp. 23-26, 1995.